Applications Potential of RADARSAT-2

Supplement One

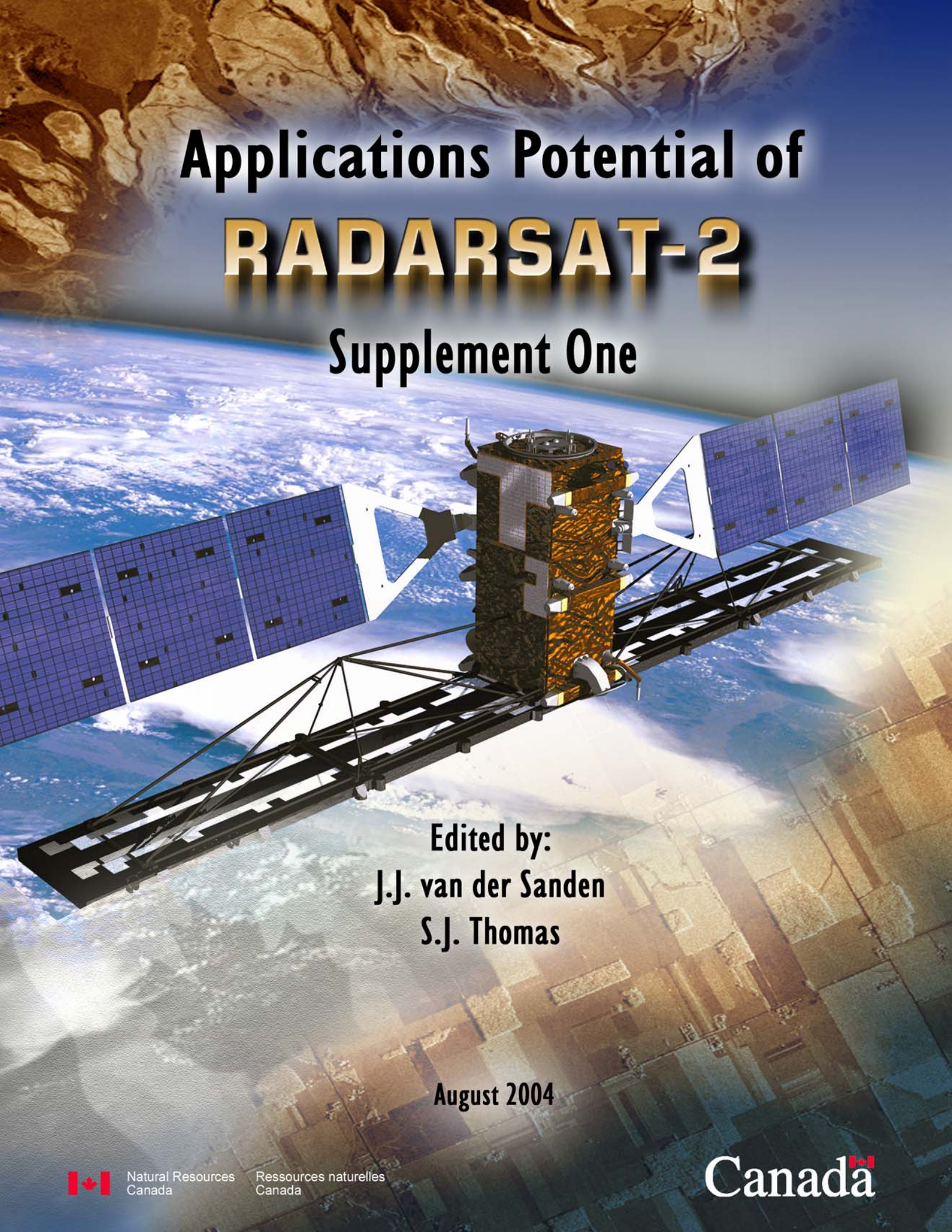

Edited by:
J.J. van der Sanden
S.J. Thomas

August 2004

Natural Resources Canada
Ressources naturelles Canada

Canada

BLANK PAGE

Applications Potential of RADARSAT-2
- Supplement One -

Prepared by:
Canada Centre for Remote Sensing
in collaboration with
Canadian Ice Service,
MacDonald, Dettwiler and Associates Ltd.,
and
Defence Research & Development Canada - Ottawa
for
Canadian Space Agency

Edited by:
J.J. van der Sanden
S.J. Thomas

Contributors:
F. Charbonneau
R. DeAbreu
Y. Du
M. Farhat
R.K. Hawkins
C. Livingstone
T.I. Lukowski
H. McNairn
B. Scheuchl
V. Singhroy
T. Toutin
R. Touzi
P.W. Vachon
J.J. van der Sanden

August 2004

BLANK PAGE

Abstract

van der Sanden, J.J. and S.J. Thomas (eds). (2004). *Applications Potential of RADARSAT-2 – Supplement One*. Ottawa (Natural Resources Canada, Canada Centre for Remote Sensing), report compiled for and with funding from the Canadian Space Agency, 115 p.

This report is the first supplement to the report entitled *Applications Potential of RADARSAT-2 – A Preview* (van der Sanden and Ross, 2001). The document discusses and demonstrates new results from case studies examining the extraction of information from RADARSAT-2 type Synthetic Aperture Radar data for applications in the fields of agriculture, cartography, disaster management, geology, coastal zones and oceans, and sea ice. This includes promising results of limited research into techniques for data fusion and the applicability of products in which RADARSAT-2 type data are fused with data from other remote sensing sources. In addition, the report introduces selected software tools for use with RADARSAT-1 and/or polarimetric SAR data. The results presented contribute to an updated assessment of a) the effect of the most important technical enhancements of RADARSAT-2 on the data information content and b) the applications potential of RADARSAT-2 relative to RADARSAT-1. The applicability of RADARSAT-2 data is anticipated to improve in a major, moderate, and minor fashion for 3, 18, and 10 of the identified applications, respectively. The recommendations emphasize a need for research and development (R&D) leading to an improved understanding of image information content as a function of polarization. This R&D is advised to focus on applications that hold the most promise for operational use of RADARSAT-2 products. The report is based on first-hand experience of applications specialists at the Canada Centre for Remote Sensing (CCRS), the Canadian Ice Service (CIS), MacDonald Dettwiler and Associates (MDA) and the Defence Research Establishment Canada (DRDC) – Ottawa. This report is an output of the RADARSAT-2 Applications Development Programme, which is led by the Canada Centre for Remote Sensing and financed by the Canadian Space Agency with Canadian Space Plan funds.

Keywords: RADARSAT, application, Canada, remote sensing, satellite, radar, multi-polarization, polarimetry, data fusion

BLANK PAGE

Executive Summary

Canada's second Earth observation satellite, RADARSAT-2, is scheduled for launch in 2005. Similar to its predecessor, RADARSAT-2 will image by means of a Synthetic Aperture Radar (SAR) system. RADARSAT-2 will provide all imaging modes of the current RADARSAT-1 satellite, as well as new modes that incorporate significant technical innovations and improvements. Hence, the satellite will offer data continuity to RADARSAT-1 users in addition to new data that will support development of new applications and refinement of existing ones. The most important technical enhancements embodied by RADARSAT-2 are reflected in its specifications in terms of look direction, spatial resolution, polarization, and orbit control.

Given the investment, it is important to all parties involved that the future RADARSAT-2 data can be applied to its full extent to meet information needs from users both within Canada and abroad. Preparation for RADARSAT-2 through applications research and development is therefore crucial to the overall success of the mission. Here, the Canadian government must take a leadership role since industry and academia generally lack the required continuity in terms of financial and human resources. The Canadian Space Agency (CSA) is well aware of this and allocates Canadian Space Plan (CSP) funds to the RADARSAT-2 Applications Development Programme led by the Canada Centre for Remote Sensing (CCRS).

This report constitutes one of the outputs of the RADARSAT-2 Applications Development Programme. It is the first supplement to the literature review conducted by van der Sanden and Ross (2001). As such it describes new results obtained since the earlier publication, with respect to the extraction of information from RADARSAT-2 type data for applications in the fields of agriculture, cartography, disaster management, geology, coastal zones and oceans, and sea ice. Certain results complement findings in the literature review conducted by van der Sanden and Ross (2001) and endorse the earlier assessments in terms of the anticipated effects on application potential of technical features new to RADARSAT-2 and the resulting overall applications potential. Other results further demonstrate the potential of multi-polarization and polarimetric C-band SAR images for specific applications through quantitative analysis. In addition, data fusion techniques and results are presented in the report. For example, products derived from RADARSAT-2 type data fused with magnetic data for mineral property mapping offer a 'strong' potential for geological mapping due to the synergistic effect resulting from the integration of these complementary data sources. A wavelet-based data fusion scheme combining RADARSAT-1 ScanSAR data and NOAA AVHRR data is also demonstrated, resulting in a product which offers enhanced potential for the detection of ocean features such as currents, eddies, internal waves and slicks. Data fusion is also discussed in the context of sea ice interpretation, where RADARSAT-1 and NOAA AVHRR data are fused into one information product using Principal Component Analysis techniques to offer improved ice-water separability.

This report allows us to further identify application fields and information extraction techniques that require additional research and development. The applicability of the current RADARSAT-1 data products is often taken as a starting-point for discussions concerning the application potential of the future RADARSAT-2 data products. In terms of application potential, the report focuses on an assessment of the data information content and thus pays little attention to other issues that may affect the promise of an application, e.g.

economic or legal preconditions. After all, these preconditions may vary widely from one geographical area to another. The report is based on first-hand experience of applications specialists at the Canada Centre for Remote Sensing, the Canadian Ice Service, MacDonald Dettwiler and Associates and the Defence Research Establishment Canada – Ottawa. Findings that other researchers have published in the literature have been consulted in some cases.

The report also includes an updated assessment of the effect of the most important technical enhancements of RADARSAT-2 on the information content and hence the application potential of its data. The differences between the ratings presented in this report and those presented in van der Sanden and Ross (2001) are minimal. Revisions include an increase in anticipated impact of the SDP mode for ship detection from minor to moderate, as well as an increase in anticipated impact of the SSP mode for currents and coastal zone applications from minor to moderate. In addition, the application of sea ice topography and structure is expected to increase from minor to moderate for RADARSAT-2's selective look direction feature. A comprehensive justification of all ratings is presented in Appendix I. Consistent with van der Sanden and Ross (2001), comparison of the ratings for the overall application potential of RADARSAT-1 and –2 shows that the biggest improvement is projected to be associated with the crop type, crop condition and sea ice topography / structure fields. This is primarily the result of the enhancement of RADARSAT-2 in terms of polarization.

The principal recommendations for applications research and development (R&D) are:

1. R&D in the context of RADARSAT-2 should focus on increasing the understanding of the image information content as a function of the polarization of the radar signal.
2. The primary R&D challenge lies in the extraction and application of the information contained in the data acquired in the Quad Polarization image mode.
3. R&D to prepare for the exploitation of RADARSAT-2's extended polarization capabilities should focus on application fields that hold the most promise for operational use of the relevant products.
4. There is a need for further studies into the in application potential of information products resulting from the fusion of RADARSAT-2 type data with data from other sources (e.g. ALOS PALSAR).
5. Calibration of Envisat ASAR data that are received and processed at the Canadian satellite receiving stations would facilitate applications R&D in preparation for RADARSAT-2.
6. Demonstration images in the data format selected for RADARSAT-2 products should be made available in support of the development of image analysis software.

The recommendations 1 to 4 were initially presented in van der Sanden and Ross (2001) and continue to remain valid.

Preface

The Canada Centre for Remote Sensing (CCRS) compiled this report in the framework of the RADARSAT-2 Applications Development Programme. This programme aims to prepare the remote sensing community for the application of data products from Canada's second radar satellite, RADARSAT-2, which is scheduled for launch in 2005. While led by the Canada Centre for Remote Sensing, the programme is financed by the Canadian Space Agency with Canadian Space Plan funds.

The report is based on ongoing applications development work at CCRS, CIS, MDA and DRDC-Ottawa. In some cases, results published by other national and international researchers were consulted. The editors wish to acknowledge the technical contributions of the following colleagues:

Francois Charbonneau	Section 3.3.1
Roger DeAbreu	Section 3.6.2
Yong Du	Section 3.5.3
Mo Farhat	Section 4.3
Bob Hawkins	Appendix II
Chuck Livingstone	Section 3.2.2
Tom Lukowski	Section 3.3.2
Heather McNairn	Sections 3.1.1, 3.1.2, 3.1.3
Bernd Scheuchl	Section 3.6.1
Vern Singhroy	Sections 3.4.1, 3.4.2
Thierry Toutin	Section 4.1
Ridha Touzi	Sections 3.3.1, 4.2, Appendix III
Paris Vachon	Section 3.5.3
Joost van der Sanden	Sections 3.2.1, 3.5.1, 3.5.2, Appendix I

In addition, Julie Allard is acknowledged for the design of the front cover and Ginette Gauvin for her assistance with the final layout of the text.

Lastly, the editors would like to encourage the readers of this report to inform them of their questions and comments by sending an email to one of the following two addresses: Joost.van_der_Sanden@ccrs.nrcan.gc.ca or Sylvia.Thomas@ccrs.nrcan.gc.ca.

BLANK PAGE

Contents

List of Tables

BLANK PAGE

List of Figures

List of Abbreviations

Abbreviation	Description
2-D, 3-D	Two-dimensional, Three-dimensional
ALOS	Advanced Land Observing Satellite
ARC	Active Radar Calibrator
ASAR	Advanced Synthetic Aperture Radar
ATI	Along-Track Interferometry
AVHRR	Advanced Very High Resolution Radiometer
BPA	Bushels per Acre
CCRS	Canada Centre for Remote Sensing
CFAR	Constant False Alarm Rate
CHS	Canadian Hydrographic Service
CIS	Canadian Ice Service
CSA	Canadian Space Agency
CSP	Canadian Space Plan
DEM	Digital Elevation Model
DRDC	Defence Research and Development Canada
DN	Digital Number
DND	Department of National Defence
DPCA	Displaced Phase Centre Antenna
EEZ	Exclusive Economic Zone
ENVISAT-1	First Environmental Satellite
ERS	European Remote Sensing Satellite
GIS	Geographic Information System
GMTI	Ground Moving Target Indication
GPS	Global Positioning System
GSC	Geological Survey of Canada
GSFC	Goddard Space Flight Center
HH	Horizontal transmit – Horizontal receive polarization
HV	Horizontal transmit – Vertical receive polarization
IHS	Intensity, Hue, Saturation
InSAR	Interferometric SAR
LAI	Leaf Area Index
LL	Left-hand circular transmit – Left-hand circular receive polarization
LR	Left-hand circular transmit – Right-hand circular receive polarization
MDA	MacDonald, Dettwiler, and Associates
MDV	Minimum Detectable Velocity
MERIS	Medium Resolution Imaging Spectrometer
MLC	Multi-Look Complex
MODEX	Moving Object Detection EXperiment
NASA	National Aeronautics and Space Administration
NDVI	Normalized Difference Vegetation Index
NOAA	National Oceanic and Atmospheric Administration
OLA	Oleyl Alcohol

Abbreviation	Description
OLME	Oleic Acid Methyl Ester
OLS	Operational Linescan System
PALSAR	Phased Array L-band Synthetic Aperture Radar
PCA	Principal Component Analysis
PDF	Probability Density Function
PWF	Polarimetric Whitening Filter
PWS	Polarimetric Work Station
QP	Quad Polarization (full polarimetric)
RGB	Red, Green, Blue
RL	Right-hand circular transmit – Left-hand circular receive polarization
RR	Right-hand circular transmit – Right-hand circular receive polarization
ROI	Region of Interest
SAR	Synthetic Aperture Radar
SARP3	SAR Polarimetric Post Processor
SDP	Selective Dual Polarization
SIR-C	Shuttle Imaging Radar – C-band
SLC	Single-Look Complex
SP	Single Polarization
SPM	Small Perturbation Model
SSM/I	Special Sensor Microwave Imager
SSP	Selective Single Polarization
STAP	Space-Time Adaptive Processing
TM	Thematic Mapper
VH	Vertical transmit – Horizontal receive polarization
VV	Vertical transmit – Vertical receive polarization
WMO	World Meteorological Organization

1 Introduction

RADARSAT-2, Canada's second Earth observation satellite is being implemented through a unique co-operation between the Canadian Space Agency (CSA) and MacDonald Dettwiler Associates Ltd (MDA) of Richmond, BC. While providing data continuity to RADARSAT-1 users, RADARSAT-2 will contain a series of technical enhancements that augment its imaging capabilities. The Government of Canada is providing approximately 60% of the overall mission costs and MDA is investing the difference. Following the launch in 2005, RADARSAT-2 will be owned, operated and commercialized by MDA. Canada's investment will be recovered through the supply of data to government agencies during the mission lifetime. Canadian businesses other than MDA will benefit from the project through the awarding of subcontracts for the satellite's development and through the sales of RADARSAT-2 derived information products once the satellite becomes operational. The arrangement between CSA and MDA is seen as the first step in the transition of spaceborne Earth observation from government to private sector.

Given the investment, it is important to all parties involved that the future RADARSAT-2 data can be applied to its full extent to meet information needs of users both within Canada and abroad. Preparation for RADARSAT-2 through applications research and development is therefore crucial to the overall success of the mission[1]. Here, the Canadian government must take a leadership role since industry and academia generally lack the required continuity in terms of financial and human resources. The CSA is well aware of this and therefore allocates Canadian Space Plan (CSP) funds to the RADARSAT-2 Applications Development Programme led by Natural Resource Canada's Canada Centre for Remote Sensing (CCRS) and implemented in partnership with other federal agencies. The RADARSAT-2 Applications Development Programme aims to:

- carry out research and development needed to devise algorithms and methods to extract information from RADARSAT-2 data in key applications areas
- support government utilization of RADARSAT-2 data by working with user agencies in the development and demonstration of new applications
- link to and support the Earth Observation Applications Development Program (EOADP), whose primary goal is the commercialization of remote sensing data, including those of RADARSAT-2.

The programme was started in 2000 and is expected to continue until the launch of RADARSAT-2. It will enable the Canadian government and, through her, the Canadian industry to build on the successes achieved with RADARSAT-1 and to expand Canada's leading role in the development of SAR-derived information products.

The present report constitutes the second in a series of reports to be delivered under the RADARSAT-2 Applications Development Programme. It is the first supplement to the literature review conducted by van der Sanden and Ross (2001). The current supplement describes the state-of–the-art with respect to the extraction of information from RADARSAT-2 type data in a large number of application fields. It focuses on scientific results achieved since the publication by van der Sanden and Ross (2001), with emphasis on data fusion techniques and results. The document therefore provides an update on the application potential of RADARSAT-2 based on the most recent research, and enables the identification of application fields, information extraction techniques and data fusion techniques that show

[1] The most important text segments in this report have been highlighted for the benefit of the reader.

promise and may require further research and development. Our emphasis continues to be on those data products that are not currently available from RADARSAT-1. However, the application potential of RADARSAT-1 data products is often used as a starting-point for our discussions. In terms of application potential, we will focus on an assessment of the data information content and thus pay little attention to other issues that may affect the promise of an application, e.g. economic or legal preconditions, which may vary widely from one geographical area to another. The report is based on first-hand experience of applications specialists at CCRS, CIS, MDA, and DRDC-Ottawa. In some instances, findings that other researchers have published in the literature have been consulted.

Following this introduction, Chapter 2 presents modifications to RADARSAT-2's general system capabilities as presented in the publication by van der Sanden and Ross (2001). These changes are shown in a light blue typeface. In Chapter 3 we review the results of relevant application studies conducted since publication of van der Sanden and Ross (2001). In particular, data fusion techniques and capabilities are emphasized. Results are drawn on to assess the applications potential of RADARSAT-2 data in the fields of agriculture, cartography, disaster management, geology, coastal zones and oceans, and sea ice. Chapter 4 presents selected software tools for use with RADARSAT-1 and/or polarimetric data. We discuss the RADARSAT-1 Stereo Advisor software package, which has the potential to be upgraded to the improved specifications of RADARSAT-2, the Polarimetric Work Station (PWS) developed at CCRS, and the SAR Polarimetric Post Processor (SARP3) developed at CSA. The report finishes with an applications summary and recommendations for further applications research and development in Chapter 5.

At the end of the introduction to this report it is fitting to highlight an additional resource for information concerning RADARSAT-2 – that is - the recent special issue on RADARSAT-2 of the Canadian Journal of Remote Sensing (June 2004, vol. 30, no. 3). The 32 papers comprised in this special issue report background material on the mission's space and ground segments, discussions of the advanced modes, commercialization and operationalization strategies, and results of case studies that delve into the advanced application opportunities. To conclude, we would like to draw attention to the Science and Operational Applications Research for RADARSAT-2 Program (SOAR). SOAR is a joint partnership program between RADARSAT International (RSI), MDA and the Canadian Government through the CSA and CCRS. Following launch, this program will provide interested users with access to RADARSAT-2 data for research and testing purposes. More information about the SOAR program including the process and time schedule for the submission of project proposals can be found at the following website: http://www.radarsat2.info/soar/rs2_soar_info.asp.

2 RADARSAT-2 System Update

This section presents modifications to RADARSAT-2's specifications as provided in the literature review conducted by van der Sanden and Ross (2001). Tables 2-1 and 2-2 summarize selected specifications of RADARSAT-2. Information within these tables that has changed since publication of the first report is highlighted in a light blue typeface.

RADARSAT-2 is currently scheduled for launch in the fall of 2005. The satellite's orbit will have a nominal eccentricity of 0.00115 and a nominal argument of perigee of 90 degrees. This will provide an altitude range of approximately 792 km to 821 km, as indicated in Table 2-1. With an inclination of 98.6 degrees, RADARSAT-2 will have a 7 day primary sub-cycle and a 3 day secondary sub-cycle, and will orbit the earth 343 times within its 24 day repetition cycle. The orbit will be sun-synchronous, and the satellite will complete 14 7/24 orbits in 24 hours. In terms of imaging modes (Table 2-2), RADARSAT-2 will provide all modes of the current RADARSAT-1 satellite, as well as some new modes and polarization options that will support development of new applications and refinement of existing ones. Changes from the earlier document include a restriction of the polarization mode of the high and low incidence beams to single polarization (HH only). Therefore these modes will not be available in the selective single polarization or selective dual polarization options as indicated in van der Sanden and Ross (2001). In addition, the nominal incidence angle range for the Fine Quad Polarization mode is 20-41 degrees, consistent with the Standard Quad Polarization mode.

Table 2-1 Selected specifications of RADARSAT-2 (MDA, 2003). Note text highlighted in a light blue typeface indicates changes from the original specifications as presented in van der Sanden and Ross (2001).

General specifications	
Expected launch date	Fall 2005
Mission life	7 years after commissioning
SAR characteristics	
Centre frequency	5.405 GHz (C-band)
Bandwidth	100 MHz
Polarization	HH, HV, VH, VV
Cross polarization isolation	< -20 dB
Aperture length	15 m
Aperture width	1.37 m
Nominal spatial resolution	3 - 100 m
Nominal swath width	20 – 500 km
Nominal incidence angle	10° - 60°
Look direction	right or left
Imaging modes	11
Orbit characteristics	
Altitude (range)	792 - 821 km
Inclination	98.6^o
Sun-synchronous	14 7/24 orbits per day
Repeat cycle	24 days

Table 2-2 RADARSAT-2 imaging mode specifications. Imaging modes not available on RADARSAT-1 are shown in a bold typeface (MDA, 2003). Note text highlighted in a light blue typeface indicates changes from the original specifications as presented in van der Sanden and Ross (2001).

Imaging mode	Nominal incidence angle (degrees)	Nominal swath width (km)	Nominal resolution (Gr Rg x Az) (m)	Nominal number of looks (Rg x Az)	Polarization mode [1)]
Standard	20 - 49	100	25 x 28	1 x 4	SSP or SDP
Wide	20 - 45	150	25 x 28	1 x 4	SSP or SDP
Low Incidence	10 - 23	170	40 x 28	1 x 4	SP
High Incidence	50 - 60	70	20 x 28	1 x 4	SP
Fine	37 - 49	50	10 x 9	1 x 1	SSP or SDP
ScanSAR Wide	20 - 49	500	100 x 100	4 x 2	SSP or SDP
ScanSAR Narrow	20 - 46	300	50 x 50	2 x 2	SSP or SDP
Multi-Look Fine	30 - 50	50	11 x 9	2 x 2	SSP
Ultra-Fine	30 - 40	20	3 x 3	1 x 1	SSP
Standard Quad Polarization	20 - 41	25	25 x 28	1 x 4	QP
Fine Quad Polarization	20 - 41	25	11 x 9	1 x 1	QP

1) SP: Single Polarization; HH acquired
SSP: Selective Single Polarization; HH or HV or VV or VH acquired
SDP: Selective Dual Polarization; HH + HV or VV + VH acquired
QP: Quad Polarization; HH + HV + VV + VH acquired (full polarimetric)

The slew capability of RADARSAT-2 as presented in Figure 2-1 will enable the satellite to acquire images to either the right or left of the sub-satellite track. Although this capability is an operational feature, the right-looking configuration is regarded as the default mode of operation. Hence, it is expected that about 75% of the imaging will be performed in this particular mode, although the left-looking mode will be deployed to meet requirements associated with Antarctic mapping and emergency situations. In general, the slew capacity will be used as a strategic rather than tactical planning feature. The current concept entails pre-defining the slew plan to maximize revisit over landmasses to 300 nm. However, the potential of overwriting the pre-defined slew plan for emergency acquisitions will exist. A slew change could be done under the emergency planning lead-time (up to 6 hours before uploading of the spacecraft payload file).

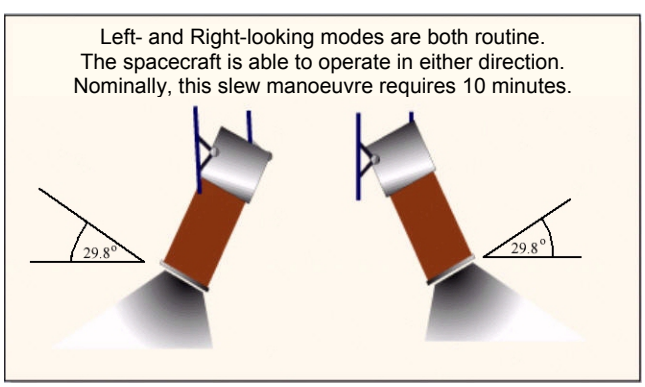

Figure 2-1 Slew planning capability for RADARSAT-2.

3 Anticipated Applications Potential

In this chapter we present and discuss results achieved since the literature review presented in van der Sanden and Ross (2001), focusing on how the new capabilities of RADARSAT-2 are expected to enhance the potential of its data for a variety of applications. The applications addressed include agriculture, cartography, disaster management, geology, coastal zones and oceans, and sea ice. Of special interest to this chapter is the topic of data fusion, and several sections address the utility and benefit of RADARSAT data fused with data from other remotely sensed and geophysical data sources. Consistent with van der Sanden and Ross (2001), the focus of the analysis presented here is on the information content of the data and not the economic viability of the application. The assessments are primarily based on results of ongoing applications development work at CCRS, CIS, MDA and DRDC Ottawa. In some cases, results that have been published in literature by other national and international researchers were consulted.

3.1 Agriculture

Farm producers and agricultural service providers require timely and reliable information on crop condition and productivity throughout the growing season. Very often crop growth is not uniform across a field due to variable soil and topographic characteristics. These variations create zones of productivity within a field. Producers can modify their management strategies if they can estimate productivity within these zones early in the growing season, and if they can establish the factors determining productivity.

Information that defines these zones can also be useful in planning management strategies from one year to the next, or in developing nitrogen management plans. Applying the right amount of fertilizer at the right location and at the right time can substantially impact farming profits and crop productivity. In addition to economic considerations, there are also obvious environmental implications for developing a sound management plan tied to crop and soil requirements. Spatial and temporal information on both soil and crop conditions will be required to formulate these management plans. Some agricultural service providers are beginning to use simple products from optical sensors on satellite platforms for land management planning, but guaranteed delivery of the imagery is problematic due to cloud cover. Information on crop growth gathered from sensors like RADARSAT-2 could aid in strategies for agricultural land use management.

Polarimetric SARs provide significantly more data relative to conventional radars. However, little is understood about the interpretation and application of polarimetric information for agriculture. To help address this knowledge gap, the Canada Centre for Remote Sensing (CCRS) has acquired airborne Convair-580 fully polarimetric data over several agricultural test sites. The data are being used to assess the sensitivity of polarimetric products to indicators of crop condition.

Results have indicated that at C-HH backscatter saturates once broadleaf crops like corn accumulate significant biomass (McNairn *et al*., 2000). This saturation effect was observed once the corn reached a height of about one metre. Although multi-polarized SAR is still useful for mapping crop type, information on crop condition for large biomass crops like corn may be restricted to early in the growing season. In contrast, two recent CCRS studies are

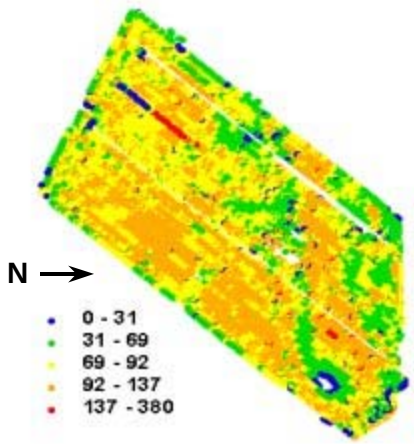

(a) Yield map for white winter wheat

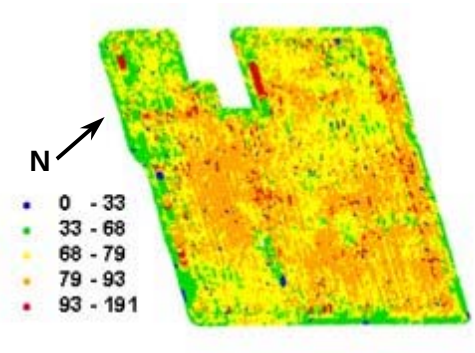

(b) Yield map for red winter wheat

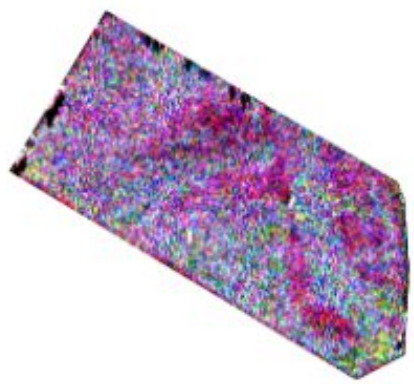

(c) SAR composite for white winter wheat

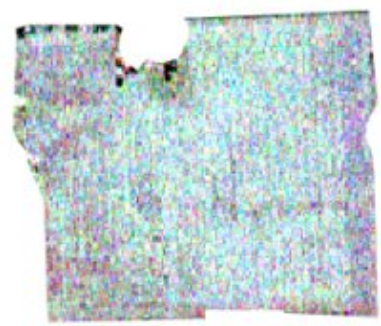

(d) SAR composite for red winter wheat

Figure 3.1.1-1 (a-d) Yield monitor maps (bushels per acre) are indicated for both (**a**) the white winter wheat field and (**b**) the red winter wheat field.; (**c, d**) the corresponding SAR images. These images are composites of the three linear polarizations (R=VV, G=VH, B=HH).

demonstrating the value of multi-polarized and polarimetric C-Band SAR for mapping the condition of other crops, in particular small grains like barley and wheat.

3.1.1 Multiple polarizations for assessing productivity in small grain crops

On June 30th 1999, airborne C-Band polarimetric SAR data were acquired over a study site approximately centred on the town of Clinton, in southern Ontario (Canada). Corner reflectors and Polarimetric Active Radar Calibrators were deployed in the study site during the airborne SAR acquisitions. Polarimetric processing and radiometric calibration of the airborne data was accomplished using the CCRS programs PolGASP and ComplexCAL. Within scene calibration accuracies were less than 1 dB (Hawkins *et al*., 1999). Image products were synthesized from the complex data using the CCRS software package POLSIG. Four linear transmit-receive polarizations (HH, VV, HV, VH), as well as the circular transmit-receive polarizations (RR, LR) were generated. The results from this study are reported in McNairn *et al.* (2002a).

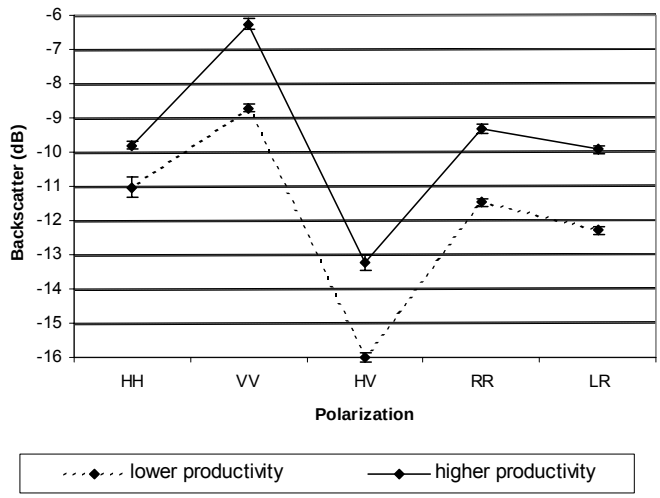

(a) Linear and circular backscatter for lower and higher producing zones in red winter wheat

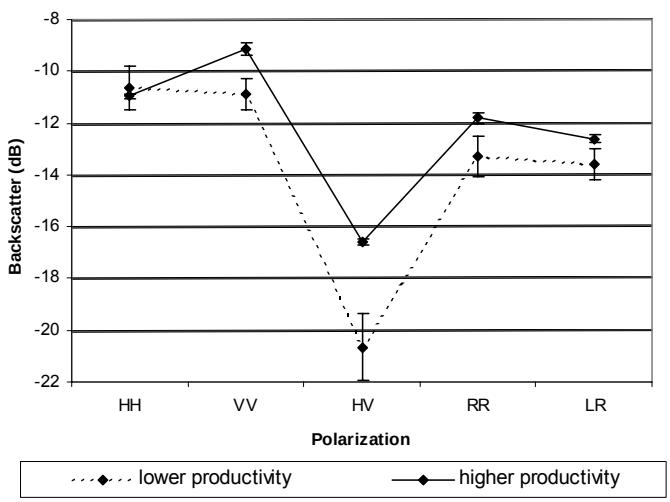

(b) Linear and circular backscatter for lower and higher producing zones in white winter wheat

Figure 3.1.1-2 (a-b) Backscatter responses are given for lower and higher yielding areas within a (**a**) red winter wheat field and (**b**) white winter wheat field. Error bars are indicated for each point.

Yield monitor data, in bushels per acre (BPA), were acquired for two wheat fields in the study site. One field was planted in soft white winter wheat and the other in soft red winter wheat. These two fields were harvested on July 14th, approximately two weeks after the radar acquisition. For these two fields of winter wheat, variations in backscatter were clearly visible on the SAR imagery (Figure 3.1.1-1). These variations matched patterns observed on the yield maps. To quantify these differences in backscatter, regions of interest (ROIs) were drawn on the SAR imagery where higher (greater than 70 BPA) and lower (less than 70 BPA) yields were recorded by the yield monitor. Under each ROI, mean values were calculated for backscatter recorded for the linear (HH, VV, HV) and circular (RR, LR) polarizations. For each wheat field, average backscatter for lower and higher yielding zones is presented in Figure 3.1.1-2. For all linear and circular polarizations, zones that produced

more bushels per acre had higher backscatter relative to zones that produced less. But the difference in backscatter between these two zones of productivity is dependent upon polarization. The linear cross-polarization (HV) exhibited the greatest contrast between these two zones. C-HV backscatter was between 2.8 dB (red wheat) and 4.1 dB (white wheat) higher for zones of greater productivity. Conversely, virtually no difference in C-HH backscatter is observed between higher and lower producing zones.

The yield map and a classified map produced from the SAR data were also compared on a pixel-by-pixel basis. The yield monitor data were normalized by area and re-coded into zones of low and high yield using the quantile classification method. Nine classes were initially identified and these were grouped into two productivity zones – lower yielding (mean yield 61.4 BPA for white wheat; 66.3 BPA for red wheat) and higher yielding (mean yield 95.6 BPA for white wheat; 82.5 BPA for red wheat). The SAR imagery was classified into ten clusters using HH, VV and HV backscatter as input and a K-Means algorithm. Based on a visual correlation with the yield maps, these ten clusters were then grouped into zones of low (clusters 1-3) and high (clusters 4-10) productivity. Zones identified as lower and higher yielding from the yield data were compared to productivity zones mapped by the SAR. The percent agreement between these two data sources was calculated. When compared on a pixel-by-pixel basis, good agreement was found between the classes derived from the SAR data, and zones of productivity derived from the yield monitor data (Figure 3.1.1-3). Areas of higher yield generally agreed with areas of higher backscatter. Percent agreement was 77% for the white winter wheat field and 62% for the red winter wheat field.

This study demonstrated that SAR data are sensitive to zones of productivity in wheat crops, but that this sensitivity is polarization dependent. For HV, a 7.4 dB difference is observed between higher producing red wheat and lower producing white wheat. As reported by Bouman *et al*. (1990), backscatter response does vary throughout the growth cycle of wheat. Hochheim and Barber (2002) discovered that particularly later in the growing season, backscatter from wheat crops is largely a function of the canopy structure, with the heads of the wheat representing the most significant biomass and moisture component in the wheat canopy. Backscatter decreases as biomass peaks, but tends to increase again as the green leaf biomass reduces and the heads start to fill. The increase in backscatter at this growth stage (grain filling) is associated with volumetric moisture within the wheat heads, which dominates the signal in high biomass areas (Hochheim and Barber, 2002).

In dry years, as experienced at this site in 1999, higher productivity can be expected in zones of higher soil moisture availability. These soil moisture differences will be related to differences in elevation and soil properties across the fields. Lower slope positions, with heavier soils and more organic matter will hold moisture in the soil longer. With access to greater soil moisture, these higher productivity zones have a longer green leaf duration. Towards the end of the growing season these zones tend to retain moisture within the canopy for a longer period of time. Stressed crops in zones of low soil moisture produce smaller and fewer wheat heads and reach maturity sooner. Crops in these zones also have less moisture in the canopy. These conditions result in a lower backscatter response when compared to higher producing zones.

3.1.2 Polarimetric SAR for establishing within-field zones of crop condition

The Clinton study demonstrated that multiple polarizations can be used to derive information related to winter wheat productivity. Although results were encouraging, the productivity

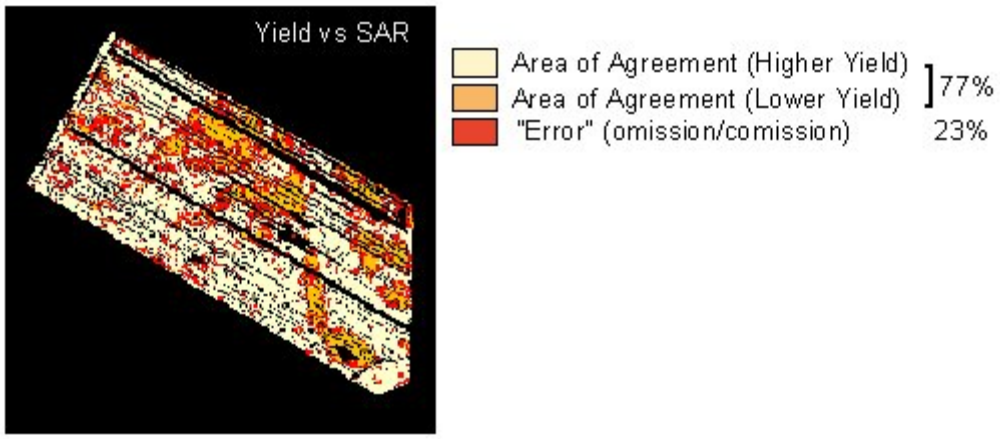

(a) Percent agreement for white winter wheat field

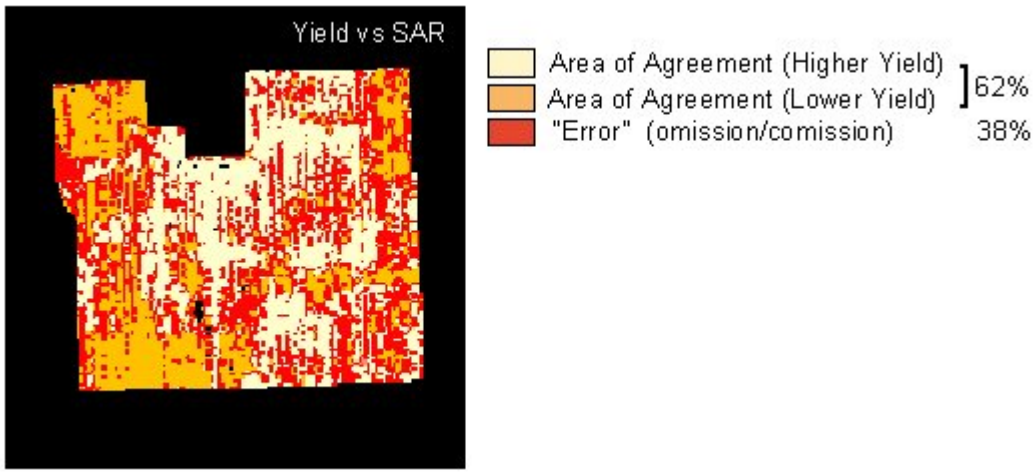

(b) Percent agreement for red winter wheat field

Figure 3.1.1-3 (a-b) Areas of agreement between the SAR derived classification maps and the yield maps for the (**a**) white and (**b**) red winter wheat fields.

information provided during this study came just two weeks prior to harvest. Thus this information comes too late in the season to be of use for remediation. Productivity maps that are available late in the season are of value, but for non-time critical applications. As an example, these applications might include zone definition for site-specific soil sampling after harvest, or for use in defining nitrogen application strategies for the following year.

On 28 June 2000, in collaboration with the Indian Head Agricultural Research Foundation, Agriculture and Agri-food Canada and the Universities of McGill, Ottawa and Manitoba, CCRS acquired airborne C-Band fully polarimetric data over a test site at Indian Head, Saskatchewan (Canada) (McNairn *et al*., 2002b). Corner reflectors and Polarimetric Active Radar Calibrators were deployed in the study site during the airborne SAR acquisitions. On the same day, airborne Probe-1 hyperspectral imagery and Ikonos (multi-spectral and panchromatic) imagery were acquired over the test site. Extensive supporting ground data on crop status and crop condition was collected coincident with the image acquisitions. Crops grown on the test site included four fields of wheat, two fields of peas and two fields of canola. Compared with the Clinton winter wheat fields, which were senescing at the time

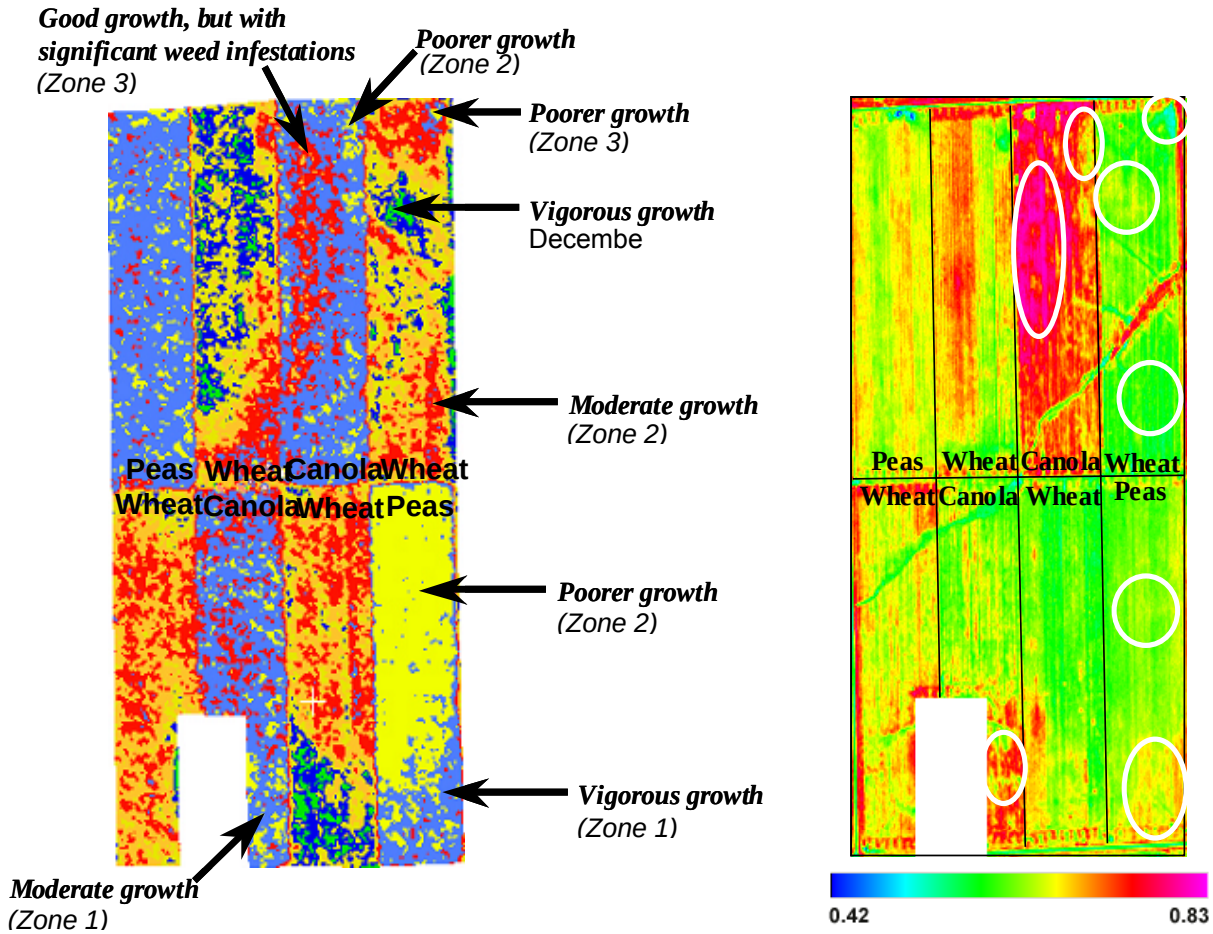

(a) (b)

Figure 3.1.2-1 (a-b) Crop condition maps generated from (**a**) an unsupervised classification of the SAR image and (**b**) NDVI from an Ikonos image. Both the SAR and the Ikonos images were acquired on June 28, 2000 over Indian Head, Saskatchewan. Circles on the NDVI map identify the general location of zones detected in the SAR image.

of the SAR acquisition, the Indian Head spring wheat crops were still in their vegetative growth stage (tillering and stem elongation) and had not yet headed. Measurements of various crop and soil indicators were acquired on the Indian Head site, including Leaf Area Index (LAI), percent ground cover, crop height and surface soil moisture. Yield monitor data and a high resolution digital elevation model (DEM) were also available.

Several polarizations were synthesized from the Convair-580 complex data, including two circular polarizations (RR and RL). Linear polarizations were synthesized by choosing an ellipticity angle (χ) of zero and by varying the orientation angle (Ψ) at 45° increments from 0° to 180°. Incidence angles over the test site, for this particular flight line, were between 42-46°. The SAR image was classified into sixteen clusters using seven of these polarizations as input and a K-Means algorithm. The polarizations used in the unsupervised classification included HH, VV, HV, RR, RL and linear polarizations with Ψ = 45° and Ψ = 135°. Extensive ground data are available to validate this classified map. However, preliminary results discussed here are based on qualitative observations from the Ikonos multispectral imagery,

field validation of the Ikonos and SAR imagery immediately following the acquisitions, and soil maps (soil type and soil moisture). Surface soil moisture was derived from 0-5 cm core samples acquired at 98 sample sites, on the day of the SAR overflight. A soil moisture map was generated from the data collected at each sample point, using an inverse distance weighted interpolation algorithm.

The 16 classes derived from the unsupervised classification could be aggregated into a number of crop condition zones, based on field observations (Figure 3.1.2-1). The unsupervised classification resulted in more classes in the wheat fields, relative to the other two crop types. For all crops, these zones of productivity were defined by the crop height and density, and were often linked to differences in soil type and thus soil moisture. For the four wheat fields, the seven polarizations separated this crop into six classes. These six classes represented three growth zones (Table 3.1.2-1). Field observations indicated that the crop condition in Zone 1 was very healthy. Here wheat plants were taller and denser.

These zones were associated with well-drained soils on upper slopes. The unsupervised classification was also able to detect zones of moderate wheat growth. Although wheat plants were shorter and growth was less dense, plants were still characterized as healthy. Saturated soil conditions were evident in pockets of gleyed soils found throughout the farm, and in regions of clayey soils in lower slopes. In these areas (Zone 3), crops were stressed. Bottom wheat leaves were yellow, suggesting a deficiency in nitrogen, and plants were shorter.

The Cloude alpha (α) and entropy (H) decomposition parameters were generated for each wheat zone, and are plotted in Figure 3.1.2-2 (Cloude and Pottier, 1997). Entropy is a measure of the dominance of a given scattering mechanism, with values close to zero suggesting that all scattering originates from a single mechanism. The alpha angle indicates the dominant scattering mechanism. The plots in Figure 3.1.2-2 demonstrate that the dominant scattering mechanism changes from the zones of healthier wheat growth (Zones 1

Table 3.1.2-1 Field observations associated with zones classified for wheat, pea and canola crops.

	Class Average Backscatter	Crop Conditions	Soil Moisture & Texture
Wheat – Zones			
Wh-Zone 1	HH (-15.1); HV (-23.3); VV (-15.8)	-taller (40-50 cm) and denser (60-90% cover) -healthier growth	-drier (20-40%) -clay loam and clay
Wh-Zone 2	HH (-11.9); HV (-20.5); VV (-12.6)	-20-40 cm high with 40-60% cover -moderate growth	-drier (20-40%) -clay soils
Wh-Zone 3	HH (-10.2); HV (-17.7); VV (-10.6)	-shorter (15-30 cm) with 40-60% cover -crop is stressed and appears yellowish (deficient in nitrogen)	-very wet (40-60%) -gleyed and clay soils
Peas – Zones			
Pe-Zone 1	HH (-9.8); HV (-16.2); VV (-10.1)	- taller (55-75 cm) and denser (90% cover) -very good growth	-drier (10-30%) -clay and clay loam
Pe-Zone 2	HH (-7.4); HV (-14.6); VV (-8.8)	-25-40 cm high but less dense -poor growth (bottom leaves yellow with brown spots)	-wetter (30-50%) -clay soils
Canola – Zones			
Ca-Zone 1	HH (-9.8); HV (-16.2); VV (-10.1)	- taller (60-70 cm) and denser (70%) -better growth	-drier (10-40%) -clay loam and clay
Ca-Zone 2	HH (-7.4); HV (-14.6); VV (-8.8)	-shorter (40-50 cm) and less dense -poorer growth	-wetter (40-50%) -clay soils
Ca-Zone 3	HH (-10.6); HV (-19.2); VV (-11.2)	-50% weeds -good canola growth (70-90 cm)	-30-50% -clay soils

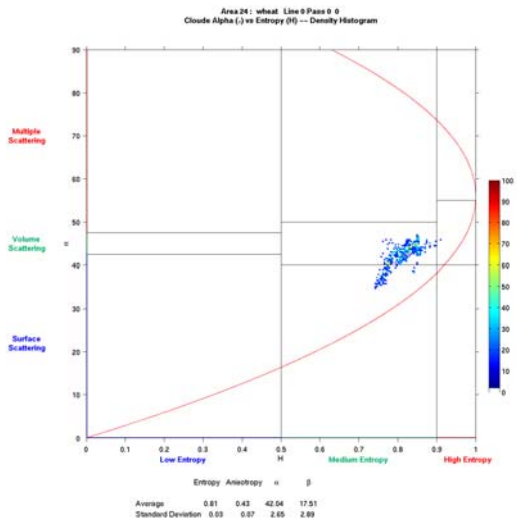

(a) Wheat Zone 1

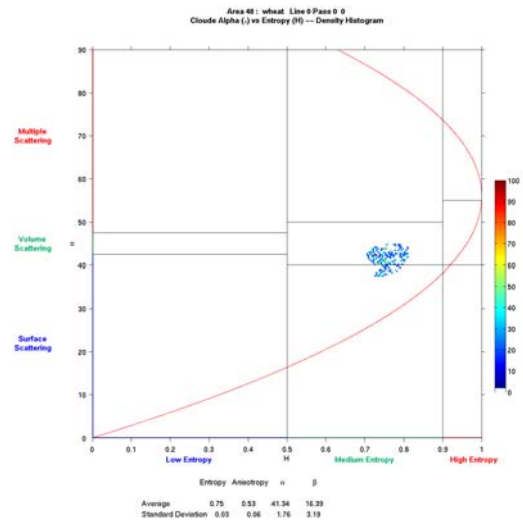

(b) Wheat Zone 2

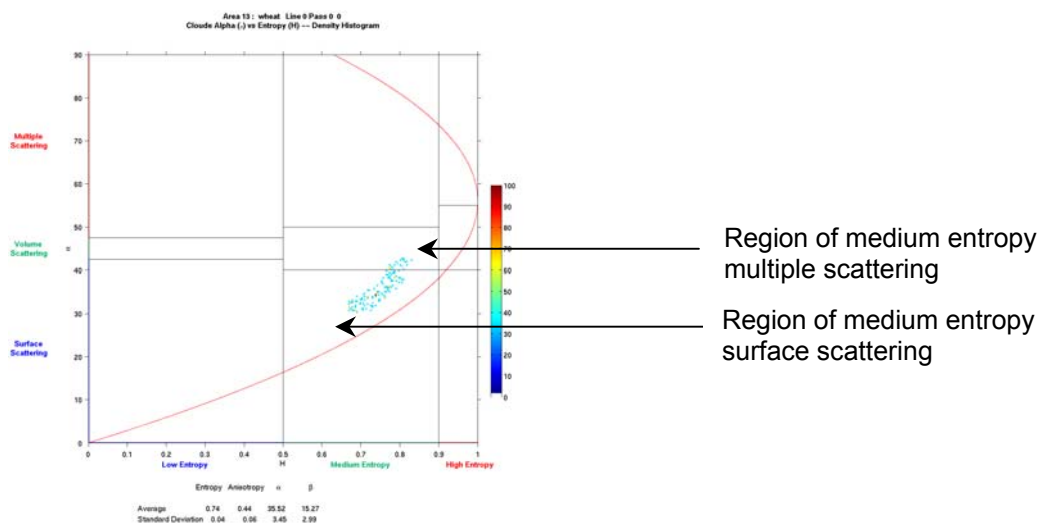

(c) Wheat Zone 3

Figure 3.1.2-2 (a-c) Cloude decomposition graphs of alpha and entropy for zones of wheat productivity represented in Figure 3.1.2-1(a). Zone 1 corresponds to the healthiest crop, while wheat plants in Zone 3 are smaller and less dense.

and 2) to Zone 3. However, more than one scattering mechanism is present in all three zones. In zones of poorer wheat condition (Zone 3), more scattering originates from surface scattering from the soil. As the plants become higher and denser (Zone 1 and Zone 2), it appears that more volume scattering from the crop and less from the underlying soil is occurring.

Fewer classes were generated for the two broadleaf crops – peas and canola. As well, backscatter differences between zones were less for these broadleaf crops (1-2.5 dB) when

compared to differences observed between zones identified for wheat (2-3 dB). Four classes were identified in the pea crops, associated with two zones of crop condition. These zones were also associated with soil type, drainage and slope position (Table 3.1.2-1). Crop condition was manifested in height and density. In zones of poor growth, bottom leaves of the pea plants were yellow with noticeable brown spots (Zone 2). Five classes of canola represented two crop growth zones (Zones 1 and 2) with a third zone characterized by significant weed infestations. In Zone 3 the canola crop appeared healthy and vigorous, but approximately 50% of the area was infested with wild oats. Vegetation (crop plus weeds) in this region was dense.

Preliminary observations from the fully polarimetric data acquired over fields of wheat, peas and canola indicate that linear and circular polarizations can detect zones of crop condition characterized by variations in crop height and density. For wheat fields at this growth stage (prior to heading) backscatter was lower in zones of healthier, taller and denser growth. Backscatter decreases as biomass peaks and this is likely due to the increased attenuation of the radar signal by the stems and leaves of the wheat canopy. However, as observed in the Clinton data set, the backscatter relationship between productivity zones can reverse after grain filling and during senescence when zones of higher productivity have higher backscatter.

3.1.3 Integrating SAR and optical imagery to derive information for agriculture

Fusion of SAR and Optical Data

End-users, including those in agriculture, seek specific information for use in decision-making. The source of the data used to derive the information is much less important than the appropriateness, quality and timeliness of the information products. SAR and optical imagery can be integrated in a number of ways to improve information extraction and to improve the characteristics of these information products.

One approach to integration is to combine or fuse data from optical and SAR sensors prior to information extraction. These multi-source and multi-dimensional data sets are created using ground control points common in each image, and a data re-sampling algorithm. An example of this approach to data fusion is provided in Figure 3.1.3-1. In this example, DRDC Ottawa first re-sampled the Convair-580 data to a 4 m x 5 m resolution and applied a 3 x 3 median filter. The hyperspectral data were then co-registered to this SAR data, and re-sampled to the SAR resolution.

Further pre-processing on the combined data sets can be applied prior to generating information products. Examples of these pre-processing techniques include Principal Component Analysis (PCA) and an Intensity, Hue, Saturation (IHS) transformation. PCA transforms multi-dimensional data sets to create linear combinations (principal components) of the original channels. PCA reduces the dimensionality of the combined data set. As well, these new channels are uncorrelated, yet account for the inherent variation of the data to the maximum possible extent. Saint-Jean *et al*. (1995) explained how Landsat TM and Convair-580 data were integrated using PCA and the IHS transformation, in order to enhance information extraction. After reducing the TM data set down to three channels using PCA, the three channel RGB was transformed to IHS colour space. The intensity channel was then replaced with the SAR image and the saturation channel was replaced by a uniform DN value. The “new” IHS image was then transferred back to RGB space.

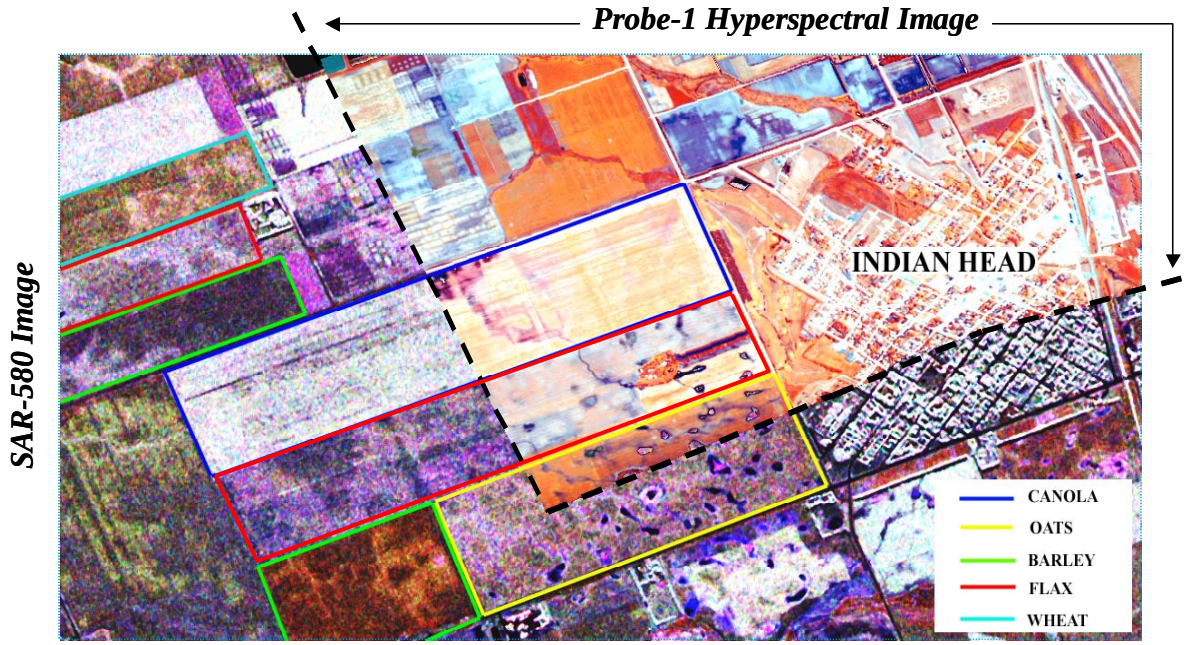

Figure 3.1.3-1 Probe-1 hyperspectral imagery merged with Convair-580 imagery. Both images were acquired over Indian Head, Saskatchewan on June 28, 2000. These data sets were resampled to a 4 m x 5 m resolution and co-registered, after first roll correcting the Probe-1 data. The Probe-1 bands displayed are R=722 nm, G=553 nm and B=491 nm. The Convair-580 RGB was created with R= HH, G=HV and B=VV. The image processing was completed by the Aerospace Radar and Navigation Section of Defence Research and Development Canada (DRDC Ottawa), and this image example provided to CCRS courtesy of DRDC Ottawa.

A number of studies have documented the advantages of combining optical and radar data for crop classification. Rosenthal and Blanchard (1984) reported that crop classification improved almost 20% when data from both radar and visible infrared sensors were combined, while Brisco *et al*. (1989) found that classification improved by 25%. Landsat TM identified summer fallow fields more accurately than the C-HH SAR, but the SAR data classified pea and lentil crops more accurately. Brisco and Brown (1995) used two dates of Landsat TM (May and July) and four dates of C-HH SAR imagery (May, June, July and August) to classify crop type. Using two TM channels from the July acquisition and two C-HH images (July and August) an overall classification accuracy of 85% was achieved. This compared to an accuracy of 74% using all four SAR images and 79% using all channels of the July TM image. The optical data were superior for separating summer fallow from grain classes, but the SAR data was better at separating canola crops.

Fusion of Information Products Derived from SAR and Optical Sensors

Although optical and radar data can be fused prior to information extraction, it is also possible to derive information products from each data set and to then combine these products in models for use in decision-making. Visible, infrared and microwave wavelengths are sensitive to very different soil and crop characteristics. Microwaves respond to the large-scale structure of the crops (size, shape and orientation of leaves, stalks, and fruit) and the dielectric properties of the crop canopy. Crop structure and plant water content vary as a

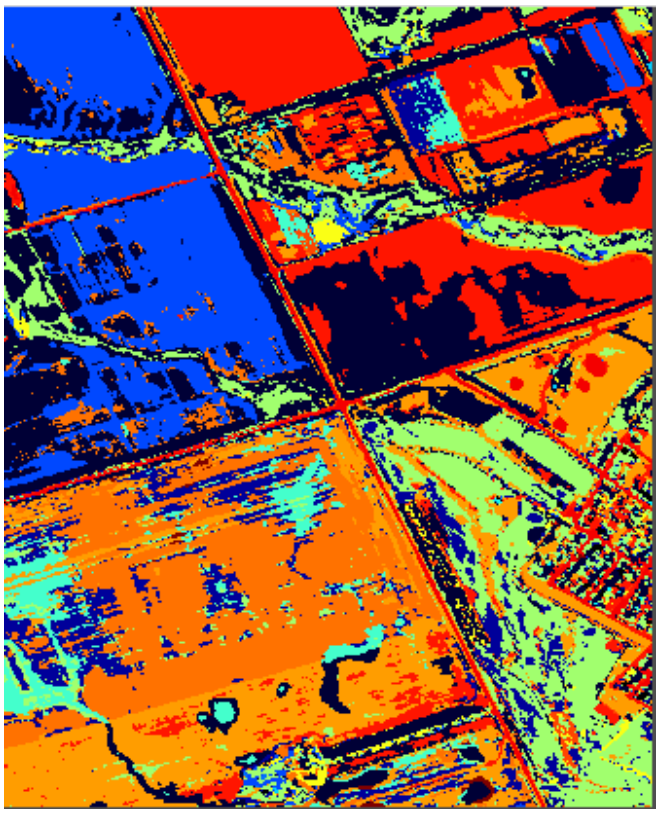

Map of the dominant endmembers derived from spectral unmixing of Probe-1 hyperspectral image
(a)

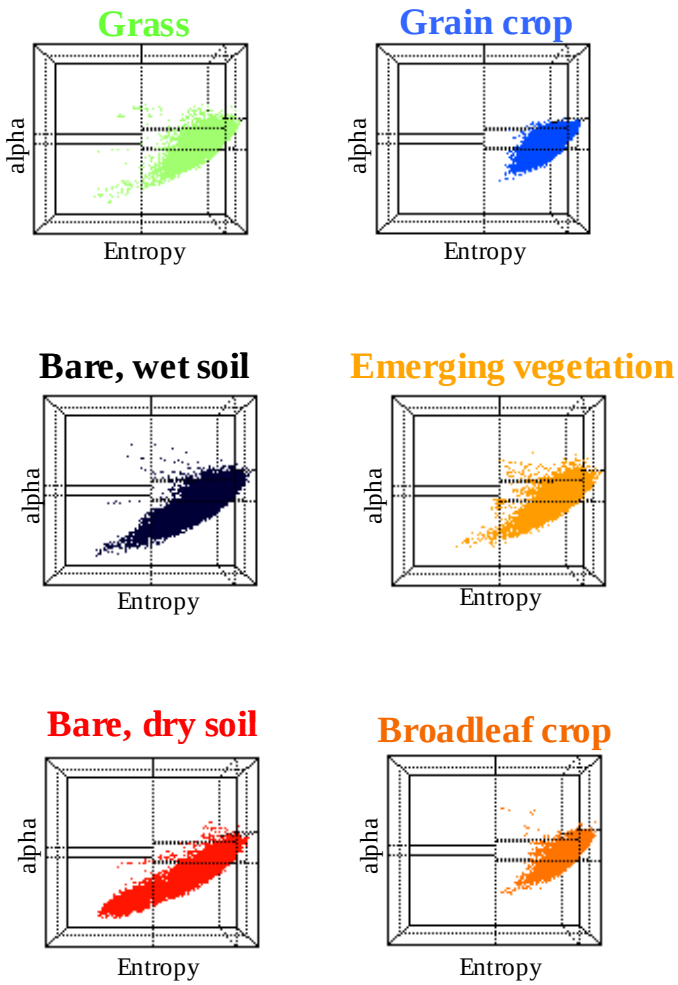

Representation of endmembers under Cloude's decomposition
(b)

Figure 3.1.3-2 (a-b) Scattering mechanisms identified from the Convair-580 imagery plotted as a function of endmembers derived from Probe-1 hyperspectral imagery. Both the Probe-1 imagery and SAR imagery were acquired over Indian Head, Saskatchewan on June 28, 2000. Spectral unmixing was performed on the hyperspectral data and this produced a number of endmember fractions. (**a**) The dominant endmembers for each pixel; (**b**) Alpha and entropy values derived from the SAR data for the regions under each endmember. The image processing and information extraction was completed by Lockheed Martin Canada. The derived endmember fraction map and decomposition plots were provided to CCRS courtesy of Lockheed Martin.

function of crop type, growth stage and crop condition. Reflectance in the visible-infrared spectral region depends primarily on the plant pigmentation and internal leaf structure. Thus crop information derived from optical and radar sensors should be considered as complementary.

The two map products in Figure 3.1.2-1 help to demonstrate the complementarity of information derived from optical and radar sensors. As described in section 3.1.2, the classified map produced from the SAR imagery delineates zones where crop height and density varied as a result of differences in soil properties. In Figure 3.1.2-1(b) an Ikonos image acquired on the same day as the SAR image was used to derive a map of NDVI (Normalized Difference Vegetation Index). NDVI maps indicate general crop condition. Higher NDVI values are generally associated with crops that are healthier or with crops that have a greater accumulation of biomass (higher and denser). This example suggests that optical imagery provides more detailed information on the condition of broadleaf crops like canola and peas. However, the SAR image clearly defines zones of wheat productivity that are not always obvious on the NDVI map.

Combining information products from several sources can also be of use during image interpretation. In Figure 3.1.3-2, Lockheed Martin Canada applied spectral unmixing to a Probe-1 hyperspectral image acquired over Indian Head, Saskatchewan. In this map, the dominant endmember in each pixel is presented. These endmembers included four classes of vegetation (grass, small grains, emerging vegetation and broadleaf (canola)) and two classes of bare soil (wet and dry). From the Convair-580 polarimetric image acquired on the same day, the Cloude decomposition (alpha and entropy) values are plotted for each endmember. The response recorded by a SAR sensor is often a result of a mixture of scattering mechanisms and in general, several types of sources and scattering mechanisms are simultaneously present in backscatter from one target. These Cloude decomposition plots indicate that surface scattering dominates bare soil. For grass and emerging vegetation, scattering comes from both surface scattering as well as some scattering within the vegetation. For small grain and broadleaf (canola) crops, most of the scattering originates within the vegetation volume.

In an approach to combine image products, Smith *et al*. (1995) and McNairn *et al*. (1998) proposed using decision trees that incorporated both optical and SAR image products. These studies suggested taking this approach for land cover and conservation tillage mapping. Smith *et al*. (1995) identified a spring TM image for mapping perennial versus annual crops. Annual cereals, oilseeds and fallow could then be distinguished using summer TM imagery. SAR is used in the fall in order to map tillage practices, since radar backscatter is correlated with surface roughness.

Erosion models such as the Revised Universal Soil Loss Equation are used to predict soil erosion risk and to determine the reduction in soil loss from improved land management practises. This model uses information on rainfall, soil characteristics, slope length and steepness, as well as soil management practices to estimate soil loss (tonnes per hectare). To provide accurate estimates requires reliable and up-to-date inputs on management practices, which are very dynamic over time, and which vary from field to field. McNairn *et al*. (1998) proposed a decision tree approach that used optical and SAR imagery for mapping soil tillage and crop residue. Tilling the soil increases the risk of erosion. Because backscatter is sensitive to soil roughness, radar imagery can be used to determine if (and when) fields have been tilled or if they have been left in no-till. Optical sensors that acquire spectral information in the short-wave infrared are well suited for providing the information

required on percent crop cover (Bannari *et al*., 2000). Residue left on the soil surface reduces the risk of wind and water erosion. These maps of tillage and residue, derived from optical and radar imagery provide information on management practices often missing in erosion estimates. Including this management information can significantly improve estimates of soil loss at the field and the watershed scales.

3.2 Cartography

3.2.1 Maritime boundary mapping

No nation can fully exercise its sovereign rights to living and non-living resources in adjoining seas and oceans without accurate knowledge of its maritime boundaries. This query to sovereignty explains the significant interest countries attach to the mapping of their borders at sea.

The outer limits of maritime jurisdictions such as the Exclusive Economic Zone (EEZ) are defined in terms of distances from the baselines of the Territorial Sea. In turn, these baselines are defined as straight lines joining headlands and islands or discrete points, such as drying rocks. Hence, reliable identification and positioning of the most seaward islands and rocks is a prerequisite for the establishment of precise maritime boundaries. Traditional methods for the mapping of these features typically include aerial surveys. However, the costs associated with such surveys can be prohibitive for complete mapping of extensive and isolated areas.

Scientists at the Canada Centre for Remote Sensing, on request of and in partnership with the Canadian Hydrographic Service (CHS), have applied RADARSAT-1 Fine mode data to map the islets and rocks as found along the North coast of Labrador. In 1997, the CHS surveyed this particular area for the presence of such features by means of visual observation from a helicopter. The RADARSAT-1 data studied were acquired during low tide conditions in August and September of 2000 and processed to images with a pixel spacing of 3.125 m by 3.125 m. Joint analysis of images of two or more dates was implemented to minimise the chance of confusion between rocks and rock look-alikes, that is, icebergs.

Figure 3.2.1-1(a) shows a section of the North coast of Labrador as imaged by RADARSAT-1 on 20 September 2000. The overlaid stars mark the GPS positions of rocks surveyed by the CHS in July and August of 1997. Figures 3.2.1-1(b) and 3.2.1-1(c) show two-date colour composites comprised of RADARSAT-1 Fine mode images acquired on 3 September 2000 (in green) and 20 September 2000 (in blue). The feature in Figure 3.2.1-1(b) is clearly imaged on both dates and represents the rock shown in the corresponding photograph (Figure 3.2.1-1(d)). In contrast, the feature in Figure 3.2.1-1(c) is imaged on September 20 only. This indicates that the feature observed is an iceberg rather than a rock.

Through visual interpretation of the RADARSAT-1 data, 19 out of 22 surveyed rocks and islets could be confidently identified. The average offset between the recorded image positions and 1997 GPS positions (accuracy ± 100 m) was less than 150 m. Hence, it can be concluded that RADARSAT-1 images are a good source of information for supporting maritime boundaries definition. Moreover, mapping approaches that make use of RADARSAT data are likely to be more cost-effective than those approaches that involve the deployment of airborne platforms.

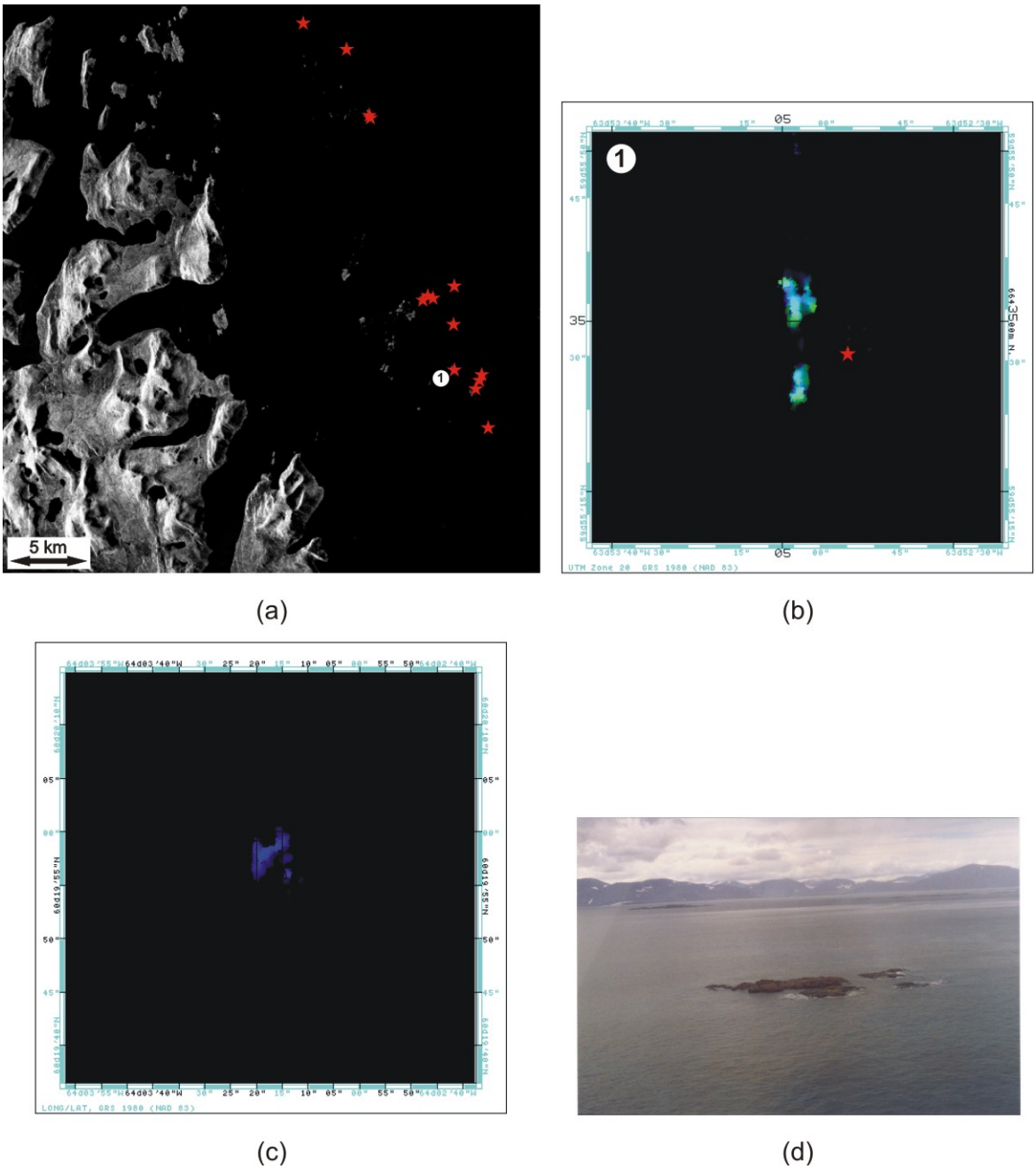

Figure 3.2.1-1 (a-d) North coast of Labrador imaged by RADARSAT-1 (**a**) Fine mode image subset acquired on 2000-09-20; the overlaid stars mark the GPS positions of rocks surveyed by the CHS in 1997 (**b**) two-date colour composite comprised of Fine mode images acquired on 2000-09-03 (in green) and 2000-09-20 (in blue); the feature conceived was clearly imaged on both dates and represents the rock shown in the corresponding photograph in (d) (**c**) the feature conceived in this two-date colour composite was imaged on the second date (2000-09-20) only and may hence be concluded to represent an iceberg.

RADARSAT-2 can be expected to offer more potential for maritime boundary mapping than RADARSAT-1. Images acquired in the Ultra-Fine resolution mode will enable the mapping of smaller rocks and islets. The selective look direction capability will facilitate the scheduling of acquisitions during low tide conditions. Improved orbit control will allow for the positioning of features within < 100 m of their true geographic location (after processing, without ground control points).

3.2.2 Moving object detection

RADARSAT-2 has been designed with an experimental, motion measurement mode known as the Moving Object Detection EXperiment (MODEX). This mode has been specified and funded by the Department of National Defence (DND) and will be used to investigate the measurement of vehicle and natural surface velocities from space based radar data. The RADARSAT-2 antenna is an active array that has dual polarized (H and V) patch radiators on two wings that are extended along the direction of flight to form the 1.5 m x 15 m aperture. For MODEX investigations the radar can transmit from the whole antenna and receive signals from each of the two wings (apertures) or can alternately transmit from each aperture and receive on both. By spatially registering the raw SAR data from each of the two apertures to correspond to times where the radar observed the scene from the same point in space, displacements of scene elements that move consistently over the duration of a SAR aperture can be measured down to fractions of a wavelength as local phase shifts. The detection of moving objects and the measurement of their radial velocity is, thus, the detection and measurement of scene changes over times corresponding to the aperture displacement time (approximately 1 ms for RADARSAT-2).

Processing Concepts

Object motion can be extracted from the two channel SAR data using SAR Ground Moving Target Indication (GMTI) techniques: Along-Track Interferometry (SAR ATI) or Displaced Phase Centre Antenna (SAR DPCA) (Thompson and Livingstone, 2000) or by applying a limited form of Space-Time Adaptive Processing (STAP) to the frequency domain representation of the data.

ATI measurements treat the two aperture outputs as interferometer channels and compute the correlation of the scene from one aperture with the complex conjugate of the scene from the other. The correlation yields a complex interferogram in which radar returns from stationary scene elements cluster about the positive real axis of the complex plane. Radar returns from moving objects appear outside of the real-axis cluster along constant-phase (constant velocity) radials. DPCA measurements subtract the images from the two apertures to null the stationary scene to the radar noise level and only moving objects remain in the difference scene. STAP measurements use the spatial and temporal diversity of the measurement set to construct a weighting function that can be used to null the stationary scene. When range-compressed data is processed in the azimuth frequency domain, moving objects can be extracted as spectral lines above a residual noise background.

Although all three approaches work with the same data and are nominally equivalent, there are differences that enhance the applicability of each in certain circumstances. STAP analysis does not require matched filters and works well to detect fast-moving objects. Weak, slow objects are suppressed along with the stationary scene. STAP processing requires extra effort to extract precise object locations. The SAR GMTI approaches require

filters accurately matched to the radial velocity of the moving object to yield precise measurement results but provide very good position information. Both DPCA and ATI analyses have equivalent performance for fast and medium speed moving objects. ATI analysis has better detection sensitivity for weak, slowly moving objects (Chiu and Livingstone, 2002). A discussion of SAR ATI and DPCA can be found in Livingstone *et al.* (2002).

Measurable Speed Ranges

In the MODEX data, moving objects displace a fraction of a wavelength over the aperture displacement time. When the wavelength fraction is small (slowly moving objects) the problem becomes one of distinguishing the object phase shift from the phase noise (radar system plus scene internal motion) of the nominally stationary world. When object dimensions are of the same order as the radar resolution cell size, the phase noise of the single-look data determines the minimum detectable velocity (MDV). For an object whose radar cross-section is 20 m^2 the RADARSAT-2 MDV is expected to be 6.2 m s^{-1} when the false alarm rate is 10^{-6} (Thompson and Livingstone, 2000). Smaller allowed false-alarm rates result in smaller MDV values. When the object is much larger than a resolution cell (e.g. an ocean current system) coherent integration can be used to suppress the phase noise at the cost of increasing the size of the resolution cell. Rough calculations suggest that coherent integration of RADARSAT-2 MODEX data to approximately 100 x 100 m (10000 m^2) cells should allow current measurements with MDVs of the order of 0.25 m s^{-1}. The upper speed range measurable with MODEX data is determined by the smallest non-resolvable displacement ambiguity (displacement of Npi radians in phase) and the lowest unresolved azimuth ambiguity. For RADARSAT-2, the first displacement ambiguity, the directional ambiguity that occurs at an object radial velocity of 55.5 m s^{-1}. For a sampling rate (pulse repetition frequency) of 2000 Hz, the first azimuth ambiguity and the absolute velocity ambiguity occur when the radial velocity of the measured object exceeds 111 m s^{-1}. It is expected that the first two ambiguities can be resolved with absolute displacement measurements in many cases.

Development of the RADARSAT-2 MODEX Processing Facility

When the moving objects of interest are vehicles, the desired velocity measurements in a MODEX scene are sparse. Any useful processor designed to extract and measure vehicle velocities must automatically detect the moving vehicles, measure their radial velocities and determine their spatial positions. A series of experiments is being conducted with an airborne ATI radar on a Convair-580 aircraft (system developed by CCRS; Livingstone *et al.,* 1995) to develop and test detection, measurement and measurement optimisation algorithms suitable for automatic processing systems. The first of these experiments was conducted in 1999 and is reported in Livingstone *et al.* (2002). Results show that automatic extraction of vehicle measurements from MODEX-like airborne data is feasible. Investigations of the phase properties of ATI processed moving objects have shown that a two-parameter phase probability density function (PDF) based on a hypergeometric function is robust for objects moving in a natural terrain background and that the parameters needed to define the PDF can be extracted from the ATI interferogram (Gierull, 2001; Gierull and Sikaneta, 2002; Sikaneta and Gierull, 2002). Further work by Sikaneta (2002) has shown that the ATI phase PDF is robust for extremely heterogeneous scenes such as urban areas. The phase PDF forms the basis for a moving-object Constant False Alarm Rate (CFAR) detector (Gierull, 2002). The problem of constructing an automatic processing/estimation system for arbitrary moving objects is under investigation and the resulting algorithm is expected to have STAP and ATI components in addition to an adaptive CFAR algorithm. A precision signal simulator developed by Sicom Inc. in 1998 is being used to extend the

results from the airborne experiments to the RADARSAT-2 geometry and radar properties (Chiu, 2000; Chiu and Livingstone, 2001; Chiu, 2002). The problem of extracting moving vessels from MODEX ocean data remains to be investigated at the time of writing.

Data Availability
MODEX has been funded by DND to further defence research interests. The data policy that governs its access is being submitted to Parliament for approval. At the time of writing, the data is considered protected and will only be releasable to government departments. Data release will require DND approval.

3.3 Disaster Management

The urgency associated with disaster management dictates that applications in this field require instantaneous and frequent image acquisition. RADARSAT-2's selective look direction capability will (on average) shorten the response time and increase the revisit frequency in all but the most northerly regions on Earth. In addition, RADARSAT-2's multi-polarization and full polarimetric modes offer improved potential for disaster management applications. In this section we present results pertaining to the use of polarimetric data for oil spill and search and rescue applications.

3.3.1 Oil spills

Annually more than 100 million liters of hydrocarbon are spilled in the world's oceans. Illegal dumping associated with tank cleaning accounts for three quarters of the amount discharged (Wismann, 1993). To mitigate this problem an effective monitoring tool needs to be developed. Recommendations of the American Coast Guard ask for an information acquisition system that can operate independent of solar and atmospheric conditions. Moreover, the information acquired must cover a large area (≥ 52,000 km^2) and allow for an evaluation of the slick type (natural or human origin) and the spilled volume or, as a minimum, the variability in the slick's thickness (Lambert *et al.,* 1992). SLAR and SAR systems have proved their efficiency in terms of climatic independence, coverage, slick/water discrimination and slick surface estimation (Solberg *et al*., 1999; Espedal and Wahl, 1999). In the context of RADARSAT-2 it is of interest to discuss what oil spill properties can be derived from C-band polarimetric SAR images.

The Small Perturbation Model (Ulaby *et al*., 1986), equation 3.3.1-1, is frequently used in the analysis of oil slicks in SAR images. This model expresses the backscattering coefficient σ^o as the product of a field factor coefficient $[\, k^2 * \cos^4\theta * |\, \alpha\,(k_r,\ \varepsilon, \theta,\ pp)\,|^2\,]$ and density spectrum term $\Psi\,(k_r\,, \theta, \phi, U)$. α is the modified Fresnel coefficient, i.e. the proportion of energy reflected by the surface, which includes the effect of surface undulation. Ψ corresponds to the density spectrum of the surface waves at the wave number k.

$$\sigma^o = 8 * [\, k^2 * \cos^4\theta * |\, \alpha\,(k_r,\ \varepsilon,\ \theta,\ pp)\,|^2\,] * \Psi(k_r,\ \theta,\ \phi,\ U) \qquad (3.3.1\text{-}1)$$

Both terms are a function of the radar wave number ($k_r = 2*\pi/\lambda_r$) and the incident angle of the radar wave (θ). The field factor coefficient is also a function of the surface dielectric constant (ε) and the polarization of reception and transmission of the radar wave (pp, for p = H or V, for Horizontal and Vertical). The density spectrum is also dependent on wind speed

(U) and the relative azimuth (ϕ), that is, the angle between the plane of incidence of the radar waves and the direction of propagation of the ocean waves. The radar signal is strongly influenced by the diffusion elements of a size similar to its wavelength, λ_r. Modulation of the backscattering coefficient is thus related to the distribution of the capillary waves at the ocean surface. Capillary waves are the spontaneous result of the interaction of the wind with the surface and their wavelength is of the order of $\lambda_{cw} \approx 1.5$ cm. One SAR resolution cell will cover several of these diffusion elements. The total power received is the resultant of the superposition of the waves backscattered by each of these elements. If the received waves are in phase, then the interference is constructive and the received energy maximum. This is Bragg's principle of constructive interference. Equation 3.3.1-1 is valid only for angles of incidence ranging from 20° to 60°. For $\theta < 20^o$, specular reflection dominates over Bragg scattering. For $\theta > 60^o$, it is necessary to account for the shadowing effect caused by the waves of larger amplitudes (amplitude > 0.5 m). The presence of oil on the ocean surface affects both terms of equation 3.3.1-1. Firstly, the density spectrum term is reduced due to the dampening effect of the oil on the capillary waves. Secondly, the oil modifies the surface dielectric constant (less effect for thin oil layers $\delta < 1$ mm).

To setup a campaign for the collection of radar data over ocean slicks is both expensive and constrained by environmental laws. CCRS was involved in an oil detection experiment with an airborne scatterometer and a SAR about 20 years ago (Singh *et al.*, 1986). The data discussed in this text were acquired during two Shuttle Imaging Radar missions in 1994 (SIR-C). The experimental setup was in the hands of German and Japanese scientists (Gade *et al.*, 1998a). During the April experiment, 200 liters of Oleyl alcohol (OLA) were applied over the ocean. OLA is widely used for this kind of experiment because its damping properties resemble those of biologic oil slicks (Alpers and Hühnerfuss, 1989). During the October experiment four different surfactants were applied, that is, IFO 180 (crude oil), OLA, Oleic acid methyl ester (OLME) and two types of triolein (pure and dissolved with n-hexane solvent). The SIR-C data, used in this study, have been acquired in the Quad-pol and Dual-pol configuration for L- and C-band. The incident angle, at the slick location, varies from 21° to 47°. Corresponding environmental ground reference data include wind speed at 10 m altitude (U_{10}) and relative wind direction ($\Delta\phi$). Examples of backscattering coefficients measured over ocean and slick are shown in Table 3.3.1-1.

The ocean - oil backscatter ratio is the most frequently used variable for the characterization of oil slicks. This ratio, which is also referred to as the damping ratio, has the advantage to

Table 3.3.1-1 Backscattering coefficients over oleyl alcohol and ocean surfaces, for the polarizations HH, HV and VV. Sub areas 1, 2, and 3 correspond to smaller patches inside the slick. SIR-C data acquired, at $\theta = 21^0$, over North of Japan, in C-Band, April 15, 1994.

Surfaces	**HH [dB]**	**HV [dB]**	**VV [dB]**
Oleyl alcohol	-6.8	-33.08	-6.74
Sub area 1	-7.26	-33.1	-7.11
Sub area 2	-6.99	-33.05	-6.71
Sub area 3	-7.44	-33.65	-7.29
Ocean	-3.4	-29.60	-3.11

be independent of the dielectric properties of the surface and the orientation of the wind. The value of this ratio is uniquely related to the contrast between the surface spectral density of ocean and surfactant surfaces, at the Bragg wave number (K_B). It has been shown in literature that the damping ratio is more important in C-band than in L-band. This can be explained from the fact the wavelengths of capillary waves and C-band microwaves are of the same order (Singh *et al.*, 1986; Gade *et al.,* 1998 a, b). Figure 3.3.1-1 shows the C-band damping ratios for different polarimetric parameters computed for the OLA spill as imaged by SIR-C on April 15, 1994 (Touzi and Charbonneau, 2002). The horizontal bars in this figure correspond to the detection threshold, which is the ratio of the backscatter level of clean ocean and the noise level. For most polarimetric parameters this threshold is not visible because it exceeds the 5 dB range of the y-axis. Ratios in excess of this threshold, i.e. for HV, Cupmin and Vumin, are not meaningful.

The VV damping ratio can be seen to exceed the HH damping ratio by approximately 0.5 dB. The damping contrasts for the Right-Right (RR) and Left-Left (LL) circular polarizations are significantly lower than those for the linear polarizations. This can be explained from the nature of the surface scattering process. High impedance surfaces, like the water, reverse the rotation angle of the incident signal ($\chi \longrightarrow -\chi$). As a result, the RR and LL return signals for ocean surfaces are weak. This in turn reduces the sensitivity of these polarizations to changes in surface roughness. The RR and LL damping ratios for other spill types were often found to be below the detection threshold. For the most part, the different polarization power parameters provide the same information. Roughly the same

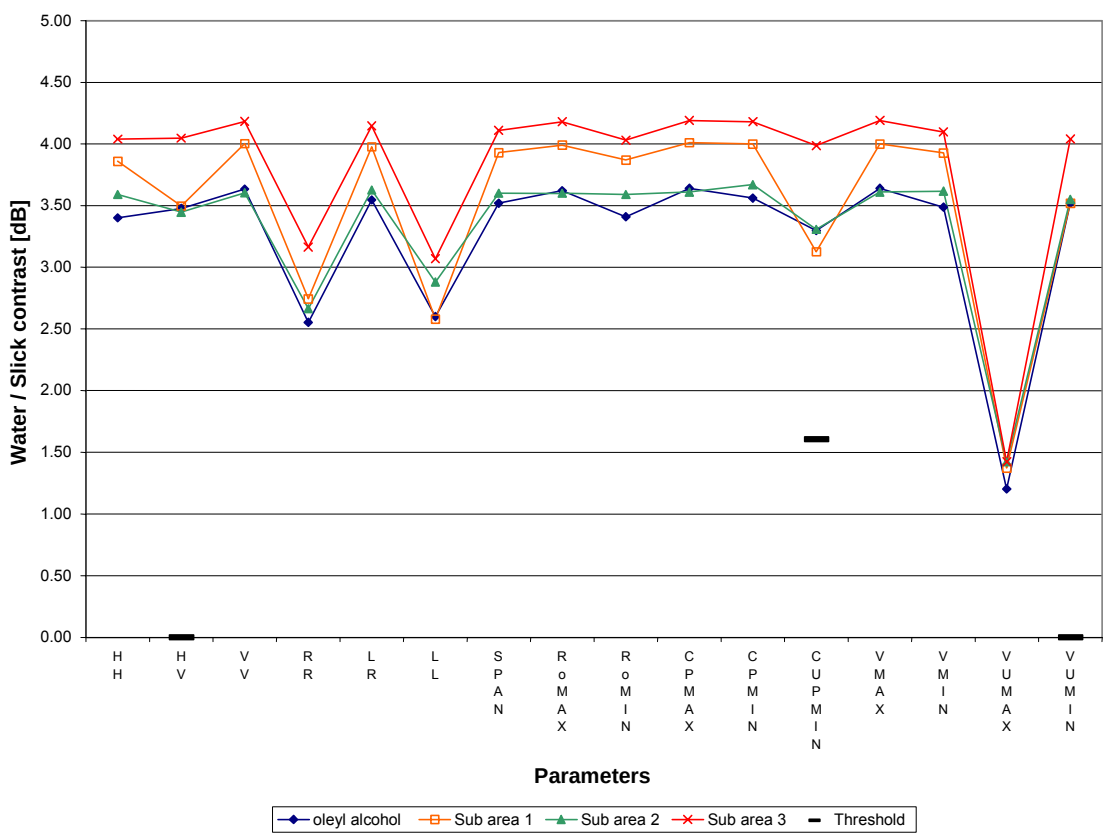

Figure 3.3.1-1 Damping ratio σ^o_o / σ^0_s between oleyl alcohol and ocean surface, for different polarimetric parameters. Sub areas 1, 2, and 3 correspond to smaller patches inside the slick. SIR-C data acquired over North of Japan, in C-Band, April 15, 1994.

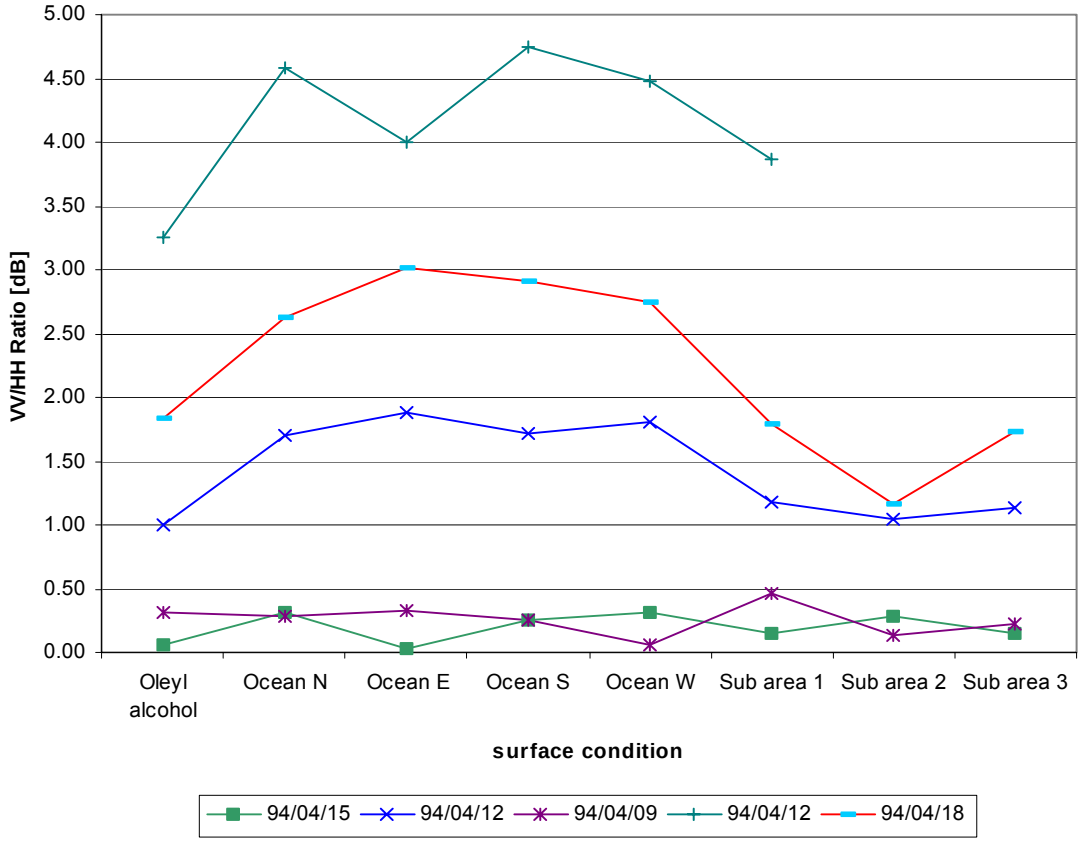

Figure 3.3.1-2 Polarization ratio σ^o_{HH} / σ^o_{VV} for different dates of SIR-C acquisitions (C-band) over Oleyl alcohol slicks. Sub areas 1, 2, and 3 correspond to smaller patches inside the slick, and Ocean N, E, S, W corresponds to the surrounding ocean polarization ratio on the North, East, South and West sides of the slick.

water-OLA contrast ratios were obtained for HH, VV, LR, SPAN, Romin, Romax, Cpmax, Cpmin, Vmax and Vmin. Where Romin, Romax are the extremas of the wave intensity; Cpmax, Cpmin are the extremas of the completely polarized wave intensity; and Vmax, Vmin are extremas of the matched power (Touzi *et al.*, 1992). Typically, the unpolarized variables (Cupmin, Vumax and Vumin; where Cupmin is the minimum power of completely unpolarized component; Vumax and Vumin are the extremas of cross-matched power) display low contrast ratios. This illustrates that the presence of a surfactant has little effect on the degree of polarization of the microwave signal. The signals from both ocean and OLA were found to have a high degree of polarization, i.e. ranging from 0.94 to 0.99. Consequently, it may be concluded that the computed unpolarized variables are of little value for the characterization of thin oil spills.

The Small Perturbation Model (SPM) can be shown to predict that the VV/HH backscatter ratio is of little value for the analysis of oil spills in radar mages. Ratioing of the two backscatters annuls the effect of the density spectrum term since the spectral densities for HH and VV are identical. The only effect remaining is embodied by the polarization dependent modified Fresnel coefficient. The variable governing that coefficient is the

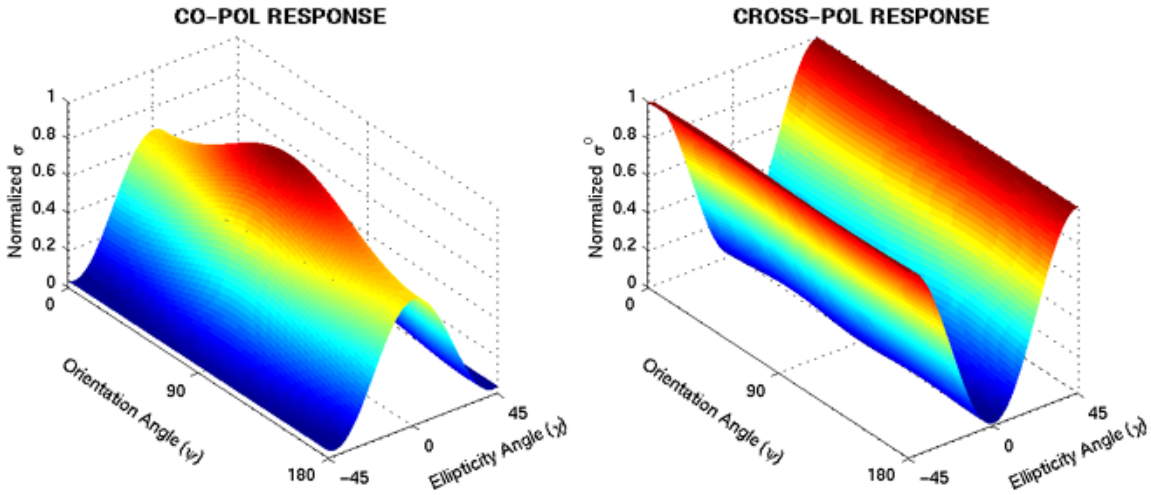

a)

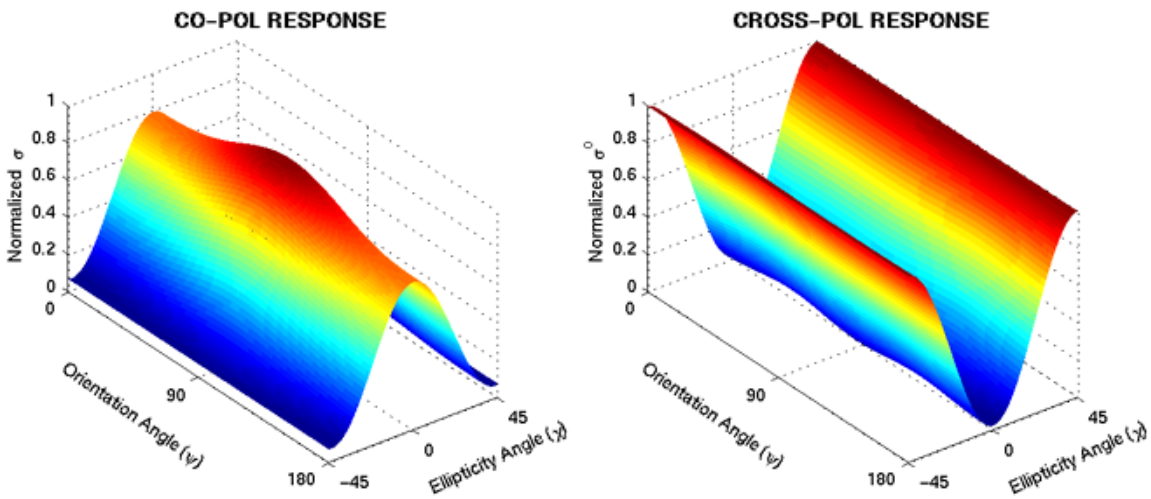

b)

Figure 3.3.1-3 (a-b) Polarimetric signatures for the SIR-C, C-band April 16, 1994 acquisition, North of Japan. **a**) Ocean North side; **b**) Oleyl alcohol (OLA), full area.

dielectric constant of the observed surface. The dielectric constants of the ocean and oil slicks are a function of the water temperature and the slick thickness, respectively. Natural surfactant films and older (dispersed) mineral oil slicks have thicknesses that are small (about 1 μm) compared to the wavelength of the incident microwaves. Moreover, the dielectric constant of oil ($\varepsilon \approx 10$) is much lower than that of salt water ($\varepsilon = 60 - 45j$). Hence, the dielectric constant of an oil slick on water is not significantly different from the dielectric constant of clean water. Based on the SPM model, the ratio of the VV/HH backscatter can therefore be expected to be insensitive to the presence of oil on water. However, the results presented in Figure 3.3.1-2 show a difference in the VV/HH backscatter ratio for OLA and clean water of up to 1.5 dB. The limited thickness of the OLA spill (about 1 μm) rules out a significant effect of the oil on the dielectric constant. The observed difference in the VV/HH ratio therefore suggests that the SPM is not the most appropriate model for analysis of oil slicks imaged by multi-polarized and full polarimetric SAR systems. A two-scale model that

accounts for the scattering behaviour of longer gravity waves is likely to be more appropriate for such analysis. The data from RADARSAT-2 will facilitate new and more conclusive research on this topic.

Figures 3.3.1-3a and 3.3.1-3b show typical co- and cross-polarized signatures for ocean and OLA, respectively. The shapes and pedestals of the OLA signatures do not deviate significantly from those for clean ocean water. The shape of the signatures is clearly indicative of a surface scattering interaction process. The low pedestals confirm that volume scattering is negligible. Results from analysis of the October data show that, at high wind speeds and high incidence angles, oils with different viscosities generate nearly identical polarization signatures. Unfortunately, all of the slicks imaged by SIR-C are very thin. Hence, the question of whether or not polarization signatures of thicker slicks ($\geq$ 1 mm) will be identifiable based on volumetric and multi-layer scattering remains unanswered.

The presented preliminary results seem to indicate that the capability to acquire multi-polarized or full polarimetric images will add little to the potential of SAR to support the detection and monitoring of oil slicks. However, we are of the opinion that the current lack of polarimetric SAR observations over actual oil spills (with different thicknesses) prohibits comprehensive studies. Hence, the acquisition and analysis of full polarimetric SAR data for oil spills of opportunity is recommended.

3.3.2 Search and Rescue

As described in van der Sanden and Ross (2001), the use of Synthetic Aperture Radar (SAR) systems to assist Search and Rescue SAR, in particular in Canada's northern regions, is being studied at CCRS. Recent work has focussed on continuing development and evaluation of techniques for use with polarimetric imagery to determine possible locations of crashed aircraft.

Polarimetry

The signatures of man-made targets in polarimetric SAR images are expected to differ from those of the adjacent natural areas in which they are found. This has been found to work for airplanes where the dihedrals formed at the tail section or between the wings and the fuselage produce target signatures which may be detected in SAR imagery (*Jackson et al.,* 1998). Three methodologies that can be used to locate such dihedral targets in polarimetric data, originally applied in the work of the SAR^2 project at the National Aeronautics and Space Administration – Goddard Space Flight Center (NASA-GSFC) (Jackson *et al.,* 1997, 1998; Jackson and Rais, 1999; Rais *et al.,* 2000) have been examined at CCRS. These include the Polarimetric Whitening Filter (PWF) (Novak *et al.,* 1993), the Cameron Decomposition (Cameron *et al.,* 1996), and the Even Bounce Analysis (Evans *et al.,* 1988).

A major concern in Search and Rescue is the minimization of the number of false targets. Such false alarms arise in two major ways: firstly, man-made targets are identified as appearing at a particular location in the image when there are in fact, no man-made targets there. Secondly, man-made targets are correctly identified, however these are not crashed aircraft but other structures. The former must be controlled in the analysis of the data. In a practical situation, any remaining targets would have to be identified and resolved through a visit by Search and Rescue personnel to determine if they are, in fact, the crashed aircraft.

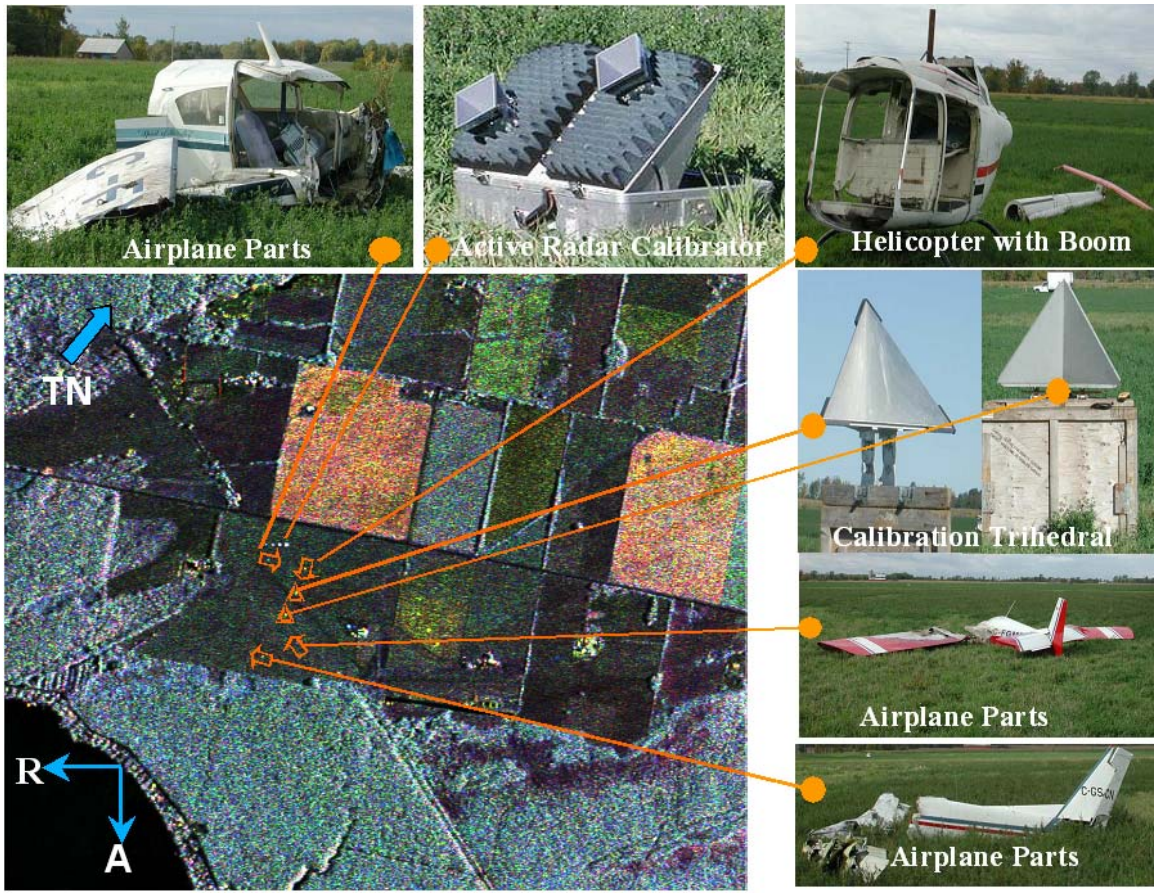

Figure 3.3.2-1 Orillia Test Site. Convair-580 SAR colour image of September 29, 2001 (R: HH, G: VV, B: HV).

In order to minimize the first kind of false alarm rate while detecting man-made targets, an algorithm combining the above three methods is being used. In analyzing the initial results, it was found that other man-made as well as natural features can have similar SAR backscatter characteristics to those of a crashed airplane, usually corresponding to a larger number of samples than a crashed airplane (as was also reported in Jackson *et al.,* 1998). Other false targets can appear in the analysis of radar imagery, but corresponding to fewer samples than would be expected for an airplane. Based on these observations, image morphology and clustering processes are being employed to assist in distinguishing false targets from crashed aircraft.

Test Sites

Orillia Test Site - Data were acquired on September 29, 2001 near Orillia by the Convair-580 SAR (Livingstone *et al.,* 1995; Hawkins *et al.,* 2002*).* Targets included previously crashed aircraft parts and calibration devices. In this experiment, the aircraft parts were positioned at various orientations including the optimal backscattering position, where the heading of the crashed airplane is perpendicular to the look direction of the radar.

All imagery acquired in support of this experiment were processed on the ground (not using the real-time processor onboard the Convair-580). A high-resolution slant range colour image of the area containing the targets is shown as Figure 3.3.2-1 with the targets shown in detail in the insets. Orange arrows indicate the locations of the aircraft targets showing

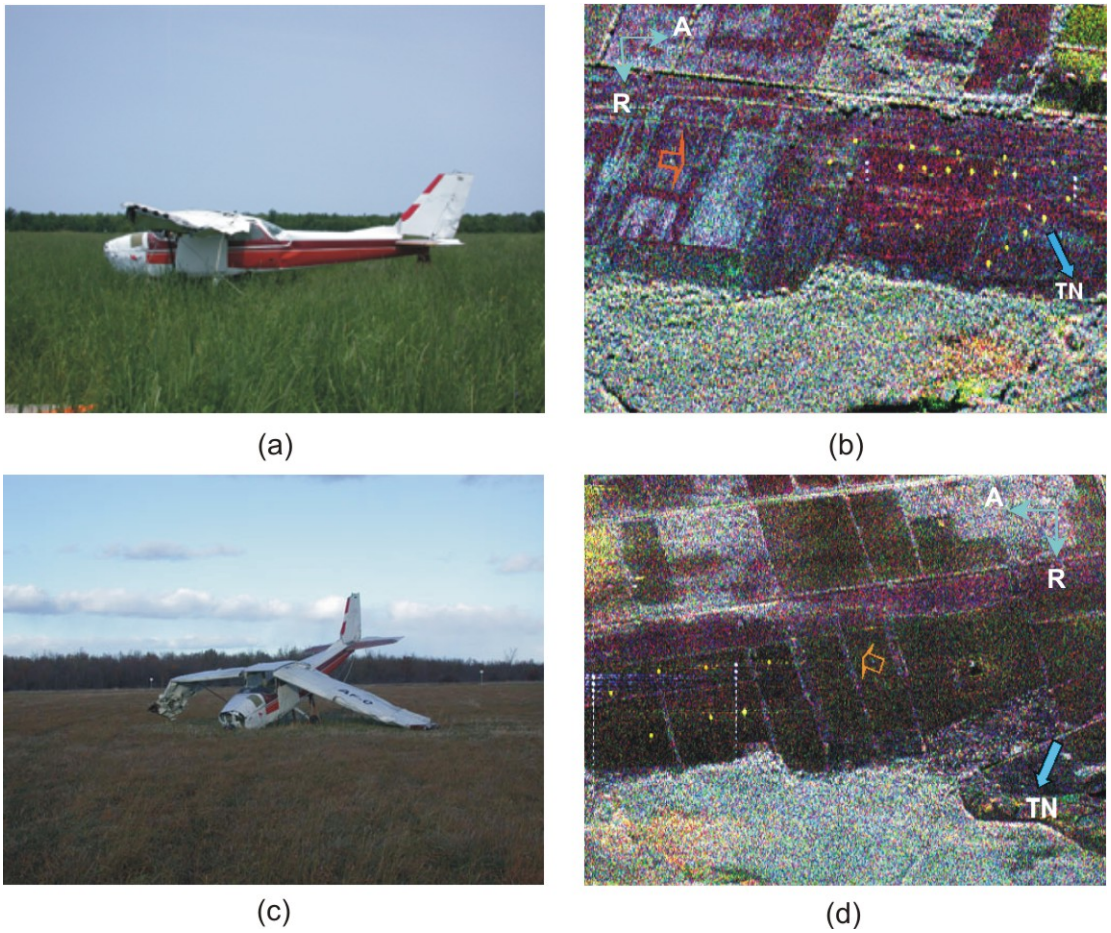

Figure 3.3.2-2 (a-d) Ottawa Test Site (**a**) Approximate ground truth on June 25, 2002. (**b**) Convair-580 image of June 25, 2002 (R:HH, G:VV, B:HV). Orange arrow indicates the "heading" of the plane. (**c**) Ground truth on Nov. 1, 2002. (**d**) Convair-580 image of Nov. 1, 2002.

their approximate "heading". Triangles indicate the locations of the corner reflectors. Note the targets are located within their respective symbols. An Active Radar Calibrator (ARC) is shown at the top of the image.

Ottawa Test Site - A previously crashed aircraft target consisting mainly of a Cessna-172 was acquired during the winter of 2001-2002 and deployed in a field on the outskirts of Ottawa. Acquisition of Convair-580 data has occurred on a number of occasions including two passes on June 25, 2002 and one pass on November 1, 2002. Trihedral corner reflectors, ARCs and the previously crashed aircraft are seen in Figures 3.3.2-2(b) and (d). In Figure 3.3.2-2(b), the heading of the plane (as shown by the arrow) is perpendicular to the look direction of the radar. In Figure 3.3.2-2(d), the plane has been oriented at 30 degrees from the "optimal" position of Figure 3.3.2-2(b).

On visual examination of these SAR images, it is clearly seen that there are differences between the calibration targets, crashed aircraft and the surrounding terrain. The trihedral corner reflectors appear yellow as there is backscatter in the HH and VV transmit-receive polarization combinations, but not in the cross-polarization HV combination. The terrain appears as multiple shades due to significant variations in the backscatter at the various

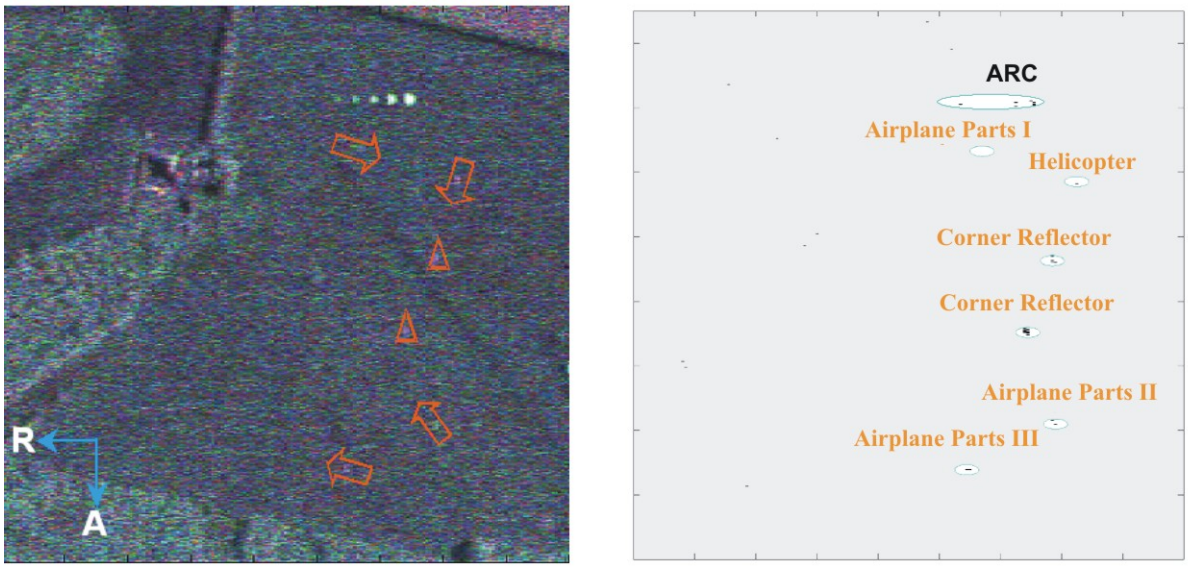

(a) (b)

Figure 3.3.2-3 (a-b) (**a**) Orillia test site Convair-580 image of September 29, 2001 (R:HH, G:VV, B:HV). (**b**) Combined detection result using PWF, Cameron Decomposition and Even Bounce Analysis. Blue ovals indicate locations of the planes, trihedral corner reflectors and ARC.

polarizations. The plane in Figure 3.3.2-2(b), as well as the ARCs in Figures 3.3.2-2(b) and (d), appear white indicating that there is significant backscatter in all three transmit-receive polarization combinations (HH, VV, HV). In contrast, the shade of the crashed aircraft in Figure 3.3.2-2(d) indicates a noticeable difference in the relative backscatter of the different polarization combinations at this orientation of the target.

Polarimetry Experimental Results

The imagery and analysis results for the Orillia test field on September 29, 2001 are presented in Figure 3.3.2-3. The results of Figure 3.3.2-3(b) were obtained by the combination of the three methods. Image samples that correspond to the actual location of a dihedral or narrow diplane are retained as possible locations of crashed aircraft parts. Blue ovals indicate the locations of the plane and calibration targets. Six of the seven targets in the image were detected. Since the signatures of trihedral corner reflectors are in general different from dihedrals and diplanes, the Cameron Decomposition should not identify trihedrals as behaving like dihedrals or narrow diplanes. However, it is believed that such scattering did occur from these two trihedral corner reflectors which were oriented with one of their sides facing the radar.

In Figure 3.3.2-3(b), the airplane target at the top left (Airplane Parts I) was not identified. It is believed that this is due to its “suboptimal” orientation (at a heading of approximately 60 degrees from the optimal position). Although the aircraft parts at the bottom of this figure (Airplane Parts III) were in a similar orientation, they were still detected. On examining this target, it is believed that this is due to a significantly larger dihedral formed by the tail of the target.

The imagery and analysis results for one of the two passes on June 25, 2002 are shown in Figure 3.3.2-4. This result was obtained using the Cameron Decomposition following

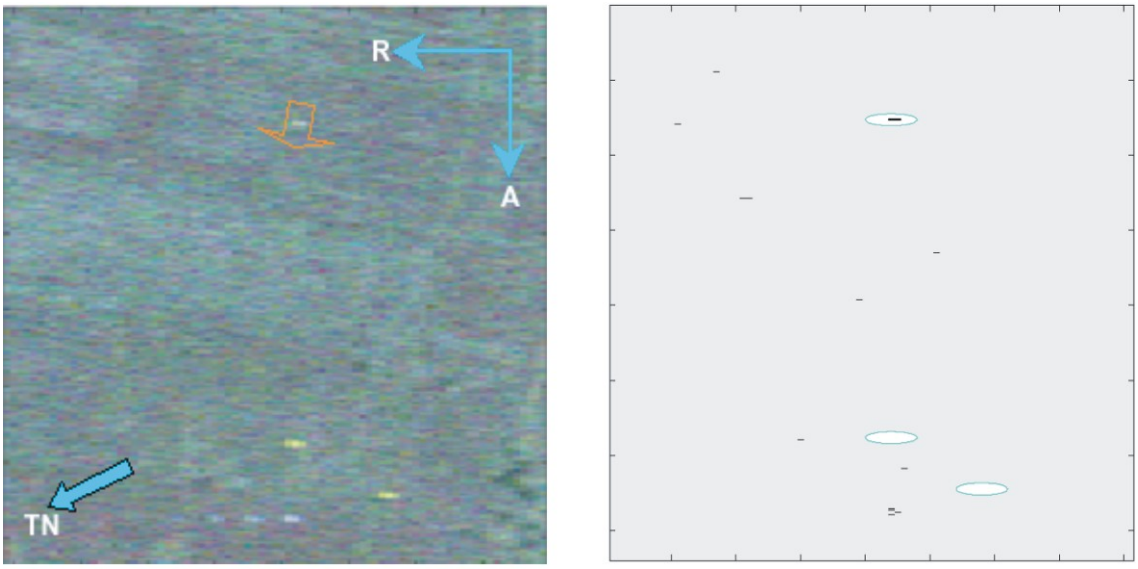

(a) (b)

Figure 3.3.2-4 (a-b) (**a**) Ottawa test site Convair-580 image of June 25, 2002 (R:HH, G:VV, B:HV). (**b**) Detection result using PWF and Cameron Decomposition. Blue ovals indicate locations of the plane and two trihedral corner reflectors.

application of the PWF. It is noted that in this scene there are samples that appear as false targets. Clustering could be used to eliminate all of the false targets visible in this example.

Figure 3.3.2-5 shows the imagery and results for the pass on November 1, 2002. Figure 3.3.2-5(b) shows the result of classification when using the Cameron Decomposition following application of the PWF. The blue oval at the bottom of the figure indicates the location of the plane. Several samples within the oval are classified as dihedrals or narrow diplanes. Figure 3.3.2-5(c) shows the distributions of the z parameters (see Cameron *et al.,* 1996) for these pixels. It can be seen that two of these samples are classified as dihedrals and three of them as narrow diplanes.

Figure 3.3.2-5(d) shows the best detection/false alarm result obtained for these data when the Even Bounce Analysis is added to the results of Figure 3.3.2-5(b) in the combination of the three methods. There is only one false alarm, located at the top right of this figure.

It is noted that the results of Figures 3.3.2-3 and 3.3.2-5 demonstrate the behaviour of the algorithms in a non-optimal orientation of the target with respect to the range direction.

Conclusions

Results using three target detection methods applied to SAR polarimetric data have been described here. The combination of the three methods has been found to generate the best detection results most of the time (i.e. targets were found with the lowest false alarm rates).

The success of these studies continues to indicate the potential use of Synthetic Aperture Radar systems for detection of man-made targets, in particular, aircraft, to assist Search and Rescue in Canada. These results support the work carried out in the studies and results of the SAR^2 Project at NASA–GSFC, applied here to the Canadian context, but restricted here to C-Band systems.

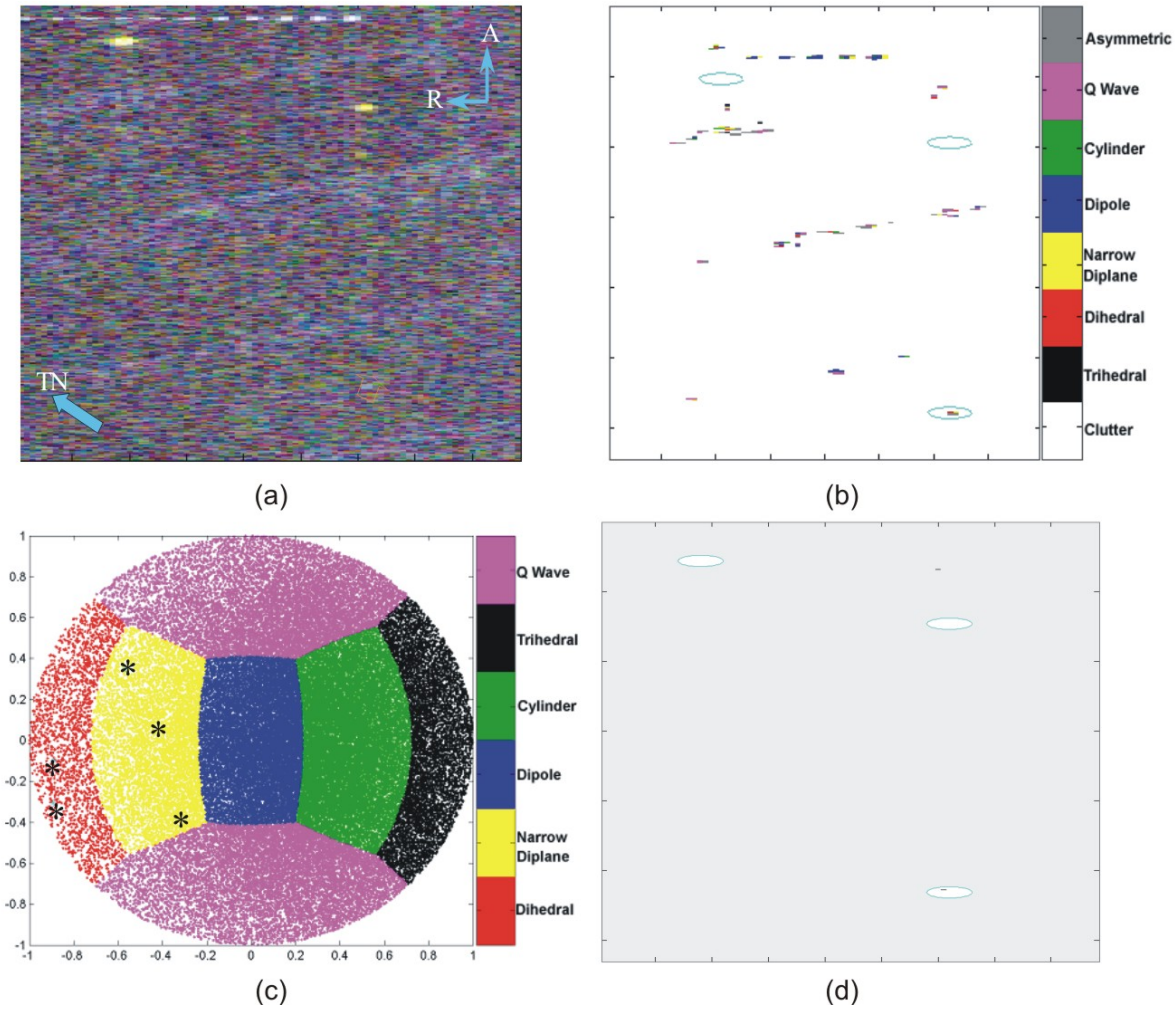

Figure 3.3.2-5 (a-d) (**a**) Ottawa test site image of Nov. 1, 2002 (R:HH, G:VV, B:HV). (**b**) Classification result using PWF and Cameron Decomposition. (**c**) The z parameter distribution of the image in the Cameron Feature Decomposition Circle. The stars indicate the detected symmetrical scatterers at the location of the plane. (**d**) Combined detection result using PWF, Cameron Decomposition and Even Bounce Analysis. Blue ovals indicate locations of the plane and two trihedral corner reflectors.

Significant further development is required to move from these results to an operational capability for detection of crashed aircraft. There will soon be an increase in available spaceborne Synthetic Aperture Radars (including RADARSAT-2) with more complex operating modes. It is hoped that they can be of assistance so that the possibility of saving lives and mitigating the effects of aircraft crashes will thus improve.

Further details are given in Lukowski *et al.,* 2002a, Lukowski and Charbonneau, 2002b, Lukowski *et al*., 2004, Lukowski and Yue, 2003a, and Lukowski and Yue, 2003b.

3.4 Geology

Recent results have shown that RADARSAT-1 C-HH images have provided geologists with useful information for geomorphology, geological structure and rock units (Singhroy and Saint-Jean, 1997, 1999; Singhroy *et al*., 1998; Saint-Jean *et al*., 1999). However, early research related to the capabilities of RADARSAT-2 images for geological mapping has shown that the high resolution stereo aspects of the Ultra-Fine beam mode will improve image interpretation techniques for terrain mapping, and that some lineament orientations are enhanced by cross-polarized images (Saint-Jean *et al*., 1999). Research spanning the last two decades has shown that radar polarimetry can provide specific information on the shape and distribution of scattering elements within a resolution cell, which has potential value for geological mapping (Skriver and Pedersen, 1995). However, in the glaciated vegetated Canadian Shield, where the majority of the mineral deposits of Canada are found, the geological application of polarimetric SAR is not fully understood. Research is now starting and results are very preliminary. In these vegetated areas, the SAR signal only partially penetrates the vegetation canopies, which are strong volume scatterers that commonly exhibit a high cross-polarized component (Zebker *et al*., 1990; Evans *et al*., 1986). Nonetheless, the information obtained from the morphology of the vegetation canopy and its relationship with terrain features is of great value for litho-structural interpretation. In arid areas, where surficial materials and rocks are exposed, Evans *et al*. (1986) have shown that polarimetric SAR images can facilitate lithologic mapping. The purpose of this section is to provide additional techniques that will enhance the uses of RADARSAT-2 images for geological mapping. We focus on high-resolution image fusion techniques for mineral property mapping and monitoring of active landslides using interferometric images.

3.4.1 High-resolution data fusion for mineral exploration

In this section, we report on the capabilities of high-resolution image fusion techniques in support of geological mapping and mineral exploration. This investigation provides evidence that the 3 m high-resolution Ultra-Fine capability of RADARSAT-2, when fused with other high-resolution geophysical data, will improve current image fusion techniques used by exploration companies and geological mapping agencies.

Singhroy (1992, 1996) has developed interpretation techniques for RADARSAT-fused images to facilitate mineral exploration programs in Canada. Mineral exploration companies, geological agencies and consulting firms now use these methods and interpretation guidelines routinely, and as such the Canadian Space Agency has supported several contracts on RADARSAT-1 data fusion techniques to service the Canadian and international mineral and hydrocarbon exploration industry. The technique involves fusing RADARSAT-1 images selectively with vertical gradient magnetic, radiometric, optical and topographic data, thus producing thematic exploration image maps at scales of 1:100 000 for regional exploration and mapping programs. With the availability of the 3 m Ultra-Fine beam mode of RADARSAT-2, together with other high-resolution topographic and geophysical data sources, the image fusion techniques shown in Figures 3.4.1-2 and 3.4.1-3 will provide an effective tool for mineral and hydrocarbon property mapping at scales of less than 1:20 000.

To produce the image maps shown in Figures 3.4.1-2b and 3.4.1-3, Convair-580 airborne high-resolution (6 m) SAR data of mineral belts of the Sudbury Basin in Ontario and the Lac Volant area in Quebec were acquired on July 27, 1988 and February 25, 1997 respectively. For the Lac Volant site, Saint-Jean *et al*. (1999) reported that some lineament orientations

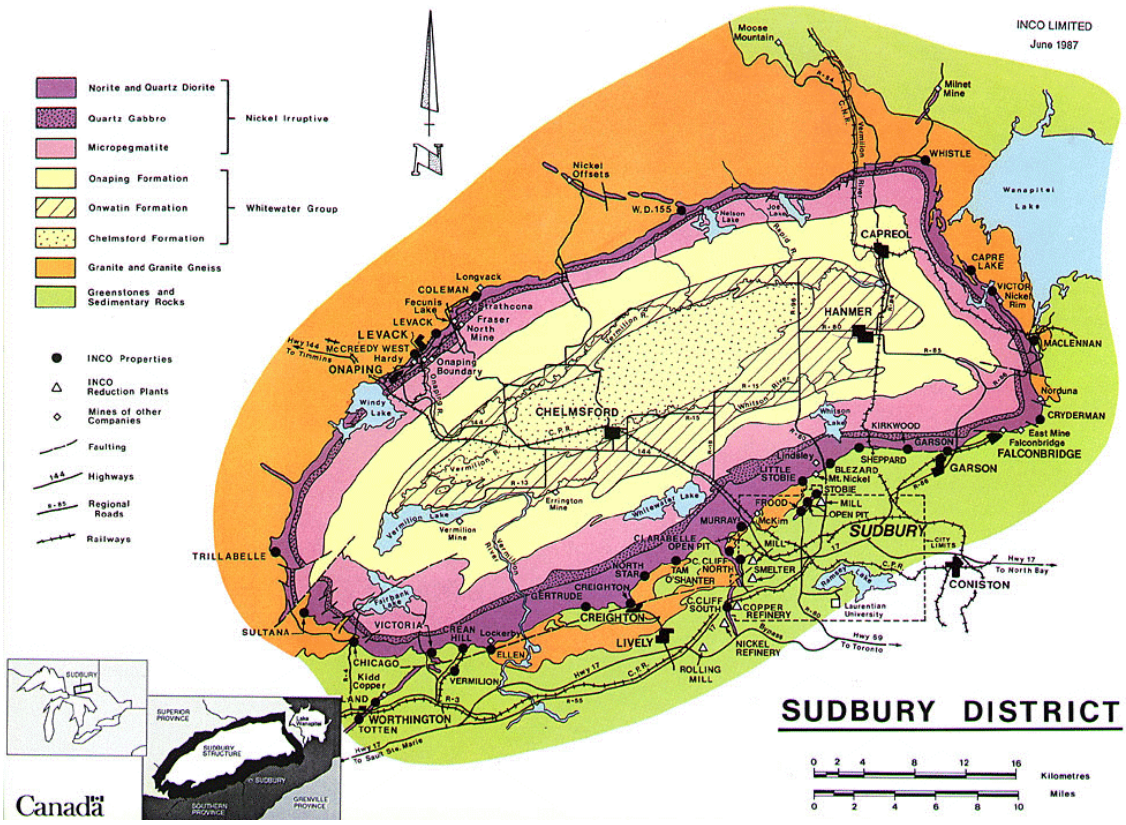

Figure 3.4.1-1 Geological setting of the Sudbury Basin. Mineralization predominantly occurs on the outer perimeter of the impact structure, which is where the mines (black dots) are located.

are enhanced by cross-polarized images. In both areas there are current active mineral exploration programs. These areas are typical Canadian Shield terrains consisting of 10-30% Precambrian outcrops, variable drift thickness and a dense to sparse forest cover.

The Sudbury Basin is one of Canada's richest mining areas, with world-class mineral deposits and the world's oldest, largest, and best-exposed meteorite impact site. This elliptical feature, known as the Sudbury Basin, is 300 km in diameter and approximately 2 billion years old. Over the past 100 years, $135 billion of nickel and copper ores have been mined from more than 90 mines distributed around the rim of the Basin. Current production is about $2 billion a year. Figure 3.4.1-1 shows some regional geologic information and the distribution of mining properties of INCO, one of the largest mining companies in Canada. This simplified geological map is used to facilitate the interpretation of the fused product of the Sudbury Basin shown in Figure 3.4.1-2(a), which consists of a Standard 1 mode RADARSAT–1 image (25 m resolution) integrated with low-resolution (200 m) magnetic data. Much remains to be learned about the structural evolution of the Sudbury Basin and the mineralized showings around it, and there are current discussions to conduct deep drilling to understand mineral emplacement and the impact structure. RADARSAT-1 images

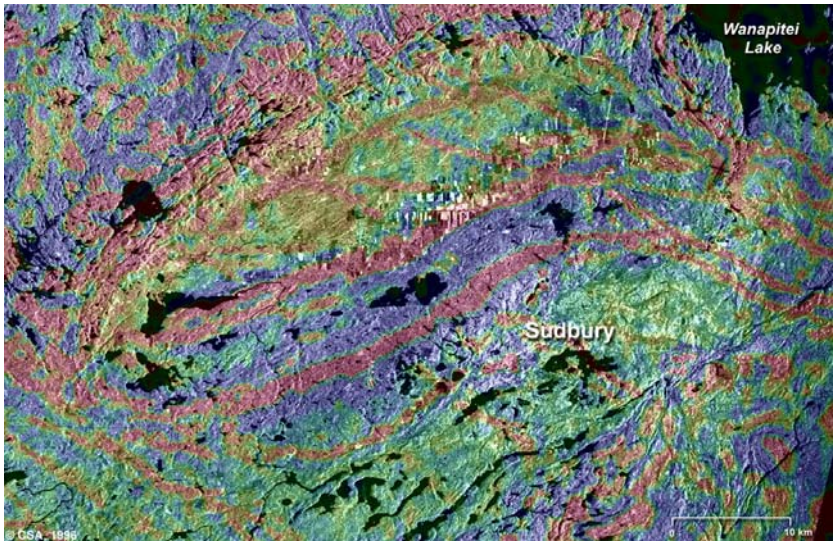

(a)

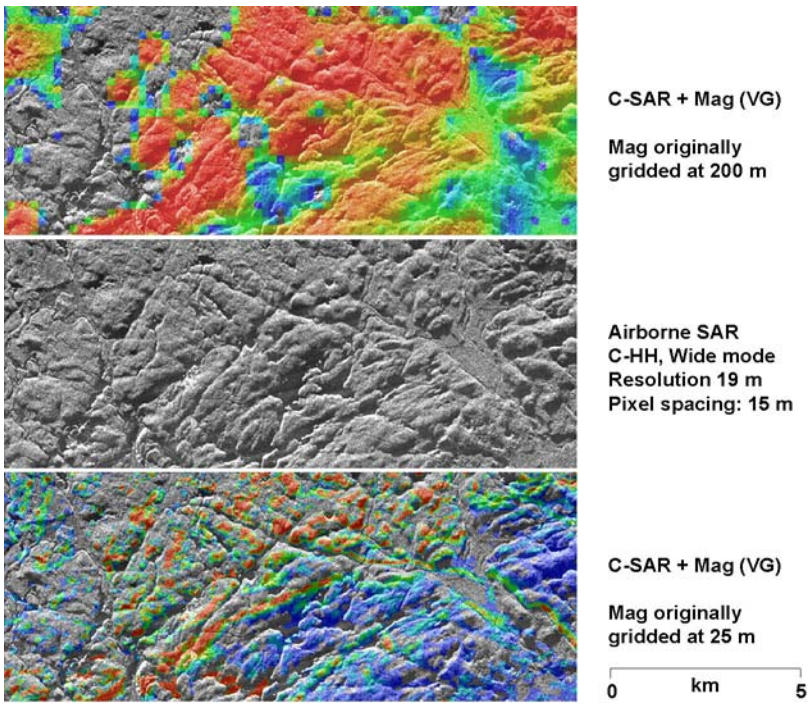

(b)

Figure 3.4.1-2 (a-b) Image fusion results for mineral and hydrocarbon property mapping, Sudbury Basin. (**a**) RADARSAT Standard 1 descending mode image (25 m resolution, acquired June 4, 1996) integrated with low-resolution (200 m) magnetic (mag) data (vertical gradient). This type of data integration can be used for interpretation on a smaller scale at a regional level. (**b**) Airborne SAR C-HH (19 m resolution, acquired July 27, 1988) fused with 25 m magnetic vertical gradient data. The integrated SAR and higher resolution magnetic data (bottom figure) reveal a higher level of detail in the geological structure of the area.

have been used to study the characteristic elliptical shape and the associated fractures around the Basin (Lowman, 1994). The Standard 1 beam mode of RADARSAT, at 20-27° incidence angle, provides an excellent view of the topography and structural features of the Sudbury area. Structure is expressed by differential erosion controlled by fractures, dykes and lithology. The fused image in Figure 3.4.1-2(a) is generated using the Intensity-Hue-Saturation (IHS) integration procedure. It involves the fusion of the RADARSAT-1 SAR image to modulate the intensity, the magnetic signatures to modulate the hue and a constant to modulate the saturation of the resulting image. The RADARSAT-1 image provides terrain information and the surface expressions of structures seen on the image, which appear as a network of linears. The low-resolution vertical magnetic gradient image, obtained from the Geological Survey of Canada (GSC), shows geological units as expressed from their magnetic signatures. The variation in the concentration of magnetic minerals can be used to trace rock units. Therefore the combined RADARSAT-1 and geophysical image map is useful in geological mapping of structures and lithology. Areas in red outline the strong magnetic signature of the Sudbury Igneous complex (also known as the nickel eruptive). Magma-filled dykes also have highly magnetic signatures. These are seen as NE-SW trending linears observed on both the RADARSAT-1 and geophysical images. The other colours shown on the synergy image correspond to different rock types with different magnetic signatures. These types of synergy images are used by geologists and mining companies to facilitate geological interpretation.

The high-resolution capability of the RADARSAT-2 Ultra-Fine beam mode will prove very useful for geological and terrain mapping. By fusing high-resolution SAR imagery with other high-resolution geophysical, topographic and optical data sources, improved results in support of geological mapping can be obtained. For example, the high-resolution magnetic and SAR-fused image shown in Figure 3.4.1-2(b) represents a similar image map that will result from fusion with RADARSAT-2 Ultra-Fine beam mode data. The structural details at the outcrop level are provided by the high-resolution Convair-580 airborne SAR image. When this information is combined with subsurface geophysical detail, the resulting large-scale (>1:20 000) fused SAR image maps will be well suited for mineral property mapping (Figure 3.4.1-2(b) - lower). High-resolution (10 m line spacing) airborne vertical gradient magnetic surveys are very expensive, and are usually flown by exploration companies to provide detailed magnetic signatures of rocks for site-specific exploration programs. The high-resolution mapping and visualization techniques will be very useful for target exploration.

High-resolution vertical gradient magnetic image data has also been fused with high-resolution airborne polarimetric images of the Lac Volant mineralized area. Our results show that the polarimetric fused magnetic images (VH/Mag), (VV/Mag), (HH/Mag) are all useful for structural and lithologic mapping (Figure 3.4.1-3). In areas of sparse vegetation and more than 20% of outcrops, cross-polarized images show more directional lineament enhancement (Saint-Jean *et al*., 1999).

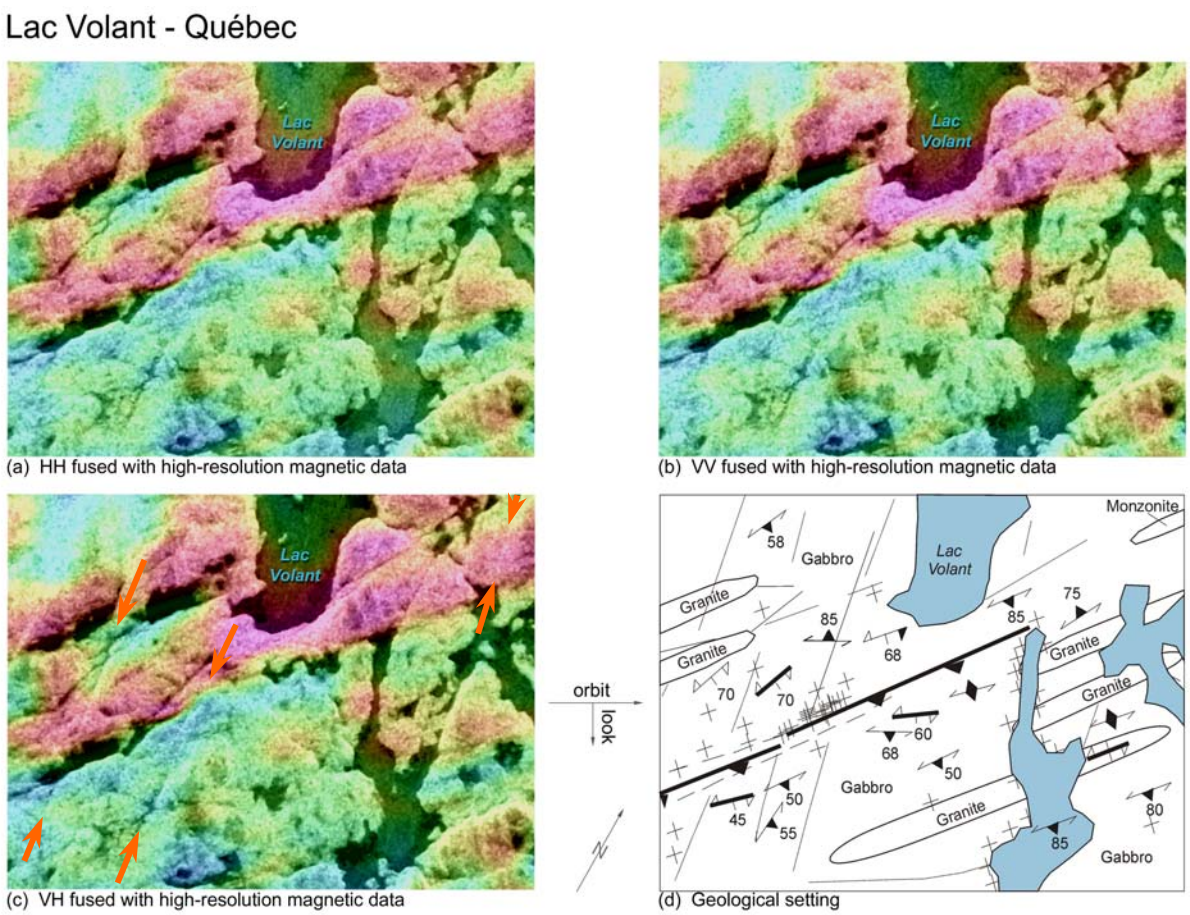

(d) Geological setting

Figure 3.4.1-3 (a-d) Fusion of polarimetric airborne Convair-580 SAR data acquired February 25, 1997 and high-resolution magnetic data, Lac Volant, Quebec. In combination, SAR and magnetic data reveal well the geologic units as depicted on the geological map (d). The best discrimination of the geologic structure in this example was achieved with the cross-polarized (VH) SAR and magnetic vertical gradient integrated image (c). The arrows highlight North-East trending lineaments not visible in the HH or VV fused images.

3.4.2 Monitoring deformation of active landslides from InSar techniques

Remote sensing techniques are increasingly being used in slope stability assessment (Murphy and Inkpen, 1996; Singhroy *et al*., 1998; Singhroy and Mattar, 2000). Recent research has shown that differential interferometric SAR techniques can be used to monitor landslide motion under specific conditions (Vietmeier *et al*., 1999; Rott *et al*., 1999). Provided coherence is maintained over longer periods, i.e. in non-vegetated areas, it is possible to observe surface displacement of a few cm per year. Using data pairs with short perpendicular baselines, short time intervals between acquisitions, and correcting the effect of topography on the differential interferogram, reliable measurements of surface displacement can be achieved.

Our study focused on the Frank Slide, a 30×10^6 m^3 rockslide-avalanche of Paleozoic limestone, which occurred in April 1903 from the east face of Turtle Mountain in the

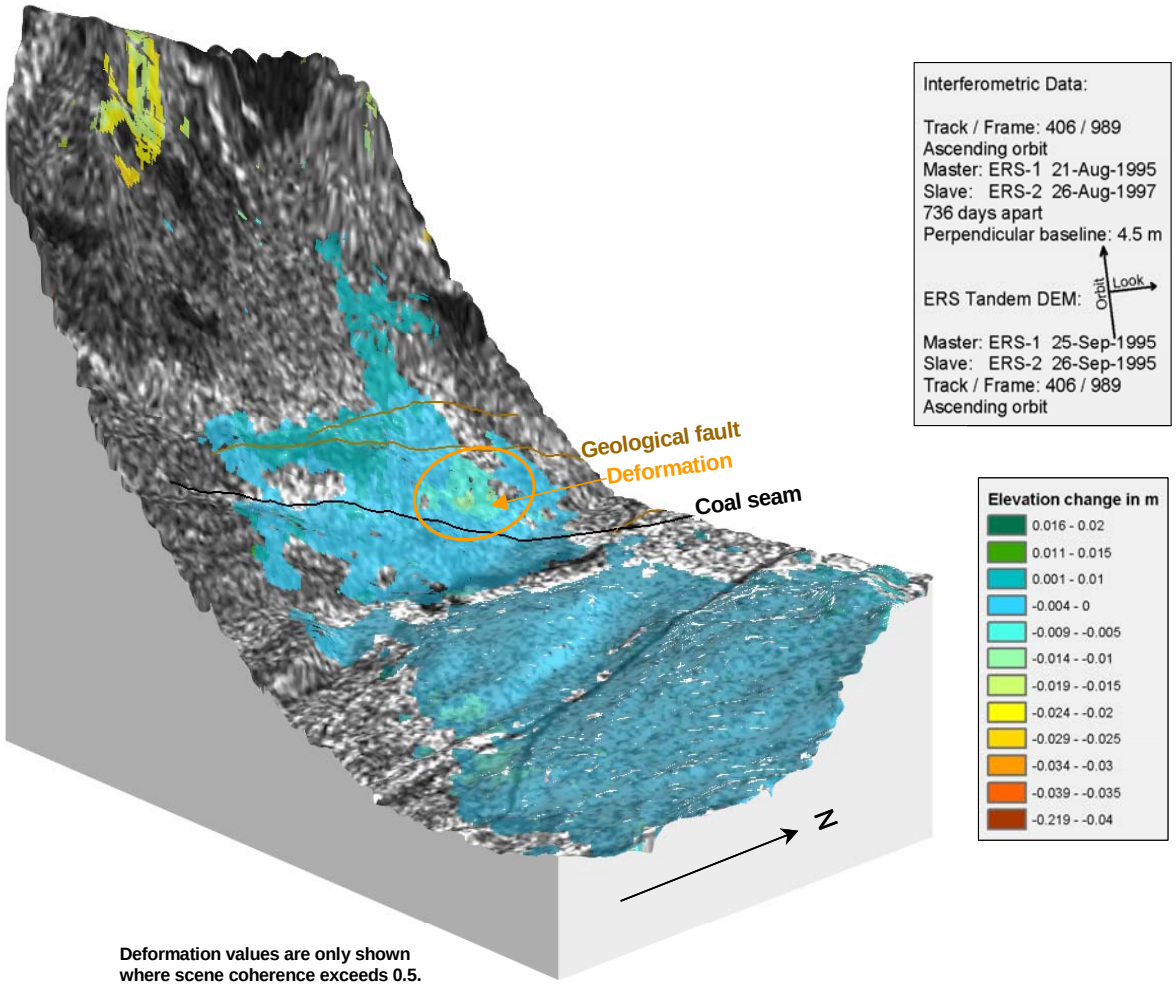

Figure 3.4.2-1 Surface deformation map, interferometrically generated from ERS data acquired August 1995 & August 1997 and draped over a high-resolution elevation model. Possible surface deformation was detected at a location between a coal seam and a geological fault traversing the slope.

Crowsnest Pass region of southern Alberta, Canada. Seventy fatalities were recorded (Cruden and Hungr, 1986). Detailed analysis on the use of SAR images for characterizing and monitoring the Frank slide is reported by Singhroy and Molch (2004). An ERS pair of images acquired August 1995 and August 1997, with a perpendicular baseline of 4.5 m, was used for the InSAR analysis. The InSAR investigation revealed the presence of a near-circular fringe in the differential interferogram. Figure 3.4.2-1 shows the interferogram draped on a high-resolution DEM. InSAR results show minor deformation along parts of the geological structure, suggesting that the Frank slide is still active. There is also a displacement of -1.3 cm, indicating gradual motion of the rock face prior to the 2001 rockslide, in which 6000 tons of rock and debris fell from the north slope of Turtle Mountain. Due to the small perpendicular baseline of only 4.5 m for this InSAR pair, topographic contribution to the differential phase was minimal and has been removed during the processing. This could not be achieved with RADARSAT-1 archival images with larger baselines. The fact that the two areas of the detected surface displacement correspond to the location of the 2001 rock fall and along the known geological fault suggests that the instability is real, and that InSAR

techniques, if carefully applied, can locate areas of instability prior to the actual failure. These findings are now being used to target the installation of *in-situ* motion detectors. Additional monitoring using RADARSAT-1 and ERS-2 images are planned on a monthly basis for 2004 (Alberta Environment, 2000) to understand the effects of freeze-thaw, snowmelt, rainfall events and other geotechnical processes on post-slide motion. If images with small perpendicular baselines are available from RADARSAT-2 due to the improved orbit control, the additional capabilities of high-resolution multi-incidence, with right and left look direction, will make it possible to monitor smaller active landslides on slopes outside the line of site of other SAR satellites.

3.5 Coastal Zones and Oceans

An expected moderate increase in overall applications potential of RADARSAT-2 vis-à-vis RADARSAT-1 for coastal zone applications results primarily from the enhancements in terms of polarization diversity and spatial resolution. In the subsequent sections, we review the potential of RADARSAT-2 polarimetric data for shoreline detection and mapping of coastal lands. We also discuss SAR and optical data fusion techniques using the wavelet transform in support of marine applications.

3.5.1 Shoreline detection

Information on the position of shorelines and changes in these positions supports maritime navigation, the definition of legal boundaries (see also section 3.2.1), the planning of infrastructural developments, and the development of strategies to control coastal dynamics.

The ability to identify a shoreline in a radar image, and indeed any other type of remote sensing image, depends strongly on the observed water-land contrast. Small angles of incidence and high winds and/or waves are known to complicate the identification of shorelines in C-band VV radar images, in particular. Figure 3.5.1-1 illustrates the effect of waves on the water-land backscatter contrast as perceived in Convair-580 SAR images with different polarizations. The images shown in Figures 3.5.1-1(a) to 3.5.1-1(c) were acquired in the HH, VV, HV polarization, respectively. The polarization of the image in Figure 3.5.1-1(d) is defined by a transmit ellipticity (χ_t) of 0.7°, a transmit orientation (ψ_t) of 1.9°, a receive ellipticity (χ_r) of –3.7°, and a receive orientation (ψ_r) of 94.5°. This polarization combination was found to be optimal for the mapping of the shoreline observed in the sense that it yields the maximum contrast between the wave crests and the land. The best performing polarization combination was computed using an algorithm developed by Swartz *et al.*, 1988. This algorithm is implemented in the Polarimetric Work Station (cf. Chapter 4). The ellipticities and orientations for the linear cross-polarization (HV) are as follows: $\chi_t = 0^\circ$, $\psi_t = 0^\circ$, $\chi_r = 0^\circ$, and $\psi_r = 90^\circ$. Hence, it may be concluded that, in this particular case, the best performing polarization combination for shoreline mapping is nearly identical to the HV polarization. This is in agreement with what can be visually perceived in the Figures 3.5.1-1(c) and 3.5.1-1(d).

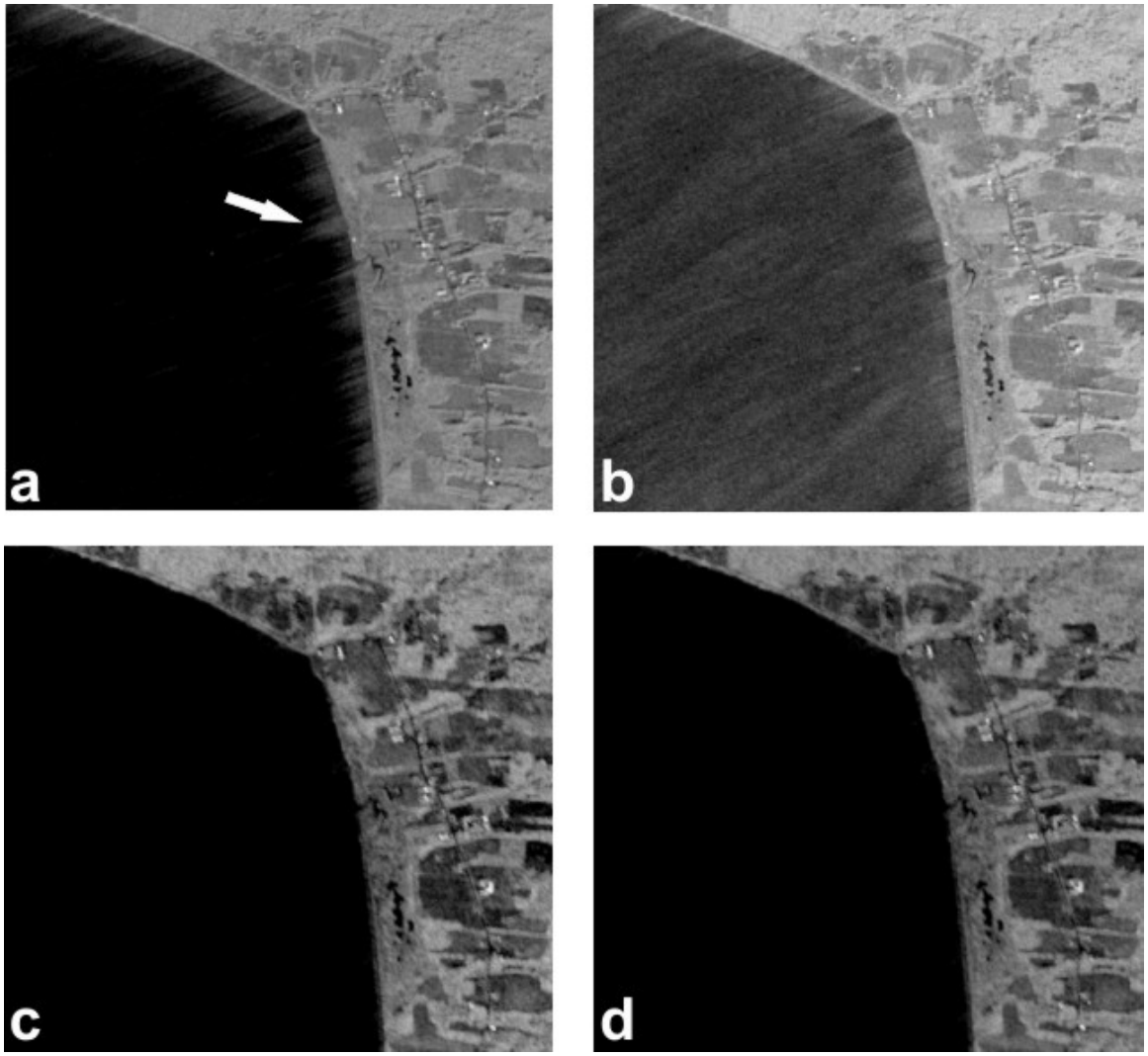

Figure 3.5.1-1 (a-d) Convair-580 SAR images showing the effect of polarization on water-land contrast; the arrow marks the presence of waves (**a**) C-band HH polarization (**b**) C-band VV polarization (**c**) C-band HV polarization (**d**) maximum contrast image; $\chi_t = 0.7^\circ$, $\psi_t = 1.9^\circ$, $\chi_r = -3.7^\circ$, $\psi_r = 94.5^\circ$.

Table 3.5.1-1 lists the backscatter values (sigma nought (σ°) rounded off to the nearest integer) for land and water as measured by the Convair-580 SAR in C-band HH, VV, HV and ee ($\chi_t = 0.7^\circ$, $\psi_t = 1.9^\circ$, $\chi_r = -3.7^\circ$, $\psi_r = 94.5^\circ$). In addition, the water-land contrasts as measured by the Convair-580 and as 'simulated' for a RADARSAT-2 Quad Polarization image are shown. The contrast values for RADARSAT-2 are derived from the Convair-580 measurements based on the assumption that the noise floor (or noise equivalent sigma nought) associated with the Quad Polarization mode will be –30 dB. The Convair-580 SAR has a noise floor of about –40 dB and is therefore more sensitive than the RADARSAT-2 SAR. Consequently, the Convair-580 SAR is capable of measuring the HV and ee backscatter signals of water whereas in the case of RADARSAT-2 SAR these signals will be recorded as being –30dB, i.e. as noise. As shown in Table 3.5.1-1, the lower sensitivity of the RADARSAT-2 SAR can result in a reduced water-land contrast in image products with

Table 3.5.1-1 Water-land backscatter values measured by the Convair-580 SAR at an incidence angle of 60°, in different polarizations (ee corresponds to: $\chi_t = 0.7^\circ$, $\psi_t = 1.9^\circ$, $\chi_r = -3.7^\circ$, $\psi_r = 94.5^\circ$). Associated measured backscatter contrasts for the Convair-580 and simulated backscatter contrasts for RADARSAT-2 are also included.

Polarization	σ° Land (dB)	σ° Water (dB)	Convair-580 measured contrast (dB)	RADARSAT-2 simulated contrast (dB)[1)]
HH	-12	-23	11	11
VV	-12	-21	9	9
HV	-21	-33	12	9
ee	-20	-33	13	10

1) Simulated available contrast in a RADARSAT-2 Quad Polarization image product (at the given incidence angle (see text); assuming a noise floor of –30 dB)

certain polarizations, e.g. HV and ee. The results of this particular RADARSAT-2 simulation indicate that the HH-polarized image provides the best contrast for water-land discrimination. However, it should be noted the backscatter values listed in the table correspond to, for satellite SAR systems, a rather extreme angle of incidence (60°). At incidence angles in the range of the RADARSAT-2 Quad Polarized image products (20°-41°) the HV (and ee) sigma nought values for water and land may well be about 5 dB higher than the ones listed. This would push the return signal for water above the RADARSAT-2 noise floor and hence enable measurement of the full contrast.

3.5.2 Mapping of coastal lands

Information on substrates and vegetation as found in coastal uplands and coastal lands under tidal influence supports coastal management in general and activities such as the mapping of habitats and environmental sensitivities (e.g. to erosion, oil spill) in specific. In addition, information on the distribution of coastal substrates and vegetation can support activities such as accessibility mapping (e.g. for military vehicles) and the planning of infrastructural works.

Figure 3.5.2-1 shows a multi-polarization composite image as acquired by the Convair-580 SAR system over Evangeline Beach, Minas Basin, Nova Scotia during low tide conditions. The HH, HV, and VV polarized channels are shown in red, green and blue, respectively. It should be noted that the backscatter contrasts as found within the dry-land area and the tidal plane were enhanced independently to account for the large difference in the radar return signal of the two targets and produce the image shown. The difference in the level of backscatter received from the dry land and the tidal plane ranges from about 13 dB in VV to about 20 dB in HH and HV. This backscatter difference is observed at a rather extreme angle of incidence (≈ 60°). The colour patterns in the image result from differences in the HH, HV and VV backscatter and can be shown to correlate to differences in beach substrate. The areas marked 1, 2 and 3 correspond to mud, friable sandstone and gravel, respectively (see photographs). The co-polarization response plots in Figure 3.5.2-2 confirm the differences in the backscatter behaviour of the three substrates. Mud displays a relatively strong backscatter response in VV, a relatively weak backscatter response in HH

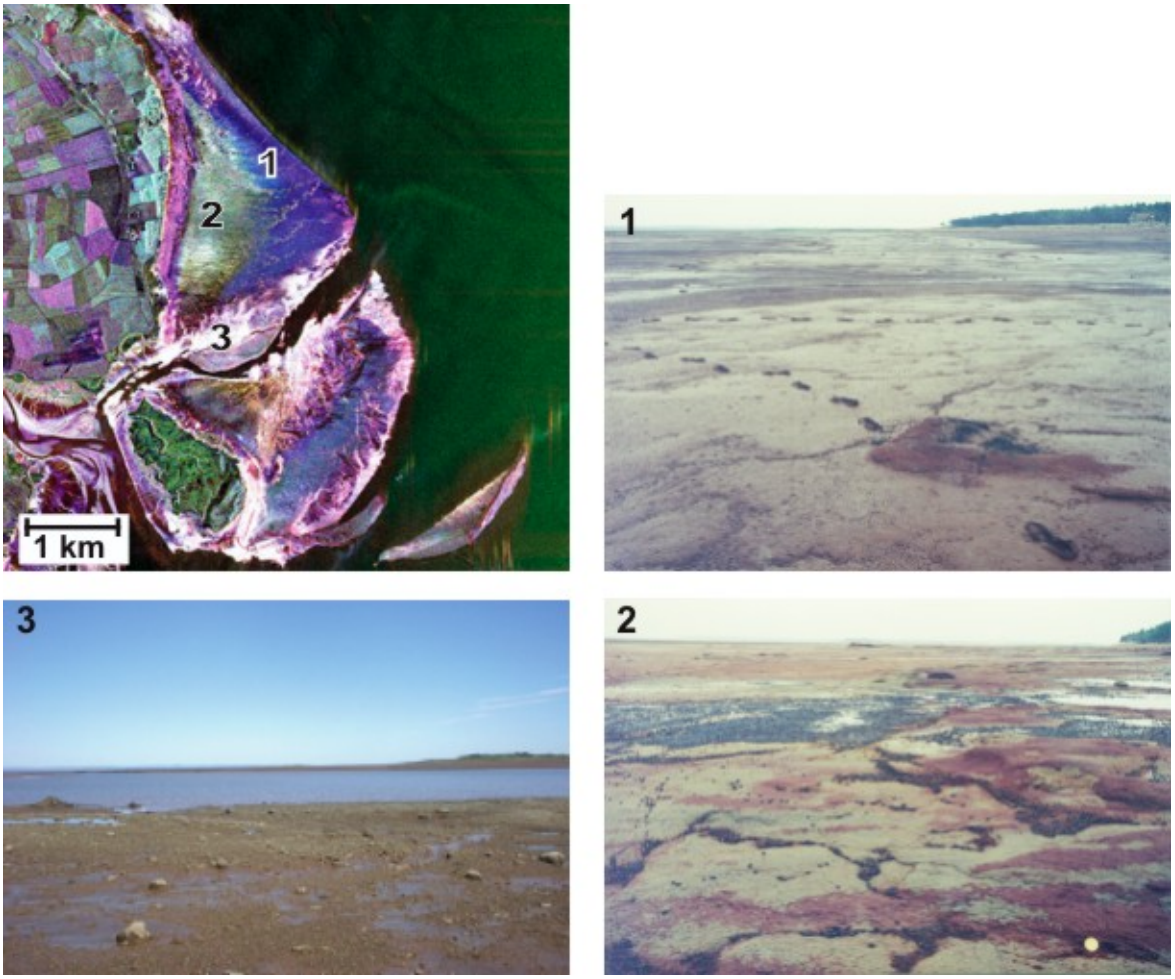

Figure 3.5.2-1 Convair-580 SAR multi-polarization composite showing Evangeline Beach, Minas Basin, Nova Scotia. The HH, HV, and VV polarized channels are shown in red, green and blue, respectively. The backscatter contrasts as found within the dry-land area and the tidal plane were enhanced independently to produce the image shown. The predominant beach substrates are shown in the accompanying photographs (1) mud (2) friable sandstone (3) gravel.

and a low pedestal height. The low pedestal height indicates that the observed radar return signal is governed by single bounce surface scattering. At the same time, the raised lips on the response plots at $\chi \approx \pm 45^{\circ}$ suggest that double bounce surface scattering contributed to the total backscatter. The apparent weakness of multiple surface scattering and multiple volume scattering, i.e. scattering mechanisms that are know to generate HV-backscatter, explains the near lack of green tones in image areas corresponding to mud. The radar response signal for mud in HV-polarization was about –44 dB. This is a value lower than the nominal noise floor of the Convair-580 SAR (–40 dB). Like mud, sandstone is characterized by a relatively strong VV response and a relatively weak HH response. However, the considerably higher pedestal suggests that a larger proportion of the total backscatter

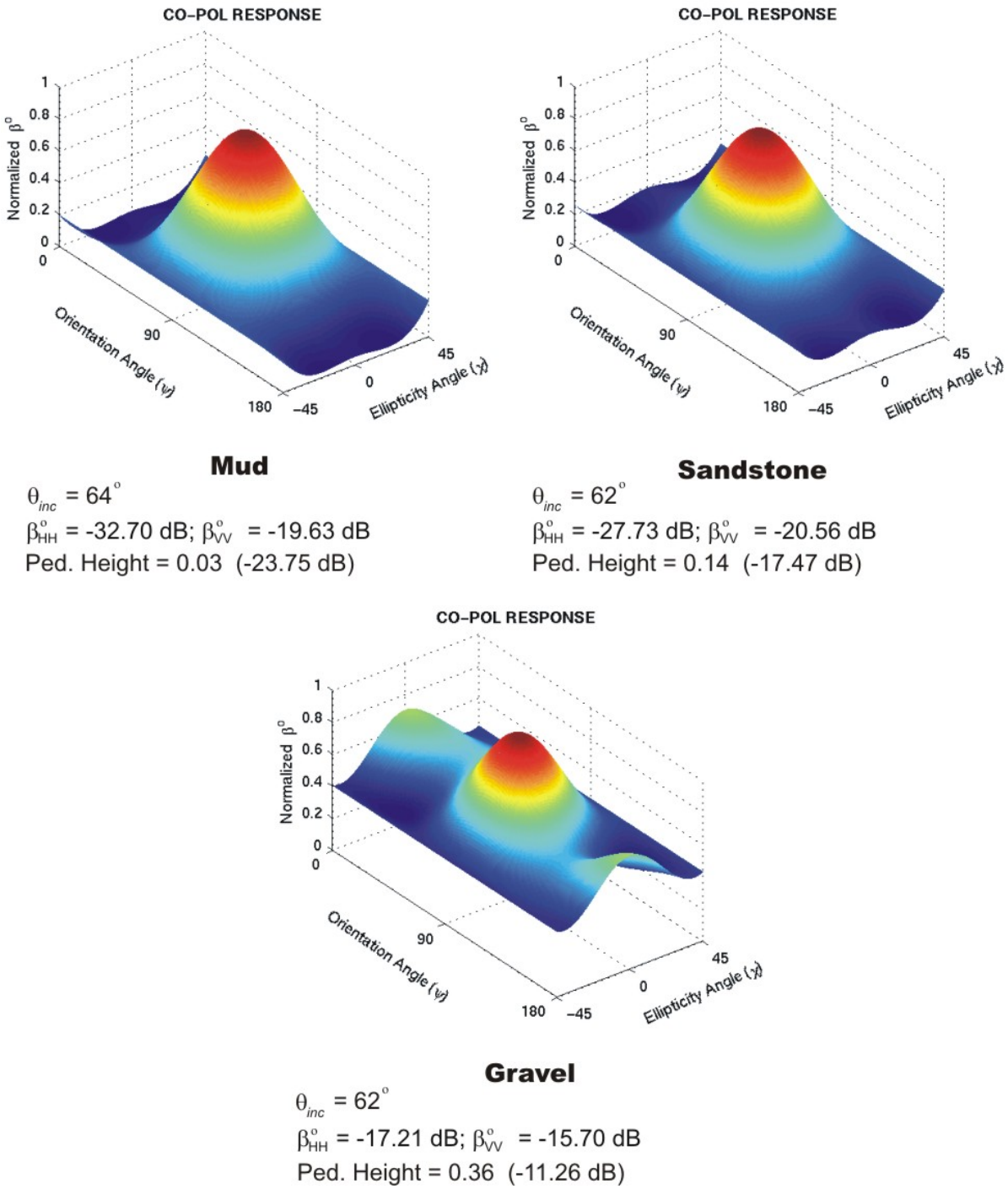

Figure 3.5.2-2 Co-polarization response plots for predominant substrates found on Evangeline beach.

results from multiple scattering. Given the limited permittivity of sandstone, the most likely form of multiple scattering to occur is multiple surface scattering. The predominantly green tone of the sandstone area in the image shown in Figure 3.5.2-1 is indicative of HV-backscatter and confirms the presence of multiple scattering. The measured return signal for sandstone in HV-polarization was of the order of –33 dB. Relative to mud and sandstone, gravel displays more equivalent HH and VV backscatter responses. The higher pedestal of

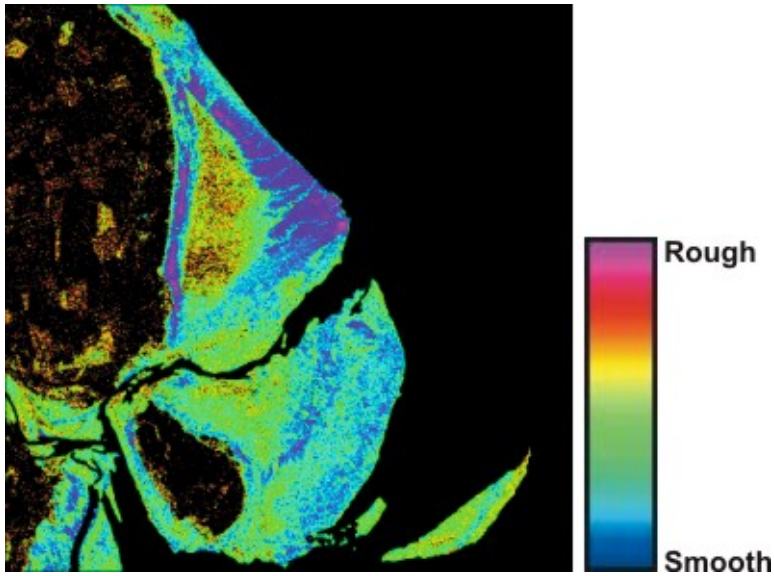

Figure 3.5.2-3 Pseudo-coloured image product showing a polarimetric attribute known as circular polarization coherence ($|\rho_{RRLL}|$). Circular polarization coherence is a function of the soil surface roughness and the local incidence angle but is independent of soil moisture and azimuth tilt.

gravel vis-à-vis mud and sandstone corresponds to a larger proportion of depolarized radar backscatter and indicates a stronger contribution of multiple scattering (most likely multiple surface scattering) to the backscattering process. The multiple surface scattering is responsible for a relatively high HV radar return signal (≈ -28 dB). Thanks to relatively high backscatter levels in HH, VV and HV, the image tone of gravel areas in Figure 3.5.2-1 is white. The differences in backscatter behaviour of the three substrate types can be explained from differences in surface roughness. This will be substantiated below.

Figure 3.5.2-3 shows a surface roughness product for Evangeline beach. The pixel values in this pseudo-coloured image product were computed from the polarimetric Convair-580 SAR data. They represent a polarimetric attribute know as the circular polarization coherence ($|\rho_{RRLL}|$) (Mattia *et al.,* 1997; Schuler *et al.,* 2002; Hajnsek *et al.,* 2002). This attribute has been shown to be sensitive to surface roughness and local incidence angle, but insensitive to surface dielectric constant (≈soil moisture) and azimuth tilt. The sensitivity of $|\rho_{RRLL}|$ to roughness is restricted to slightly rough random surfaces. These are surfaces with an electromagnetic roughness, expressed in units of wavelength ($k\sigma$), in the range of $0.2 \le k\sigma \le 1$ where k is the wave number ($k = 2\pi/\lambda$) and σ is the standard deviation of the surface height (or rms height). For C-band systems like the Convair-580 and RADARSAT-2 that operate with wavelengths (λ) of the order of 5.6 cm, the rms height corresponding to $k\sigma$ equal to 0.2 and 1 is 0.18 and 0.89 cm, respectively. For bare soil surfaces (that show azimuthal symmetry; i.e. $\langle S_{HH} S_{HV}^* \rangle = \langle S_{VV} S_{HV}^* \rangle = 0$) the circular polarization coherence is given by:

$$\left|\rho_{RRLL}\right| = \frac{\left\langle \left|S_{HH} - S_{VV}\right|^2 \right\rangle - 4\left\langle \left|S_{HV}\right|^2 \right\rangle}{\left\langle \left|S_{HH} - S_{VV}\right|^2 \right\rangle + 4\left\langle \left|S_{HV}\right|^2 \right\rangle} = \frac{T_{22} - T_{33}}{T_{22} + T_{33}} \tag{3.5.2-1}$$

With s_{xx} and T_{xx} representing elements of the scattering and coherency matrix, respectively. The value of attribute $\left|\rho_{RRLL}\right|$ increases from 0 to 1 with a decrease in surface roughness. $\left|\rho_{RRLL}\right|$ can be shown to be a function of two surface roughness parameters, i.e. the rms height and the surface correlation length (l). According to Schuler *et al.* (2002) the relationship between $\left|\rho_{RRLL}\right|$, the surface variables σ and l, and the local incidence angle (θ_{inc}) can be described as:

$$\left|\rho_{RRLL}\right| = e^{-16\left(\sigma^2 / \left(l^2 \sin^2(\theta_{inc})\right)\right)} \tag{3.5.2-2}$$

In the case of azimuth symmetric scatter, $\left|\rho_{RRLL}\right|$ is equivalent to a polarimetric attribute known as anisotropy (*A*). However, in contrast to the circular polarization coherence, anisotropy is strongly affected by system noise.

The $\left|\rho_{RRLL}\right|$ values for the mud, sandstone and gravel areas on Evangeline beach (i.e. the samples shown in Figure 3.5.2-2; $\theta_{inc} \approx 62^\circ$) were found to be of the order of 0.79, 0.58 and 0.64, respectively. This suggests that mud is the smoothest target while sandstone is the roughest. However, it can be seen in Figure 3.5.2-3 that for sandstone in particular the variability in the $\left|\rho_{RRLL}\right|$ and thus surface roughness is considerable. Overall, the patterns shown in the Figures 3.5.2-1 and 3.5.2-3 are very similar. However, unlike the patterns in Figure 3.5.2-1, the patterns in Figure 3.5.2-3 are strictly related to soil roughness and not to possible differences in soil moisture. Also, Figure 3.5.2-3 provides considerably more detail about the variability in the roughness of the sandstone plateau and other areas (e.g. the areas showing uniformly white in Figure 3.5.2-1).

3.5.3 SAR and optical image fusion with wavelets for marine applications

Image fusion is the combination of two or more different images to form a new image that contains enhanced information. The wavelet transform, which allows the decomposition of an image into its constituent spatial scale layers, has previously been applied to multi-sensor image fusion. We have developed a new image fusion scheme (Du *et al*., 2002) that is based upon the wavelet transform and that emphasizes the real information content of the images; the images are fused while minimizing the degree of re-sampling required. We are particularly interested in RADARSAT-1 ScanSAR and NOAA AVHRR visible-infrared images, which are being studied as a precursor to contemporaneous SAR and electro-optical data that will be available from the ASAR and MERIS sensors on ENVISAT. Data acquired off the British Columbia coastal area in 1999 (Figure 3.5.3-1) were selected (see van der Sanden *et al*., 2000). Due to their different physical characteristics, SAR and visible-infrared images provide different sea surface information; the purpose of radar and visible-infrared image fusion is mainly for feature enhancement.

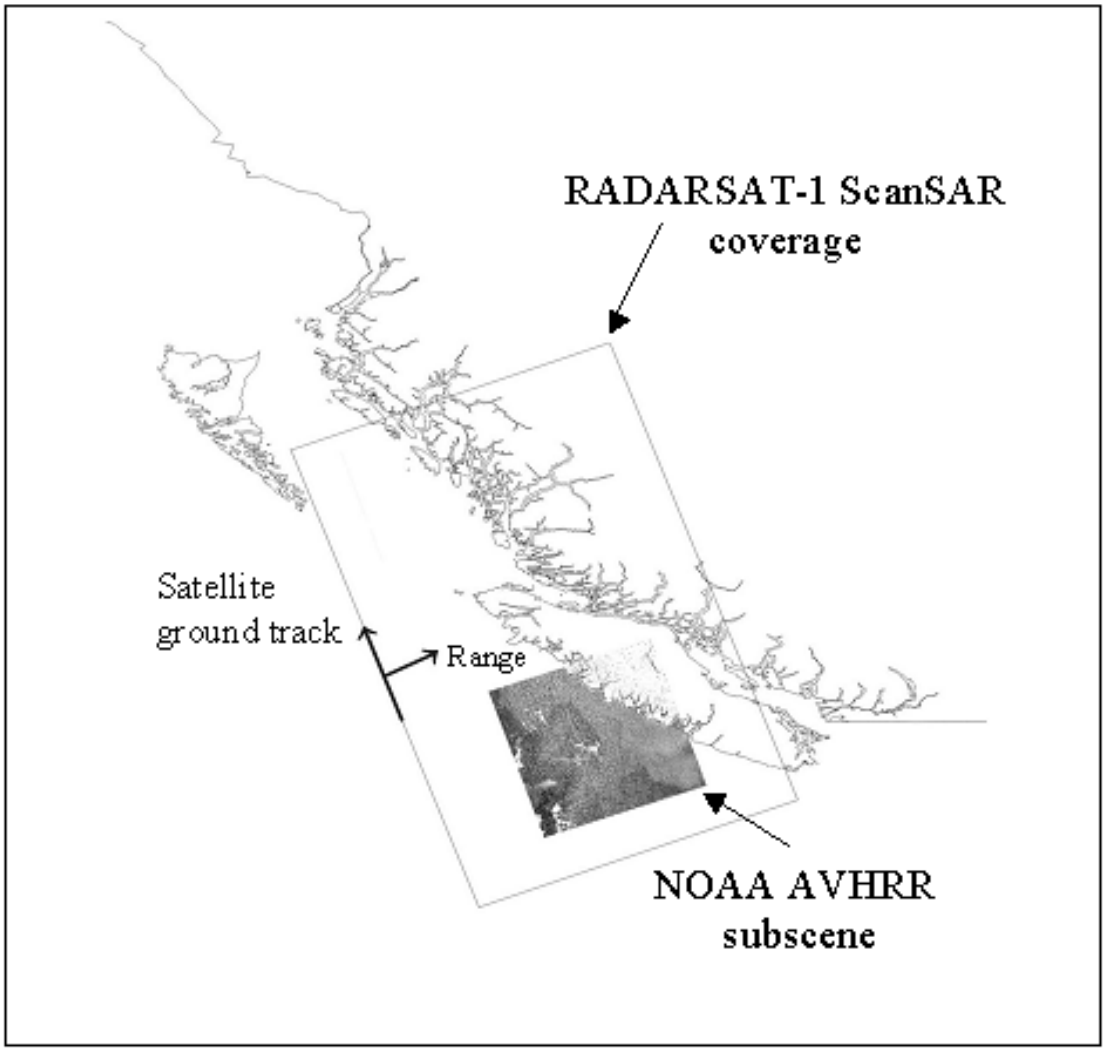

Figure 3.5.3-1 The test area off the West Coast of British Columbia.

Wavelets arose in signal processing theory to help analyze the temporal variability of signals. Wavelets can be generalized to two-dimensional signals such as satellite remote sensing images. Wavelet decomposition represents the details of a signal in an alternative manner to conventional temporal and Fourier descriptions. At a particular scale, the signal is approximated by a sum of scaling functions. The difference between the scales (termed the detail at the finer scale) can be expressed by a sum of wavelet functions. For certain scaling and wavelet functions, this hierarchical or multi-scale representation can be constructed using scaled versions of the same functions at each scale (Horgan, 1998). Figure 3.5.3-2 shows an example of an orthonormal wavelet decomposition of an image with four levels. By using the wavelet transform, an image can be decomposed into multi-scale frames in which each portion has distinct frequency and spatial properties.

Assume that we wish to fuse images A and B that have pixel sizes P_a and P_b ($P_a >> P_b$), respectively (see Figure 3.5.3-3). Let $P_a = S \times P_b$, and take $S_n \leq S$ to be a power of 2, with n chosen to satisfy $min(S - S_n)$. Image A is first re-sampled to image A' with $P_{a'} = S_n \times P_b$, such that the pixel size of image A decreases to the minimum extent possible. If $S = S_n$, the original pixel size of image A will be preserved exactly. The re-sampling in conventional

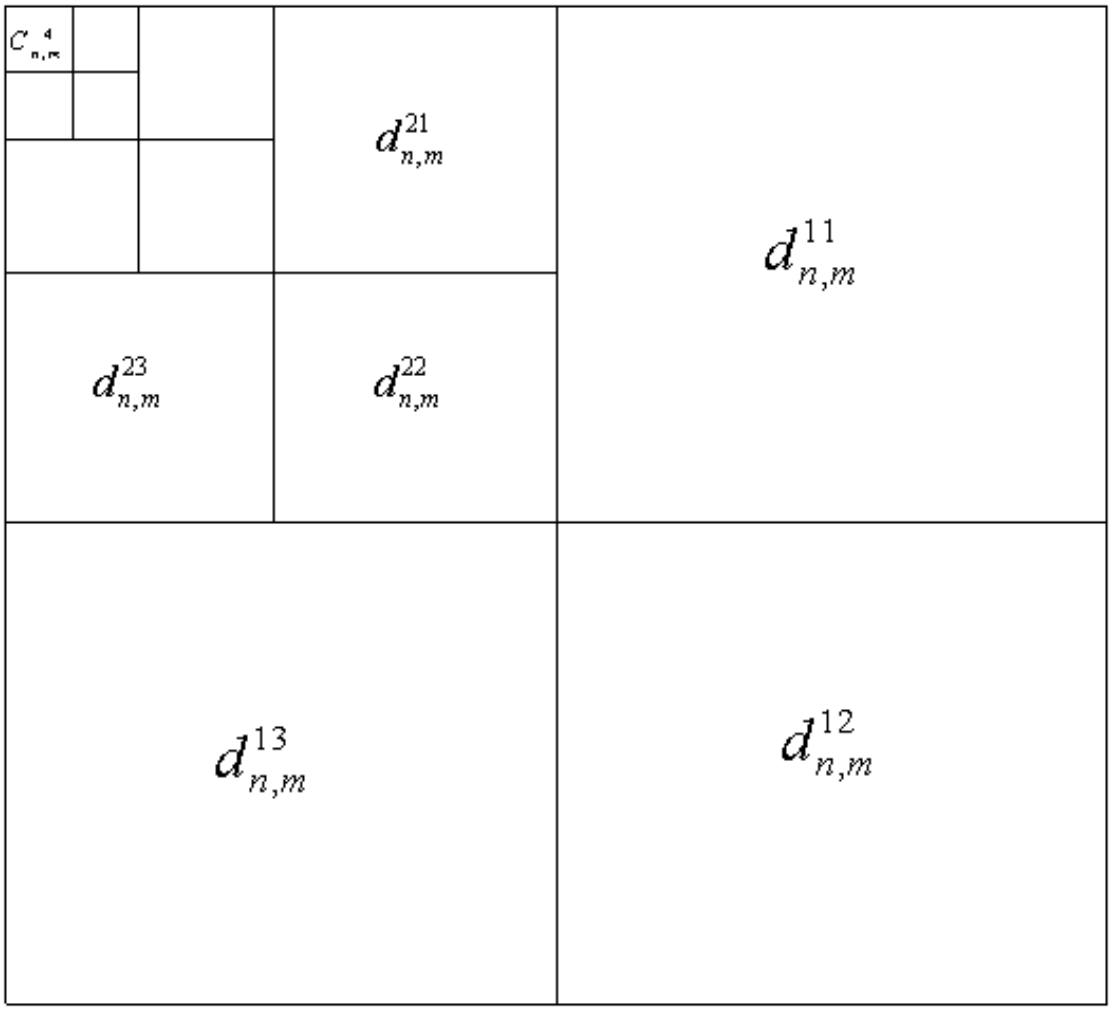

Figure 3.5.3-2 A standard orthonormal decomposition using a wavelet transform with four levels: $\{d^{k1}_{m,m}\}$ is the horizontal detail component of level *k*, $\{d^{k2}_{n,m}\}$ is the vertical detail, $\{d^{k3}_{n,m}\}$ is the diagonal detail, and $\{C^{k}_{n,m}\}$ are the low frequencies.

image fusion could be considered to be the special case of n = 0, which forces the original pixel size of both images to be re-sampled to a common grid.

The pixel size of image A' is now 2^n times that of image B. Image B can be decomposed by using a wavelet transform. The different scale levels of approximation can be obtained with a pixel spacing of 2^n times that of the original image. For example, if the pixel spacing of image B is 100 m, then the pixel spacing of level 1 is $2^1 \times 100$ = 200 m, the pixel spacing of level 2 is $2^2 \times 100$ = 400 m, and that of level 3 is $2^3 \times 100$ = 800 m. Image A' can be registered to the common grid as image B in its level *n* approximation (i.e., with pixel spacing that is the same as that of image A'). Generally, image B with its original pixel spacing is registered to a certain grid (e.g., a map projection) as image B'. The registered image B' is then decomposed by using wavelet transforms to the *n*-th scale level of approximation with the same pixel spacing as image A'. Image A' can be registered to the *n*-th scale level of approximation of image B' and retains its pixel spacing.

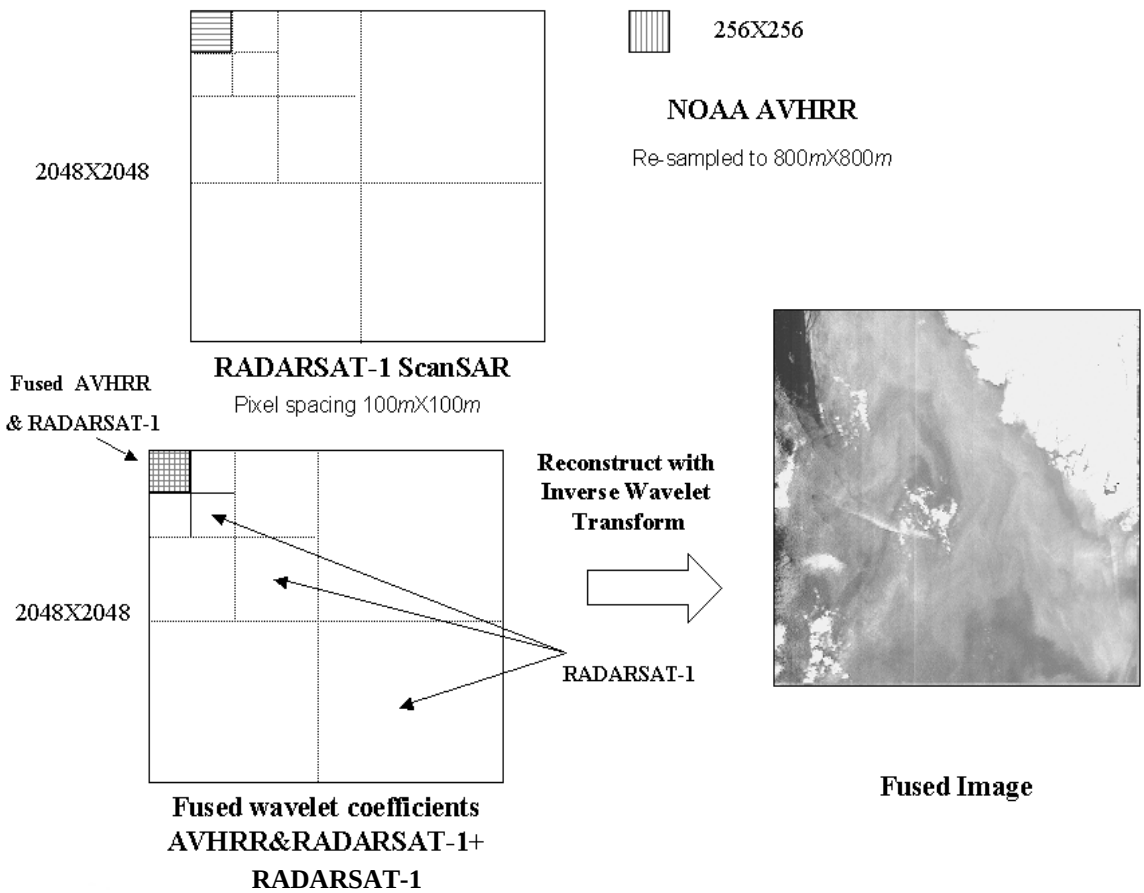

Figure 3.5.3-3 Fusion scheme for RADARSAT-1 ScanSAR (2048X2048 pixels, pixel size 100 m by 100 m) and NOAA AVHRR (256X256 pixels, pixel size 800 m by 800 m).

When the spectral properties of two input images are different, the format and scale of the digital values in the two files might be very different as well. The comparison of two sets of data requires that they be transformed to the same format, and normalized to a reasonable scale. At first, the normalization should ensure that the data of the final fused image is not beyond the range of the stored data format. In addition, the weights of the different input images should be determined depending on the purpose of the image fusion. Generally, important features in the different images should appear in the fused image. Therefore, radiometric normalization may be necessary. One approach is to use a linear regression across the area of interest in the two images. In this case, the values of the digital numbers of different images are adjusted to a common level by using a gain and an offset. Another approach is adjustment of the maximum and minimum values of the two images. Principal Component Analysis (PCA) can also be used to normalize the input images.

In some wavelet-based image fusion schemes, the two images are first re-sampled to the same pixel spacing prior to wavelet decomposition. The wavelet coefficients at the various scales are then analyzed in the corresponding levels. If the pixel sizes of the input images are on a similar scale, the re-sampling may not result in a significant error. When the pixel sizes of the input images are significantly different, the impact of re-sampling on the final image should be considered.

In our case, the quasi-original image A' is the same size and has the same pixel size as the *n*-th level decomposition of image B'. It should be noted that B' records features with scales from $P_{b'}$ to $P_{a'}$ and greater than $P_{a'}$, but A' only records features with scales greater than $P_{a'}$. That is, there are no features with scale smaller than $P_{a'}$ in image A'. Therefore, the wavelet coefficients of A' and B' may be fused from the *n*-th level of the B' decomposition, which corresponds to the zero level of A'. Depending on the application, there are several different image fusion algorithms, including multiplication, average or maximum value selection, PCA, etc.

The wavelet coefficients of two images can be calculated and combined into a single new set, which can be considered as the decomposition of a new image. By using the inverse wavelet transform, the new set of wavelet coefficients can be used to reconstruct the fused image. The new image contains some features with scale greater than $P_{a'}$ from A' and all features with scale greater than $P_{b'}$, and smaller than $P_{a'}$, and some features with scale greater than $P_{a'}$, from B'. This reconstructed image does not contain features smaller than $P_{a'}$ from A', which is an important factor in avoiding interpolation-induced artifacts. The original pixel size $P_{b'}$ is maintained in the reconstructed image without any loss of spatial information.

As a demonstration, the SAR image was first decomposed to three levels: 1024×1024, 512×512 and 256×256. The quasi-original AVHRR image was kept in its original size 256×256 (level zero). The AVHRR image (256×256) was then registered to the level three approximation of the decomposed SAR image (256×256).

A multiplication algorithm was then used to merge the wavelet coefficients. The approximation coefficients of level three of the SAR image then multiplies the registered AVHRR image, which is then normalized by the mean of the AVHRR image. Therefore, the synthetic wavelet coefficients of approximation are built at level three. In the detail images of the first three levels, only the wavelet coefficients of the SAR are considered because the AVHRR image does not contain spatial information at scales that are less than 800 m. The inverse wavelet transform was used to reconstruct the final fused image (Figure 3.5.3-4) with the fused wavelet coefficients, including levels 1, 2, and 3 details, and the synthetic approximation image of level three. The size of the final fused image is 2048×2048 pixels with a 100 m by 100 m pixel size. There are no residual artifacts and the fine pixel spacing of the SAR image is maintained.

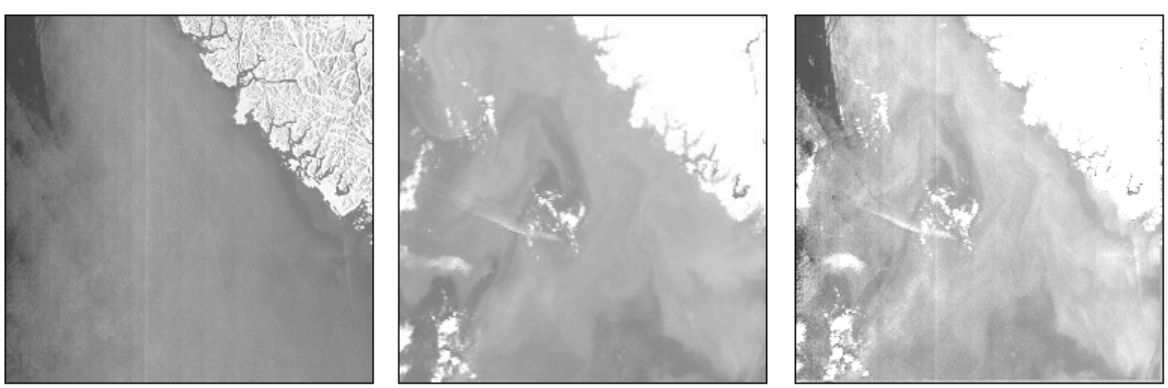

Figure 3.5.3-4 The original RADARSAT-ScanSAR (left) and NOAA AVHRR images (centre), and the resulting fused image (right).

Our results are superior to conventional image fusion in terms of spatial information preservation and artifact rejection (Du *et al*., 2002). This fusion scheme should be used when there is a significant difference in pixel sizes, a factor of 2 or more, between the original input images.

3.6 Sea Ice

Of the many information requirements for operational Ice Centres such as the Canadian Ice Service (CIS), the following three are most important (Scheuchl *et al.,* 2004):

- Ice edge location
- Ice concentration
- Stage of development (sea ice type)

Ice Centres around the world use spaceborne single channel SAR data to obtain these parameters on an operational basis. These data are often supplemented with other optical and microwave imagery from sensors such as the NOAA AVHRR and the Special Sensor Microwave Imager (SSM/I). At the CIS, RADARSAT-1 is the primary data source for the production of daily ice charts. The requirement for daily revisit makes wide coverage modes like ScanSAR the modes of choice for operational use. In many cases the resolutions available for these modes are sufficient to satisfy strategic requirements.

RADARSAT-2 will offer dual polarization ScanSAR, thus providing one co-polarization and one cross-polarization channel. Nghiem and Bertoia (2001) study the potential of multi-polarization SAR data for sea ice monitoring and conclude that the availability of the cross-polarization channel in addition to a co-polarization channel results in a higher information content. The fully polarimetric modes of RADARSAT-2 have narrower swaths and are therefore less attractive for operational purposes. Nevertheless, these modes offer the opportunity to collect fully polarimetric SAR data of sea ice over one or more ice seasons. Such a data set will improve the understanding of ice signatures and their development during growth and decay. The following sections discuss the improved capabilities of multi-polarization and polarimetric SAR data, as well as data fusion techniques to enhance the information content of RADARSAT and AVHRR images.

3.6.1 Multi-polarization and polarimetric SAR for sea ice mapping / monitoring

Data Visualization

In the CIS operational environment, ice analysts visually interpret much of the data. Data visualization is therefore important to assure optimal information retrieval. The availability of more than one channel, as with the RADARSAT-2 SDP and QP modes, makes colour a natural choice for data visualization. Figure 3.6.1-1 shows an example how the RGB representation of an ENVISAT ASAR alternating polarization image increases the information content compared to either of the two greyscale images. The two-channel information is available in one single image thus making visual interpretation easier. Open water, easily visible in HV but not in HH can clearly be identified in the colour image (blue). Landfast ice, located at the southern coast of Anticosti Island, is easily visible in HH but not in HV. In the colour composite landfast ice shows as a dark stripe between the island and the open water area.

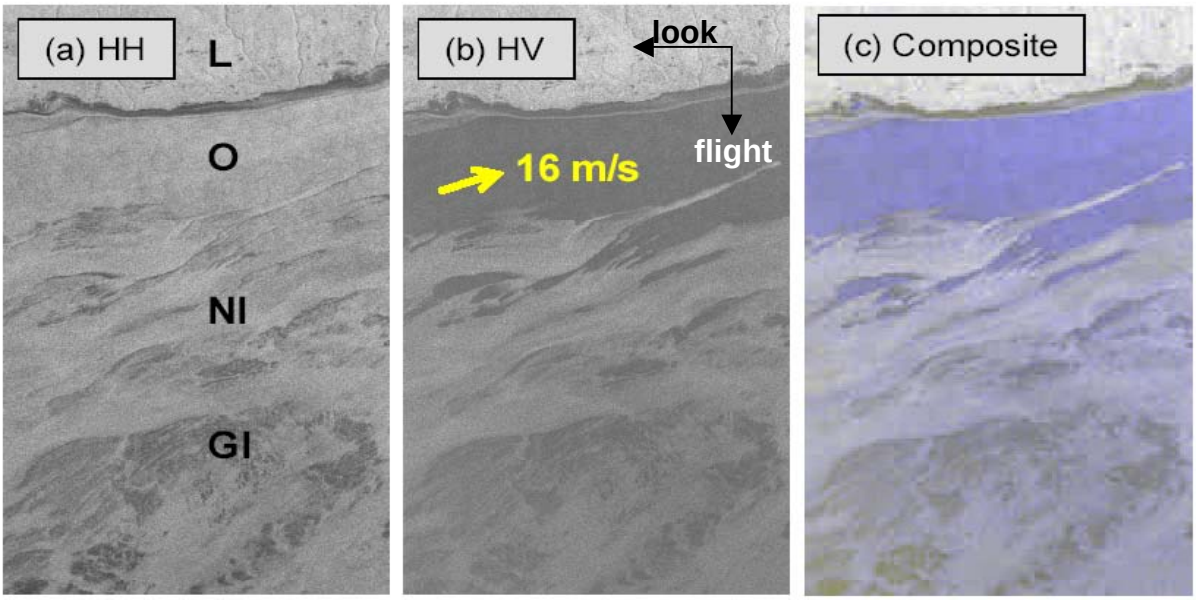

Figure 3.6.1-1 Marginal ice zone subset of Feb. 7, 2003 ENVISAT ASAR alternating polarization image acquired in beam IS4 (31-36º): (a) HH, (b) HV and (c) colour cross-polar composite (HV (Red, Green), HH (Blue)). L= land, O= open water, NI= new ice and GI= young ice. Modelled wind speed and direction shown in (b) The image dimensions are approximately 67.5 km in range and 100 km in azimuth. (DeAbreu *et al.,* 2003)

While colour can be used to represent information in fine detail, it needs to be carefully applied as there is also a high risk for misinterpretation.

- For long term colour consistency, the use of calibrated data is suggested.
- Pre-defined value ranges are recommended to enhance the contrast in the images. Value ranges need to be carefully chosen to represent possible situations throughout an ice season.
- The colour of specific ice types will change with incidence angle. This is particularly the case for low incidence modes due to high variation in the surface backscatter component.

SAR Data Classification

In principle, the three key ice information requirements present challenges for classification. For both ice edge location detection and ice concentration estimation the ability to distinguish between open water and sea ice is critical. The backscatter of sea ice and open water are often different, thus allowing the separation of the two. The most problematic situation occurs when environmental conditions are such that the backscatter of sea ice is very similar or equal to the backscatter of open water. High winds, for example, will raise the backscatter of water whereas melting conditions will lower the SAR return from sea ice. The availability of more than one channel shows great potential for resolving some of these ambiguities (Figure 3.6.1-1). In this example, the cross-polarized channel provides vital information on the ice edge as open water shows good contrast to new ice. No such contrast can be seen in the co-polarized channel due to a wind roughened water surface.

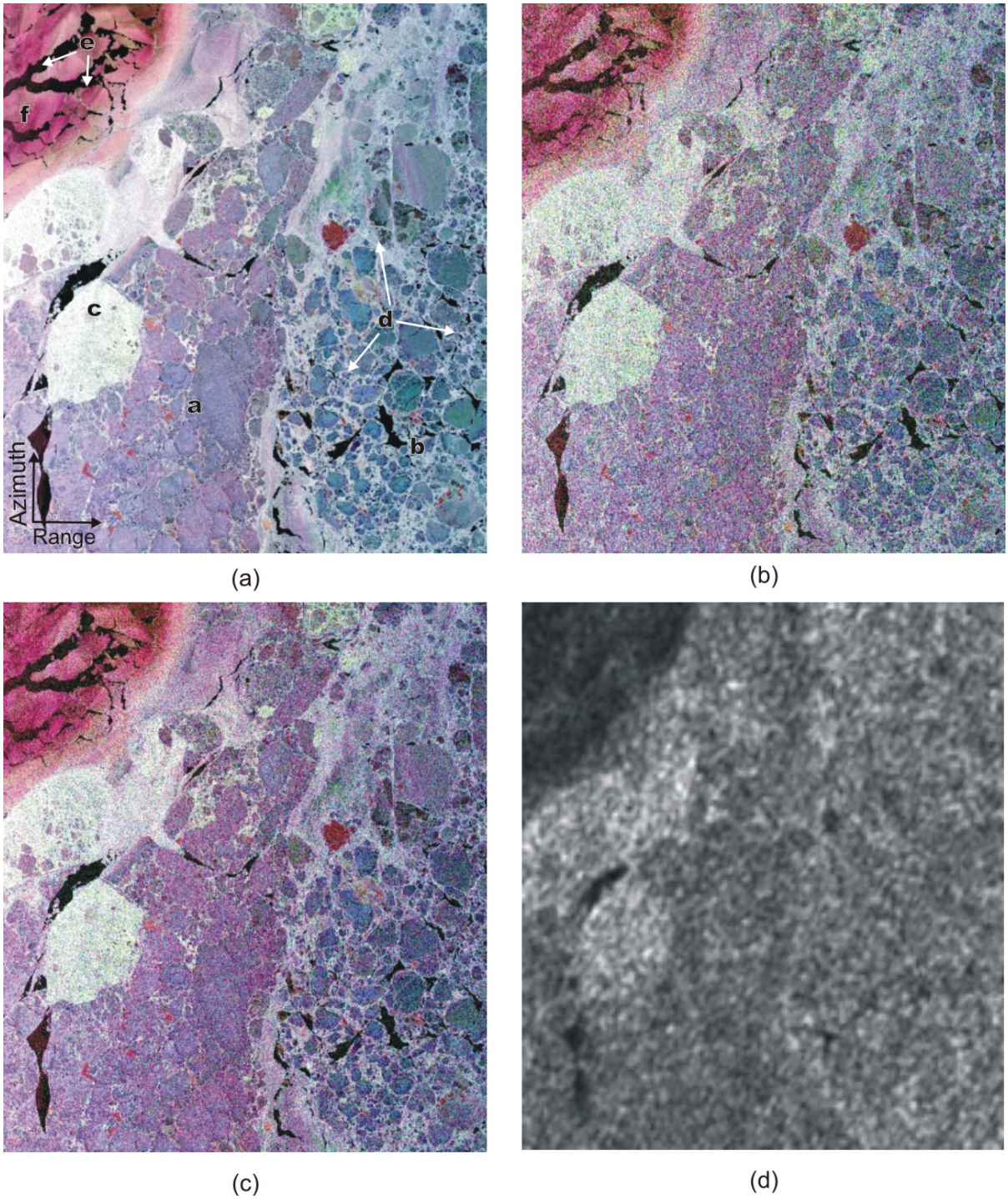

Figure 3.6.1-2 (a-d) Polarimetric data of sea ice (VV Red, HV Green, HH Blue). The image dimensions are approximately 6.4 km in range and 8 km in azimuth. The data are shown in comparable pixel dimensions (between 12 and 17 m); pixel averaging was performed. (**a**) Convair-580 polarimetric data (40x4 pixels averaged) in comparison with (**b**) simulated RADARSAT-2 data in Standard mode (3x1 pixels averaged) and (**c**) Fine mode (3x3 pixels averaged). (**d**) The grey scale image is a 50 m resolution RADARSAT-1 ScanSAR image (only approximate coverage here, look and flight direction differ from the other scenes).

Previous research also shows great potential of fully polarimetric SAR data for sea ice classification, i.e. the estimation of ice stages of development (Drinkwater *et al*., 1992; Eriksson *et al*., 1998; Rignot *et al*., 1992; Scheuchl *et al*., 2001a,b). The Canadian Ice Service relies on human interpretation of single polarization SAR images and other satellite data to produce daily ice charts. Ice concentration and the ice stage of development for up to three classes are presented in the WMO defined egg code (MSC 2002). Multi-polarization and polarimetric SAR data provide more information content compared to a single channel SAR image and will help in the interpretation of classification results. The presentation of ice information is very specific making fully automated information retrieval nearly impossible. While automated classification methods are being researched, human expertise will remain crucial for sea ice classification in the near future due to the high variability of ice signatures over an ice season.

Figure 3.6.1-2 shows an example of an airborne polarimetric SAR scene of first-year sea ice. The data was acquired in the Northumberland Straight on March 8, 2001 in freezing conditions. Also shown in Figure 3.6.1-2 are simulated RADARSAT-2 fully polarimetric data. The simulations are based on the Convair-580 acquisition. The airborne data was filtered in the range and azimuth directions to reduce the bandwidth to that of RADARSAT-2 data and noise was added to raise the noise level to values representative of the spaceborne system. For better comparison of the images adjacent pixels were averaged to achieve comparable pixel dimensions (between 12 and 17 m). The different levels of averaging affect the amount of speckle visible in the images. The Convair-580 image shows the least speckle as 160 pixels were averaged. Not representative for RADARSAT-2 is the incidence angle range covered by the data (41° to 64° compared to 20° to 49° for RADARSAT-2).

The scene can be divided into 6 different classes:

a) large, smooth first-year ice floes in near range (purple)
b) smooth first-year ice floes in far range (blue)
c) rough floes (grey to white)
d) compressed or ridged ice (white)
e) leads of open water or possible new ice (black)
f) large area of young ice (grey ice) in near range (red – at top left corner of the image). Other patches of the same ice type are scattered throughout the image.

Figure 3.6.1-3 (a) shows an example classification result for the airborne data using the complex combined H/A/alpha - Wishart classifier (Lee *et al.,* 1999). The method was slightly adjusted as only 6 classes are desired. The result corresponds well to a visual interpretation of the airborne RGB image. Scheuchl *et al*. (2003 a,b) present more detailed information on the data analysis.

Applying the same classification concept to the simulated RADARSAT-2 data (Figure 3.6.1-3 (b)) leads to a result where the higher noise level and the fact that significantly fewer looks were averaged causes some confusion between far range first-year ice floes and leads. The cross-polarized channel is particularly affected by the increase in the noise floor as it is usually around 10 dB below the co-polarized return. This is a greater issue for sea ice applications than for land as backscatter from sea ice is generally lower. Nevertheless, the information content of polarimetric data exceeds the information content of single polarization data of comparable resolution.

The rich information content of fully polarimetric data is illustrated in Figure 3.6.1-4. Here example information for two different classes is presented. This information can be used to

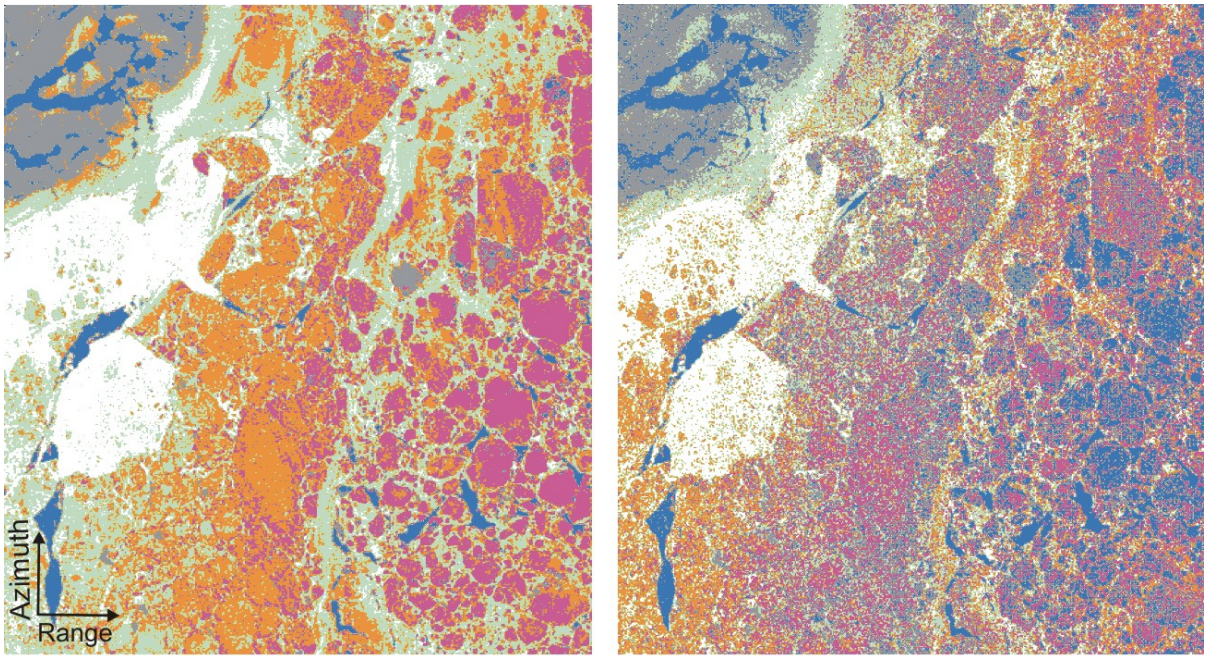

(a) (b)

Figure 3.6.1-3 (a-b) (**a**) Convair-580 classification result (40x4 pixels averaged) in comparison with (**b**) classification of simulated RADARSAT-2 data in Fine mode (3x3 pixels averaged). Less averaging and an increased noise level result in a decrease of classification performance compared to airborne data, nevertheless, there is potential for the discrimination of ice stages of development.

interpret the classification result. Not only are a large number of different parameters available, some of them allow a direct physical interpretation of the scattering. Examples of these parameters are the entropy (H), anisotropy (A), and α-angle which are based on the eigenvalue decomposition of the Coherency matrix (Cloude and Pottier, 1997), or the Freeman-Durden components which represent surface (Ps), volume (Pv) and dihedral (Pd) scattering (Freeman and Durden, 1998). The polarization response plots show a significant difference between the two classes presented.

Some of the parameters are summarized for all six classes in Table 3.6.1-1. A number of parameters show differences in the classes rather well, while others have only subtle differences. For example, the signatures of leads and young ice are similar except for the total power (TP). In particular the co-polarized ratio (HH/VV < -5 dB) as well as the ratio between the Freeman-Durden surface and volume scattering components (Ps/Pv > 7 dB) separate the two from first-year ice classes. The polarimetric Entropy (H < 0.5) also provides a clear separation. Not as conclusive are the magnitude of the complex correlation ($|\rho_{HHVV}|$), the Anisotropy (A) and the α-angle. An entropy value of < 0.5 in combination with a low α-angle (<40°) indicates dominant surface scattering, which is supported by the surface to volume ratio of the Freeman-Durden components. An increased contribution of volume scattering can be noted for the first-year ice classes. This contribution is relatively small compared to the surface scattering component for these classes except for the rough first-year ice class, where Ps/Pv reaches 3 dB.

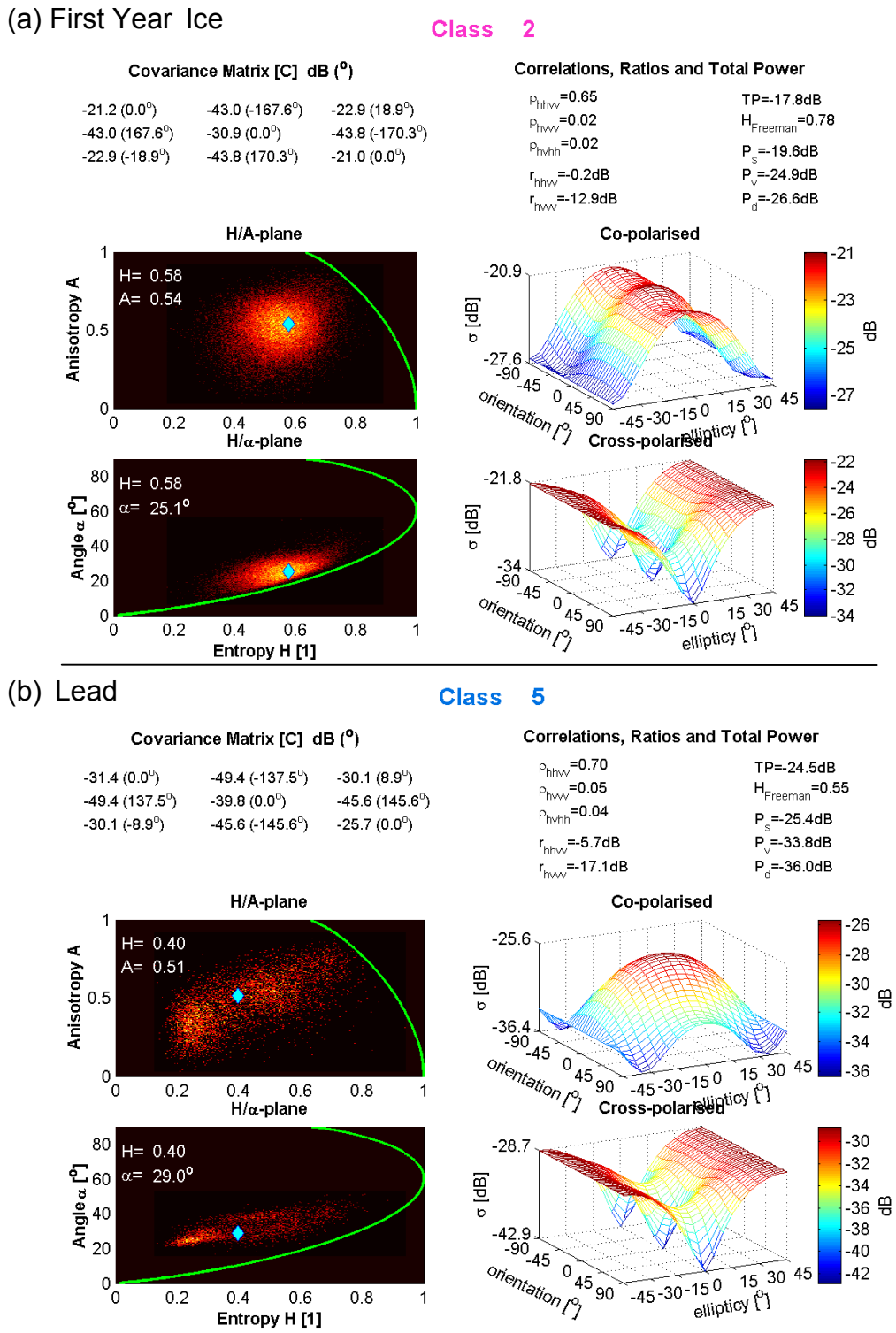

Figure 3.6.1-4 (a-b) Convair-580 data class mean information for (**a**) first-year ice and (**b**) leads. Information provided includes the covariance matrix (C), channel correlation magnitudes (ρ), channel ratios (r), the total power (TP), target decomposition parameters for Freeman-Durden (Ps,Pv,Pd) and Cloude-Pottier (H,A,α) as well as polarization response plots.

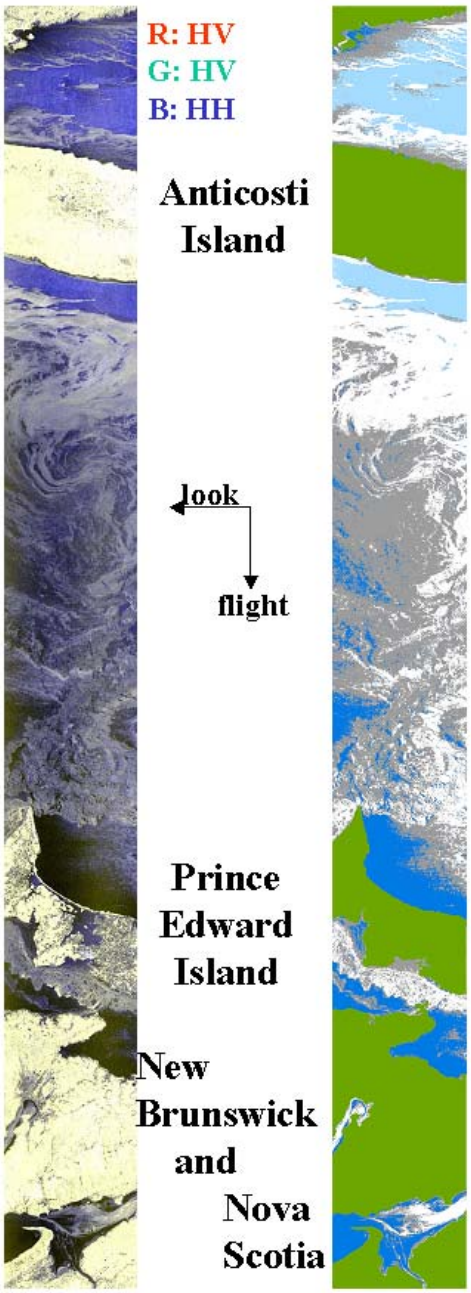

Figure 3.6.1-5 RGB representation (left) and classification result (right) for an ASAR alternating polarization medium resolution product (IS4). The scene was acquired on February 7, 2003. A subset available in higher resolution is shown in Figure 3.6.1-1. Land areas were excluded from the classification and are shown in green. Dark blue describes new ice (for the most part), light blue is interpreted as wind roughened open water. White and grey are used to indicate sea ice types.

Table 3.6.1-1 Class average values for polarimetric parameters (see text for description)

Ice Type	TP [dB]	HH/VV [dB]	Ps/Pv [dB]	$\lvert\rho_{HHVV}\rvert$ [1]	H [1]	A [1]	α [°]
Leads	-24.5	-5.7	8.4	0.70	0.40	0.51	29.0
Young Ice	-16.1	-5.7	10.0	0.84	0.28	0.41	25.7
FYI (floes, far range)	-17.8	-0.2	5.3	0.65	0.58	0.54	25.1
FYI (floes, near range)	-15.0	-0.5	5.6	0.69	0.54	0.50	23.8
Ridged FYI	-12.9	-0.4	4.9	0.68	0.57	0.46	22.9
Rough FYI (strong HV)	-10.3	-0.5	3.0	0.70	0.60	0.27	22.2

The classification of dual polarization data is possible using, for example, a modified Wishart Classifier. Figure 3.6.1-5 shows a classification result for ENVISAT ASAR alternating polarization medium resolution data (equivalent number of looks = 50). The result corresponds well to the RGB image; in particular open water is well separated from sea ice. This example illustrates the high potential of dual polarization data for sea ice monitoring.

Summary

The new RADARSAT-2 capabilities will enhance the information content retrievable from spaceborne SAR data. For sea ice monitoring the *combined* use of a co-polarization and a cross-polarization channel are beneficial for both visual and machine interpretation. The noise level of the system will affect classification performance as the cross-polarized channel intensity of sea ice is generally low and there is potential for it to be masked by noise in some areas. Multi-looking or the application of filters is recommended to reduce the effect of speckle.

Fully polarimetric data provides even more information, specifically on the nature of the scattering. The increased information needs to be traded off with greatly reduced coverage, thus making fully polarimetric RADARSAT-2 modes less attractive for operational sea ice monitoring. There is a high research value in collecting and investigating fully polarimetric SAR data over a full ice season to better understand sea ice signatures.

3.6.2 RADARSAT-1 and AVHRR image data fusion

The CIS promotes safe and efficient maritime operations and protects Canada's environment by providing reliable and timely information about ice and iceberg conditions in Canadian waters. The CIS relies on a suite of both airborne and spaceborne remote sensors to operationally monitor ice conditions in Canadian coastal and inland waterways. Currently the CIS receives daily RADARSAT-1, AVHRR, QuikSCAT (Seawinds), SSM/I, and Operational Linescan System (OLS) image data. Ice analysts select and view georeferenced, coregistered imagery within a GIS-like environment. Information from these data must be extracted within a time-sensitive operational production schedule. RADARSAT-1 serves as the primary dataset given its spatial resolution and ability to provide data regardless of illumination or cloud conditions. Unique, complementary ice information is acquired from the other sensors, albeit at coarser resolutions and over wider swaths. Given the limited time available to analysts to examine imagery, CIS actively pursues methods to maximize their ability to extract relevant ice information from all sensors in their image catalogue. As such, methods to consolidate ice information from more then one sensor into a single product or image for analysts is an active research area at the CIS.

Figure 3.6.2-1 Subset of July1, 22:28 GMT (2001) RADARSAT ScanSAR Wide Scene (Copyright Canadian Space Agency, 2001).

A popular goal of image data fusion investigations is the integration of high resolution single channel datasets with coarser resolution multispectral datasets. The ultimate goal is the creation of one image with useful multispectral information at the high resolution of the monochromatic dataset. The two primary image datasets at the CIS are ScanSAR Wide RADARSAT-1 data (single channel, high resolution (100 m)) and multispectral AVHRR data (5 visible and infrared channels, nominal resolution 1.1 km). Both datasets offer unique ice information. RADARSAT-1 provides detailed information on ice type (e.g. thinner ice vs. heavier pack ice), ice roughness and, conditions allowing, good ice-water separation (Figure 3.6.2-1). Analysts can find most of their ice information in RADARSAT-1 data. However, the contrast between ice types and water is often much reduced in RADARSAT-1's near-range due to the comparably high backscatter from wind-roughened open water areas. The landfast ice edge and an adjacent large ice flow are barely visible in the RADARSAT image in Figure 3.6.2-1. Unfortunately, RADARSAT-1 is not always capable of separating ice and open water areas – a critical task for the ice analyst.

At a coarser resolution and with more frequent coverage, AVHRR data (Figure 3.6.2-2) provides dependable ice-water separation, sea ice melt information and ice temperature information, useful for assessing new and young ice thickness. Unlike RADARSAT-1, AVHRR's sensitivity to the snow layer covering sea ice precludes it from providing ice roughness over most sea ice surfaces. However, for the same reasons, it is effective at mapping and monitoring spring sea ice melt. Also, due to their high contrast in optical and thermal characteristics, ice and open water are consistently separated using spring and summer AVHRR channels 1 and 2 (visible, near infrared) and winter and spring AVHRR

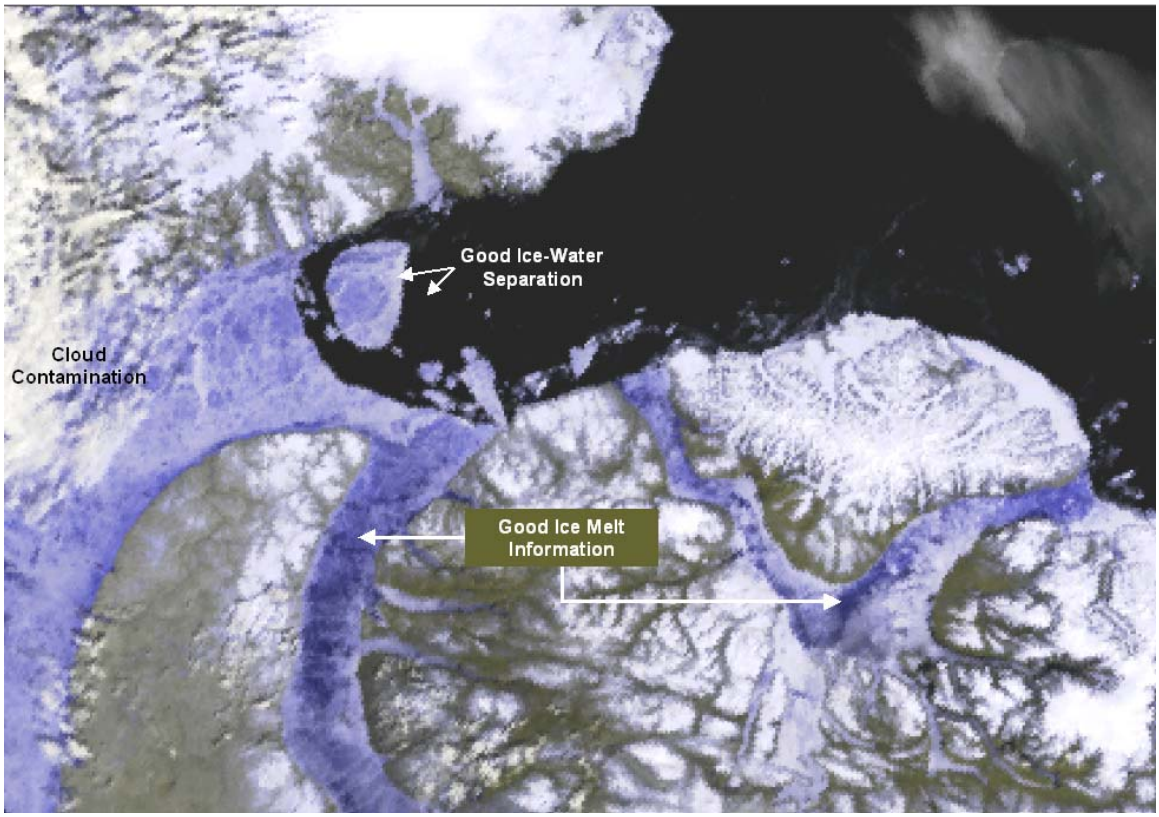

Figure 3.6.2-2 July 2, 16:36 GMT (2001) AVHRR composite image (Red-Ch. 2, Green-Ch. 2, Blue-Ch. 1)

channels 4 and 5 (thermal infrared) data. Unfortunately, these types of data cannot image the surface through cloud cover and fog. The AVHRR image in Figure 3.6.2-2 is a multi-band composite of the visible and infrared channels – Ch. 2 (red), Ch. 2 (green) and Ch. 1 (blue). This composite provides realistic image colouring and is effective at both providing ice-water separation and monitoring sea ice melt.

CIS analysts typically examine RADARSAT-1 data first and then will turn to other datasets (often AVHRR) to solve any ambiguities present in the interpretation of the SAR data or to derive other sea ice information not available in the SAR. CIS is currently examining methods of producing a fused image that offers the ice information of RADARSAT-1 and AVHRR in one product. Ideally, CIS analysts would eventually consult one fused image instead of two separate datasets. At the minimum, any fused product should preserve the high-resolution information of the SAR data and preserve the colour fidelity of the AVHRR composite. This will be the baseline metric to assess the variety of fusion techniques available. The CIS goal of data fusion goes beyond a data reduction exercise. Also of interest is the potential of any fused product to provide new sea ice information, not available in the two original products.

Figure 3.6.2-3 contains one example of a fused image based on the RADARSAT-1 and AVHRR composite discussed above. The image was created using a common image fusion technique based on Principal Component Analysis. This spectral domain technique involves transferring the multispectral 5-band AVHRR image into new spectral space by extracting its five principal components. The first principal component image was then replaced with the higher resolution SAR image and the results were transformed back into image space using

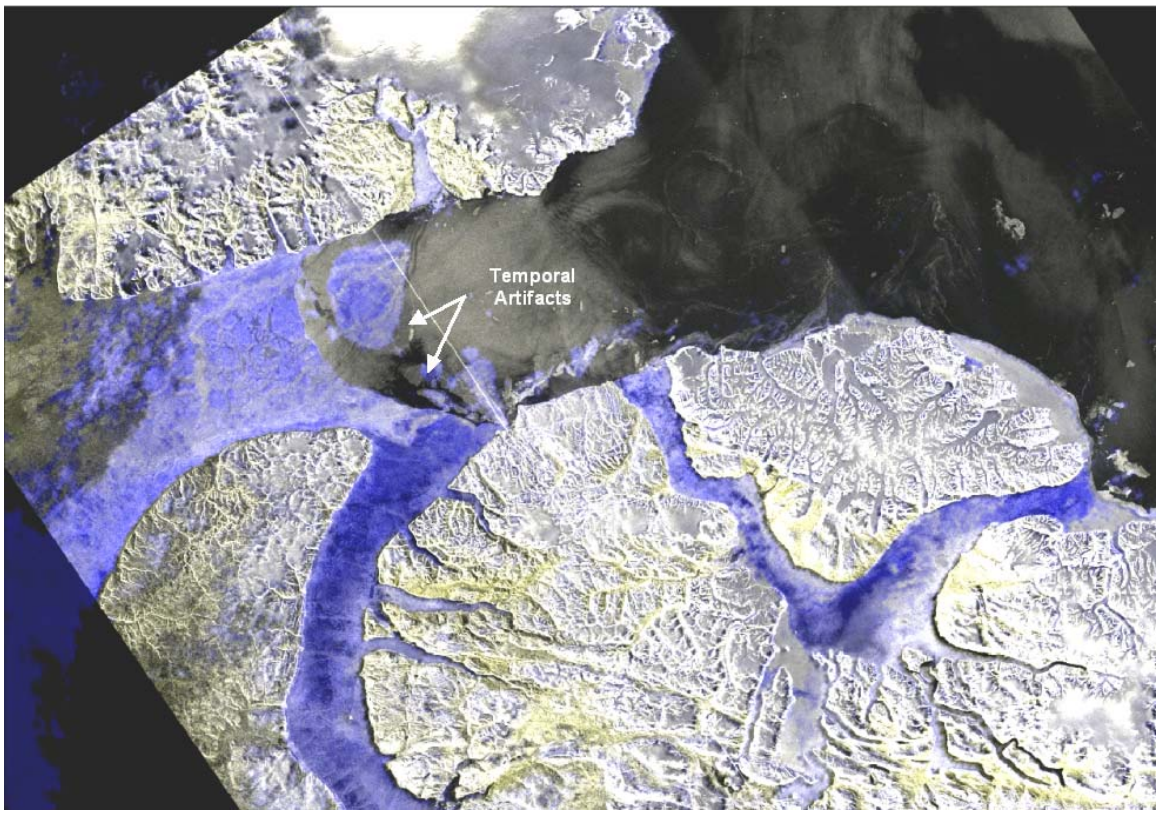

Figure 3.6.2-3 Fused image-based RADARSAT-1 ScanSAR Wide (acquired July 1, 2001, 22:28 GMT) and AVHRR composite (acquired July 2, 2001, 16:36 GMT).

the inverse principal component transformation. Although computationally intensive compared to other techniques, this approach has been found to be effective at maintaining the radiometrics of the original multispectral image, an important trait for CIS purposes. The resultant image appears for the most part to preserve the important radiometrics and information of the AVHRR data, while providing the high-resolution information of the RADARSAT image. The example images shown here were acquired more than 24 hours apart, so any movement of ice in the scene resulted in temporal artifacts in the product. The CIS will be investigating this and other fusion techniques in the near term to determine the optimal method of integrating these two image datasets within an operational environment.

BLANK PAGE

4 Selected Software Tools

In this chapter we present selected software tools for use with RADARSAT-1 and/or polarimetric data. We discuss the RADARSAT-1 Stereo Advisor software package, which has the potential to be upgraded to the improved specifications of RADARSAT-2, the Polarimetric Work Station (PWS) developed at CCRS, and the SAR Polarimetric Post Processor (SARP3) developed at CSA.

4.1 RADARSAT Stereo Advisor

Mapmakers and other illustrators have traditionally used rendering techniques such as shading, overlapping and perspective views to give an impression of three dimensionality. In the last 200 years, many advances in representing three dimensions have been made. Stereo models, anaglyphs, chromo-stereoscopic images and holograms can provide three-dimensional (3-D) information about our planet that flat, two-dimensional (2-D) images cannot.

Why is it important that the third dimension be conveyed? Humans are naturally able to see in three dimensions. The 'naturalness' of a 3-D representation of reality enhances our ability to interpret 2-D imagery. Cartographers, engineers, geologists, hydrologists, and other scientists use 3-D viewing methods, such as stereo viewing of aerial photos and satellite images, in order to better understand the Earth's surface. Representation of the third dimension supplies important information about relationships between land shape and structure, slopes, waterways, surface material and vegetative growth.

A training package has been designed at CCRS to demonstrate the feasibility and potential of stereoscopy with respect to RADARSAT-1 data. However, it will also apply to RADARSAT-2. In fact, RADARSAT-1 and -2 imagery are both well suited to be used in stereo because the imagery can be collected from different look directions, beam modes, beam positions, and at resolutions fine enough to provide a good level of detail of the Earth's surface. The training package is intended to provide the background needed to use RADARSAT data in stereo, and can be accessed at:
http://www.ccrs.nrcan.gc.ca/ccrs/learn/tutorials/stereosc/stereo_e.html
The package is not intended to review and discuss in great detail the topics in each section. A bibliography has been provided for those interested in pursuing any of the topics in greater detail.

Following the introduction, the second section provides background on 3-D visual ability. In this section, human visual perception with regards to both depth and colour is discussed. The third section is a description of various methods used, historically and presently, to display 3-D information. The fourth and fifth sections discuss stereo and radar basics respectively. The sixth section provides a short description of RADARSAT and its ability to acquire data specifically for stereo usage. Lastly, examples of RADARSAT and other remotely sensed data are used to illustrate concepts discussed in the previous sections and to showcase RADARSAT imagery in stereo. This section provides users of this manual with hands on experience and should enable them to decide on how to generate the best stereo pair for a given application.

The RADARSAT-1 Stereo Advisor is intended for anyone interested in Earth sciences (hydrology, geology, forestry, agriculture, cartography, etc.) and/or in the three-dimensional representation of the land surface. The advisor can benefit users who wish to create a digital elevation model from RADARSAT images, either to represent the land topography or to geometrically correct images for the extraction of thematic information. It will assist the users, in an interactive way, in making the best choice of a RADARSAT image pair for creation of stereo pairs. However, it is not intended for people interested in selecting only one image. According to the type of thematic information the user wants to extract, the characteristics of the study site and the user-specified requirements or constraints related to image acquisition, the RADARSAT-1 Stereo Advisor makes one or two recommendations (Cyr and Toutin, 2001).

The Stereo Advisor is a web-based tool used to help in the selection of stereo RADARSAT images (see http://www.ccrs.nrcan.gc.ca/ccrs/data/advisor/advhlp_e.html for more information). The user must input information related to the specific application and study site (Figure 4.1-1). The advisor will then:

define the user's needs and constraints in the matter of stereoscopy;

evaluate geometric and radiometric parameters involved and related to the sensor, to the observed terrain, to the application domain and to the user's focus of interest (type of information that the user wants to extract); and

suggest one or two stereo pair(s) most appropriate to the situation.

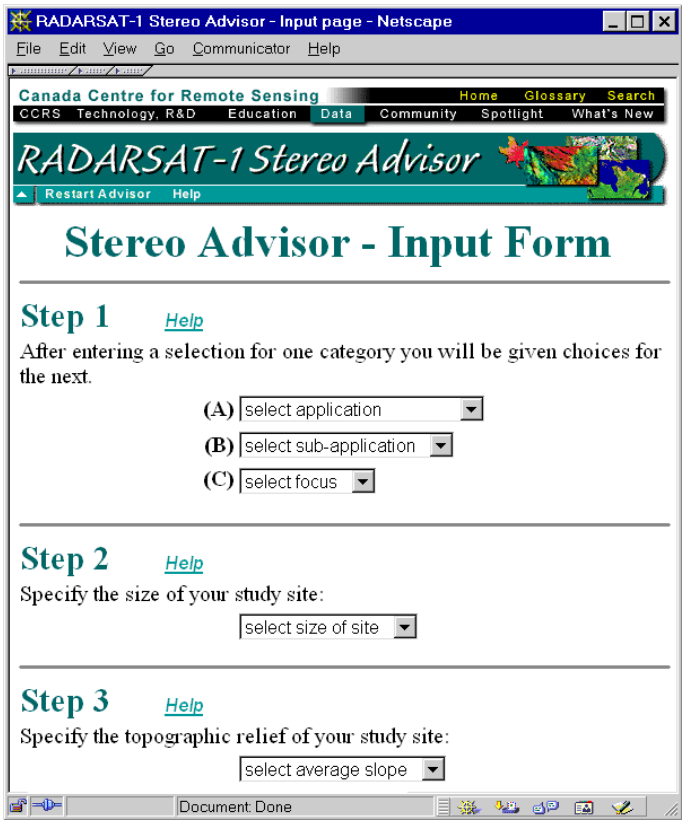

Figure 4.1-1 RADARSAT-1 Stereo Advisor input form to be completed by the user.

The suggested stereo configuration will be accompanied by explanations, comments and recommendations that will help the user understand the reasons why these stereo pairs are suggested. However the user must make the final choice according to his/her own criteria.

The advisor has the advantage of providing one or two solution(s) that are adapted to each situation and each user scenario. The user must then run the Stereo Advisor for each application. Therefore, different stereoscopic configurations could be suggested for the same study site as a function of the user-specified requirements. In the case where the user has already acquired one RADARSAT-1 image, the advisor will recommend a second image to complete the stereo pair.

Educators are invited to make use of the module to provide an interactive didactic tool to their students for studying the topic of radar imagery for stereo applications. The context-specific comments provided here with each stereo image pair recommendation are particularly useful for explaining the rationale of RADARSAT-1 beam mode selection. In addition, the "Further Study" section links this tool to other related and useful resources on the CCRS Web site, and to suggested bibliographic references.

While this advisor makes recommendations for selecting images by specifying beam modes of RADARSAT-1, it could be upgraded to RADARSAT-2 images by taking into consideration its new specifications (Ultra-High resolution and polarimetry) and new research and development. The Ultra-Fine mode of RADARSAT-2 would enable the generation of DEMs with accuracy better than 5 m using ground control points. Conservative estimates of accuracy range from 5-10m. In addition, the improved orbit control of RADARSAT-2 will facilitate more accurate absolute positioning of features.

4.2 Polarimetric Work Station

To facilitate research and application development with full polarimetric SAR data, CCRS staff have developed a software suite referred to as the ‘Polarimetric Work Station’ (PWS). The user-friendly PWS software is built on over ten years experience in polarimetric image analysis and includes a knowledgeable selection of polarimetric tools reported in the open literature. On request, PWS will be licensed for free to Canadian government institutions and academia. Canadian industry may obtain a PWS licence for a symbolic price.

4.2.1 System requirements

Although developed using MATLAB® software, the PWS toolkit can be run independent of a licence for this software on any PC platform operating with Windows NT or Windows 2000. Graphics display is optimized for 21” monitors but there are no special requirements in terms of the video card.

4.2.2 Compatible SAR data sources

PWS can read data from the following sources:

Convair-580 SAR

- Single-Look Complex (SLC); 8-byte complex, 4 polarization channels (HH, VV, HV, VH)
- Georeferenced; 10-byte, compressed cross-products of scattering matrix
- Geocoded; 10-byte, compressed cross-products of scattering matrix

Shuttle Imaging Radar (SIR-C)

- Single-Look Complex (SLC); 8-byte complex, 4 polarization channels (HH, VV, HV, VH)
- Multi-Look Complex (MLC); 10-byte, compressed cross-products of scattering matrix

NASA/JPL AIRSAR

- Single-Look Complex (SLC); 8-byte complex, 4 polarization channels (HH, VV, HV, VH)
- Precision data; 10-byte, compressed elements of the Stokes scattering operator (sometimes loosely referred to as Stokes matrix or Mueller matrix).

4.2.3 PWS functional description

PWS comprises a series of tools for:

- loading of compatible image types (see section 4.2.2)
- synthesis of images for any transmit-receive polarization combination
- synthesis of images comprised of pixels representing polarimetric variables
- image display
- computation of polarimetric variables for definable image areas of interest.

Please refer to Appendix III for a detailed description of the functionality of PWS.

4.3 SARP3: Polarimetric SAR Training Tool

The SAR Polarimetric Post Processor (SARP3) is a freeware training tool, developed at CSA to prepare the RADARSAT-2 user to utilize the new fully polarimetric SAR imaging modes. Users can perform polarimetric synthesis, extract polarimetric signatures, and conduct signature decomposition and threshold filtering using various fully polarimetric SAR data products acquired by a variety of SAR sensors. Related outputs can also be viewed. SARP3 is Windows based, developed using Visual Basic and the Windows 2000 (and above) operating system.

The tool (Figure 4.3-1) can ingest various image data formats including Convair-580 data formats, SIR-C compressed Stokes matrix and single look complex scattering matrix. Currently seven data formats can be ingested. Internally the tool keeps both scattering and stokes matrix representations.

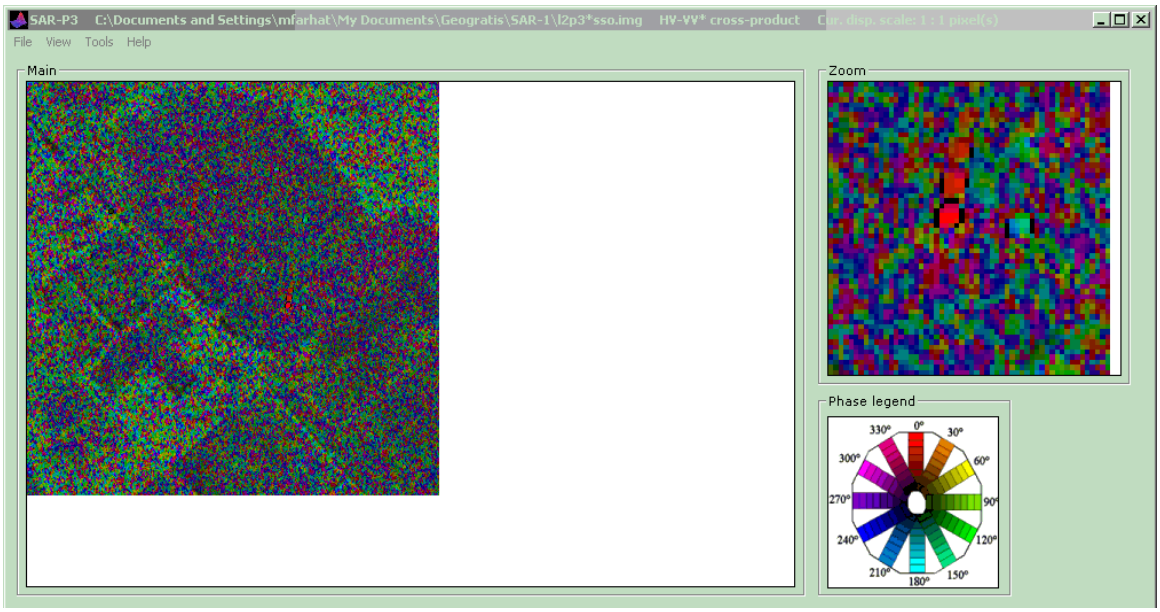

Figure 4.3-1 SARP3 main window

Images can be displayed in grey levels or using various 8-bit colour schemes to represent amplitude and phase. Image selection functionality allows the user to choose a rectangular region on the synthesized image for further analysis. Zoom functionality as well as polarimetric signature extraction can be performed on the selection.

4.3.1 Image synthesis

The software is able to synthesize the following images from the Stokes matrix: Total power, HH, VV, HV, HH HV VV composites, phase only, HH-VV, HH-HV, and HV-VV (Figures 4.3.1-1(a) and (b)). Note the last three combinations are cross-products taken from the Stokes matrix and combine phase and intensity information.

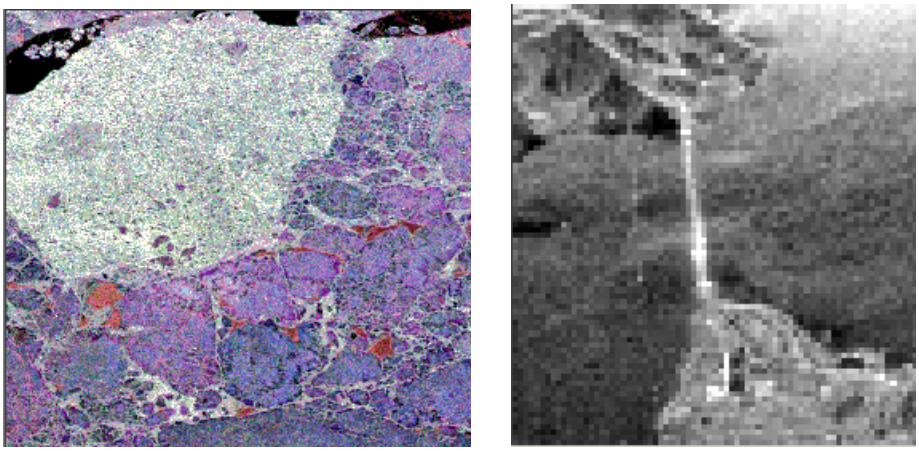

(a) (b)

Figure 4.3.1-1 SARP3 synthesized imagery. (a) Sea Ice, HH HV VV composite image. (b) Golden Gate Bridge.

4.3.2 Polarimetric signatures

Image selection is used to generate polarimetric signatures (Figure 4.3.2-1). If more than one pixel is selected then an average Stokes matrix of target pixels is computed to obtain the signature. Signatures are computed using a range of values of ellipticity and orientation. Both co-polarized and cross-polarized signatures can be computed. For the co-polarized case, both Stokes vectors are set with identical values, whereas in the cross-polarized case, the ellipticity of the receive antenna is set orthogonal to the transmit antenna ellipticity value by subtracting 90°. The software also comes with prototype theoretical signatures computed for simple geometrical shapes. These shapes are: the sphere, the dihedral, the cylinder (selective orientation) and the helix.

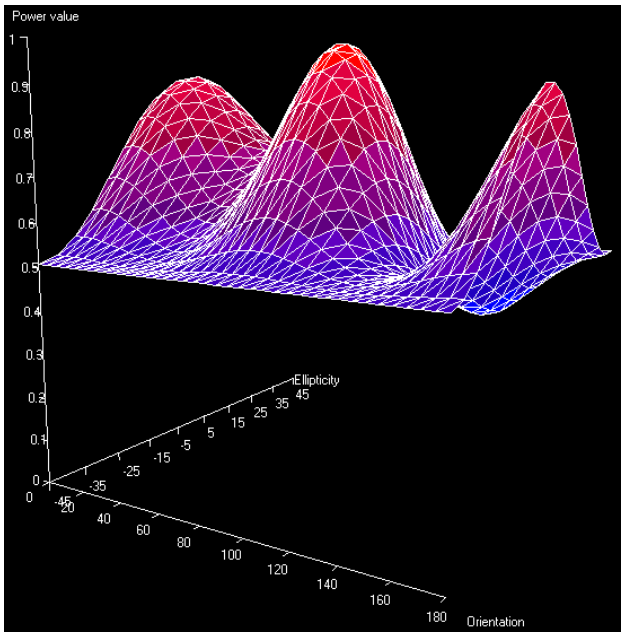

Figure 4.3.2-1 Golden Gate Bridge polarimetric signature

4.3.3 Signature decomposition

SARP3 also offers polarimetric signature decomposition using the Krogager coherent decomposition method (Figure 4.3.3-1). This function is applicable to complex scattering matrix data and yields an image representing an absolute contribution of three basic shapes: the sphere (odd number of reflections), the dihedral (even number of reflections) and the helix.

Two files are output from the signature decomposition: a colour coded graphics file and a text file representing three channels (signatures) of data.

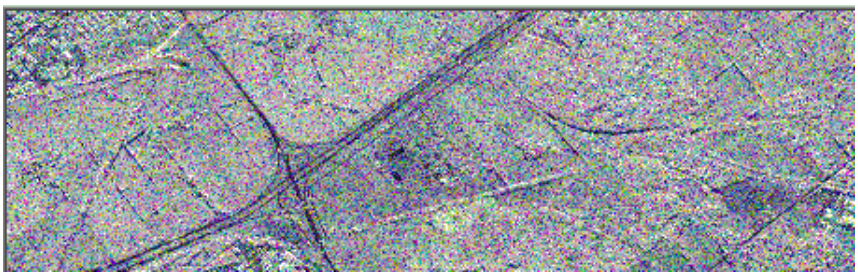

Figure 4.3.3-1 Agricultural fields - polarimetric decomposition using the Krogager coherent decomposition method.

4.3.4 Polarimetric filter

The polarimetric filter is used to threshold the output from the signature decomposition algorithm, i.e. three channels representing helix, sphere and dihedral scatter. The outcome of threshold filtering is an image where the pixels in the three channels are either set to the same output of the decomposition function or set to zero (Figure 4.3.4-1). This means decomposition values are not modified, just switched on or off depending if they meet threshold criteria. Thresholds are either band-pass or band-stop and are set by the user.

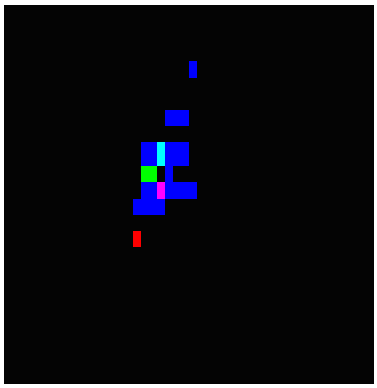

Figure 4.3.4-1 Ship pixels filtered using the SARP3 polarimetric filter.

4.3.5 Conclusion

A SAR polarimetry freeware training tool has been developed and made available to a wide range of potential RADARSAT-2 users. An essential representative subset of fully polarimetric SAR image synthesis and analysis functions have been implemented. The tool is a critical component for hands-on introductory polarimetry workshops being delivered with a set of polarimetric images and instructional material. To acquire a copy of the SARP3 contact Polarimetry.Workshops@space.gc.ca

BLANK PAGE

5.0 Applications Summary and Recommendations

5.1 Applications Summary

Table 5.1-1 shows our revised assessment of the improvements in data information content and hence applications potential resulting from the most important technical enhancements embodied by RADARSAT-2. Our latest expectations regarding the combined effect of these technical enhancements on the overall applications potential of RADARSAT-2 are rated in Table 5.1-2. The differences between the ratings presented in this text and those presented in our first RADARSAT-2 applications report (van der Sanden and Ross, 2001; Tables 3.9-1 and 3.9-2) are minimal. Changes include an increase in anticipated impact of the SDP mode for ship detection from minor to moderate, as well as an increase in anticipated impact of the SSP mode for currents and coastal zone applications from minor to moderate. In addition, the application of sea ice topography and structure is expected to increase from minor to moderate for RADARSAT-2's selective look direction feature. Ratings that have been adjusted since publication of our first report are shown here in a light blue typeface. A comprehensive justification of these latest ratings is given in a paper published in the special issue on RADARSAT-2 of the Canadian Journal of Remote Sensing (van der Sanden, 2004). For convenience, a copy of this paper is included in Appendix I of this report.

In the remaining paragraphs of this section, we summarize the results of the case studies presented in earlier sections of the current document and discuss, in general terms, how these contribute to the ratings shown in Tables 5.1-1 and 5.1-2. The presented results of combining RADARSAT-2 type products with those from other sensors are far from complete. However, they do illustrate clearly the increase in information content and hence applications potential of fused data products vis-à-vis radar data products alone.

The section on agriculture elaborated on the potential of multi-polarization and polarimetric C-band SAR imagery for application to the assessment of crop productivity (see 3.1.1) and crop condition (see 3.1.2). In addition, section 3.1.3 introduced and demonstrated the fusion of SAR and optical image data as well as of derived information products for the mapping of crop type, crop condition, soil tillage, and crop residue. Results presented in section 3.1.1 demonstrated that SAR data are sensitive to zones of productivity in wheat crops, but that this sensitivity is polarization dependent. The linear cross-polarized backscatter (HV) was found to be most sensitive to differences in wheat crop productivity. However, it was noted that growth cycle related changes in the canopy structure (e.g. grain filling) have a significant effect on the backscatter. Section 3.1.2 discussed preliminary observations from the polarimetric data acquired over fields of wheat, peas and canola. These observations indicated that linear and circular polarizations can be used to detect zones of crop condition characterized by variations in crop height and density. Section 3.1.3 drew from case studies and results reported in literature to convey the potential of data fusion for the generation of agricultural information products. Typically, SAR and optical image data can be considered as complementary sources of crop information.

In the cartography section we discussed the potential of spaceborne SAR in support of two application fields not specifically addressed in van der Sanden and Ross (2001), i.e. maritime boundary mapping (see 3.2.1) and moving object detection (see 3.2.2). Maritime

Table 5.1-1 Anticipated effect of new RADARSAT-2 features on applications potential in terms of data information content. Key: '-' minor, '-/+' moderate, '+' major.

	RADARSAT-2 Feature					
Application	**Selective Single Polarization**	**Selective Dual Polarization**	**Quad Polarization**	**Ultra-Fine Spatial Resolution**	**Selective Look Direction**	**Improved Orbit Control**
Agriculture						
Crop type	-	-/+	+	-	-	-
Crop condition	-	-/+	+	-/+	-/+	-
Crop yield	-	-	-/+	-/+	-	-
Cartography						
DEM interferometry	-	-	-	+	-	+
DEM stereoscopy	-	-	-	+	-	-/+
DEM polarimetry	N.A.	N.A.	+	N.A.	-	-/+
Cartographic feature extraction	-	-	-/+	+	-	-/+
Disaster Management						
Floods	-	-	-	-	+	-
Geological hazards	-	-/+	-/+	-/+	+	- (+) [1]
Hurricanes	-/+	-	-/+	-	+	-
Oil spills	-/+	-	-	-/+	+	-
Search and rescue	-	-	+	-/+	+	-/+ (+) [1]
Forestry						
Forest type	-	-	-/+	-/+	-	-
Clearcuts	-/+	-	-	-/+	-	-
Fire-scars	-/+	-	-	-/+	-	-
Biomass	-	-	-	-	-	-
Geology						
Terrain mapping	-	-/+	-/+	-/+	-	- (+) [1]
Structure	-	-/+	-/+	-/+	-	-
Lithology	-	-	-	-	-	-
Hydrology						
Soil moisture	-	-	-/+	-	-/+	-
Snow	-	-	-/+	-	-/+	-
Wetlands	-	-/+	-/+	-/+	-	-
Oceans						
Winds	-/+	-	-	-	-	-
Ships	-/+	-/+	-/+	+	-/+	-/+
Waves	-	-	-/+	-	-	-
Currents	-/+	-	-	-	-	-
Coastal zones	-/+	-/+	-/+	-/+	-	-
Sea and Land Ice						
Sea ice edge and ice concentration	-/+	-	-/+	-	-/+	-
Sea ice type	-	-	-/+	-	-	-
Sea ice topography and structure	-/+	-	-/+	-	-/+	-
Icebergs	-/+	-	-/+	+	-/+	-/+
Polar glaciology	-/+	-	-/+	-	+	- (+) [1]

1) Using InSAR techniques.

Table 5.1-2 Application potential of RADARSAT-1 and RADARSAT-2 [1]. Key: '-' minimal, '-/+' limited, '+' moderate, '++' strong.

	Satellite	
Application	**RADARSAT-1**	**RADARSAT-2**
Agriculture		
Crop type	-/+	++
Crop condition	-/+	++
Crop yield	-	-/+
Cartography		
DEM interferometry	+	+
DEM stereoscopy	++	++
DEM polarimetry	N.A.	-/+
Cartographic feature extraction	+	++
Disaster Management		
Floods	++	++
Geological hazards	-/+	+
Hurricanes	+	+
Oil spills	+	+
Search and rescue	-/+	+
Forestry		
Forest type	-/+	-/+
Clearcuts	-/+	+
Fire-scars	-/+	+
Biomass	-	-
Geology		
Terrain mapping	-/+	+
Structure	+	++
Lithology	-/+	-/+
Hydrology		
Soil moisture	-/+	+
Snow	-/+	+
Wetlands	-/+	+
Oceans		
Winds	+	++
Ships	+	++
Waves	-/+	-/+
Currents	-/+	+
Coastal zones	-/+	+
Sea and Land Ice		
Sea ice edge and ice concentration	+	++
Sea ice type	+	+
Sea ice topography and structure	-/+	++
Icebergs	-/+	+
Polar glaciology	-/+	+

1) Use of single date images assumed.

boundary mapping can be seen as a special case of cartographic feature extraction. RADARSAT-2's Ultra-Fine mode, selective look direction capability and improved orbit control are anticipated to improve the potential of this system in support of this application when compared to that of RADARSAT-1. Unlike its predecessor, RADARSAT-2 will offer the capability to detect moving objects and measure their radial velocity when operating in an experimental mode known as the Moving Object Detection Experiment. This unique feature has application to the detection of moving vehicles and vessels as well as to the measurement of moving natural targets such as ocean currents. MODEX data will be considered protected and will only be made available to other government departments with approval from the Department of National Defence.

Section 3.3 focused on the disaster management application field. The results of a case study examining the potential of C-band polarimetric SAR imagery for the characterization of oil spills were reported in section 3.3.1. These results complement the findings of the literature review presented in van der Sanden and Ross (2001) and confirm our earlier assessments regarding the anticipated effect of RADARSAT-2's new features on data information content and the satellite's overall applications potential. At the same time, a lack of polarimetric SAR observations over actual oil spills is noted to prohibit more comprehensive and hence more conclusive studies. Section 3.3.2 discussed the results of new case studies in the detection of crashed aircraft with the help of polarimetric SAR systems. Again, these results support our earlier assessments concerning the utility of the technical enhancements embodied by RADARSAT-2 and continue to indicate the potential use of this satellite system in support of Search and Rescue activities.

Applications in the field of geology were addressed in section 3.4. In 3.4.1 we discussed and demonstrated the fusion of RADARSAT-2 type data with magnetic data for mineral property mapping. The fused image products comprise information on terrain features and geological structures that originates from the radar data and information on geological units or lithology that is contributed by the magnetic data. The synergistic effect resulting from the integration of these two complementary data sources is seen in the 'strong' potential of the fused product for geological mapping. As discussed in van der Sanden and Ross (2001), and as shown once again in Table 5.1-2 of this text, the application potential of RADARSAT data alone for lithologic mapping is rated 'limited'. Section 3.4.2 expanded on our earlier discussion (section 3.3.2 in van der Sanden and Ross, 2001) concerning the application of spaceborne SAR data to the mapping and monitoring of geological hazards. The case study presented here illustrates the potential of repeat-pass InSAR techniques for the detection of deformation in landslide areas. It is anticipated that RADARSAT-2's enhancements in terms of spatial resolution, look direction and orbit control will benefit the application since they will enable the monitoring of smaller landslides on slopes outside of the line of sight of other SAR satellites.

In section 3.5 we discussed the use of data of the type to be expected from RADARSAT-2 and fused radar / optical image products in support of coastal zone and ocean applications. Section 3.5.1 reported on the potential of C-band SAR images with different polarizations for application to shoreline detection and section 3.5.2 discussed the potential of polarimetric SAR data for the mapping of coastal substrates. The results presented in 3.5.1 substantiate our earlier assessment regarding the higher potential utility of the HV polarization (relative to HH and VV) for shoreline detection in SAR images where the water-land backscatter contrast is reduced by high wind/wave conditions. In fact, the results indicate that the HV polarized image shows a backscatter contrast that is very close to the maximum possible backscatter contrast provided by the best performing (elliptical) polarization combination.

However, the lower sensitivity of the RADARSAT-2 SAR when acquiring HV or quad polarization images is pointed out as a potential threat to the measured contrast. Results shown in 3.5.2 demonstrate the potential of polarimetric C-band SAR data for the mapping of beach substrates and the quantitative assessment of the roughness of bare soil surfaces, subject to local incidence angle, but independent of variations in soil moisture and azimuth tilt. Section 3.5.3 introduced a new image fusion scheme based upon the wavelet transform and demonstrated its performance in a product created from the combination of a RADARSAT-1 ScanSAR image and a NOAA-AVHRR image (channel 4, thermal). The resulting product offers enhanced potential for the detection of ocean features such as currents, eddies, internal waves, slicks, etc.

The last section of chapter 3 – that is – section 3.6 addressed sea ice applications. In 3.6.1 we discussed the findings of case studies examining the potential of dual-polarization and polarimetric SAR data for the mapping and monitoring of the ice edge, ice concentration and ice type (i.e. stage of development). The sea ice type classification results support our earlier assessment with regard to the effect of the quad polarization feature on RADARSAT-2's potential in support of sea ice type mapping and monitoring. Fusion of RADARSAT and NOAA AVHRR data for the purpose of resolving ambiguities in ice-water identification is discussed and demonstrated in section 3.6.2.

5.2 Recommendations for Research and Development

The principal recommendations for applications research and development (R&D) are:

1. R&D in the context of RADARSAT-2 should focus on increasing the understanding of the image information content as a function of the polarization of the radar signal.
2. The primary R&D challenge lies in the extraction and application of the information contained in the data acquired in the Quad Polarization image mode.
3. R&D to prepare for the exploitation of RADARSAT-2's extended polarization capabilities should focus on application fields that hold the most promise for operational use of the relevant products.
4. There is a need for further studies into the in application potential of information products resulting from the fusion of RADARSAT-2 type data with data from other sources (e.g. ALOS PALSAR).
5. Calibration of Envisat ASAR data that are received and processed at the Canadian satellite receiving stations would facilitate applications R&D in preparation for RADARSAT-2.
6. Demonstration images in the data format selected for RADARSAT-2 products should be made available in support of the development of image analysis software.

The recommendations 1 to 4 were initially presented in our first RADARSAT-2 applications report and continue to remain valid.

Results reported in the present text are in agreement with these recommendations as they improve the understanding of the information content of RADARSAT-2 type multi-polarized and quad polarization data in a number of application fields. This includes applications in the fields of agriculture and sea ice – that is – applications which are expected to benefit the most from the technical enhancements embodied by RADARSAT-2. However, the increased complexity in dealing with the quad polarization data in particular continues to make research into its information content for different applications both valuable and challenging. The results of case studies that involved the fusion of RADARSAT-2 type data with other image data or derived information products are consistent with the fourth recommendation.

However, our discussion regarding data fusion methods and the application potential of fused data products is limited. Data fusion is not only a very broad topic but also remains an area of active research in most application fields. One reason for this is the growing availability and diversity of spaceborne imaging systems. The forthcoming Phased Array L-band SAR (PALSAR) onboard the Japanese Advanced Land Observing Satellite (ALOS) can be named as an example. This satellite system is scheduled for launch in 2004. Like RADARSAT-2, the ALOS PALSAR system will have the capability to acquire single polarization, dual polarization and polarimetric data. Many applications can be expected to benefit from the enhanced information content of the multi-frequency products that will result from the fusion of RADARSAT-2 and PALSAR data. Studies that examine the combined application of RADARSAT-2 and ALOS PALSAR data are therefore recommended.

In our first RADARSAT-2 applications report, we identified the Envisat ASAR system as a valuable future source of data for applications R&D in preparation for RADARSAT-2. Indeed, Envisat was successfully launched by the European Space Agency (ESA) on March 1 of 2002. Dual-polarized Envisat ASAR data products (HH+VV, HH+HV and VV+VH) have become available to the larger community of researchers and other users since late 2002. Although these advanced products were initially difficult to obtain, they are now more readily available. Hence, applications R&D activity using Envisat ASAR data products continues to be recommended. The results of such work are expected to provide better insight into the application potential of the RADARSAT-2 Selective Dual Polarization data products in particular.

The Canadian satellite receiving stations in Prince Albert, Saskatchewan and Cantley, Quebec have been receiving Envisat ASAR data since December 2002. The derived data products are readily available to selected government agencies (for more information see http://www.ccrs.nrcan.gc.ca/ccrs/data/order/details_e.html#envisat) but are not radiometrically calibrated and the tolerances on calibration (either absolute or relative) are unknown. This limits the applicability of these data sets because it precludes comparison of different (e.g. multi-temporal) images and extraction of reliable quantitative information. Initiatives leading to the calibration of Canadian Envisat ASAR products would certainly facilitate R&D efforts in preparation of RADARSAT-2 and are therefore recommended.

The airborne Convair-580 SAR continues to be the sensor of choice for the acquisition of polarimetric C-band data within Canada. Since publication of our first report in 2001 a series of pre-existing and newly acquired Convair-580 SAR images has been posted for download by interested parties on the following GeoGratis website from Natural Resources Canada:
http://geogratis.cgdi.gc.ca/clf/en?action=entrySummary&entryId=325&entryType=productCollection&keymap=outlineCanada.
These images, in combination with the software tools discussed in sections 4.2 and 4.3, represent a recommended basis for applications R&D in preparation for RADARSAT-2. A complete listing of the available images can be found in Appendix II of this report. Finally, it is recommended that demonstration images in the data format selected for RADARSAT-2 products (i.e. the GeoTIFF format) are made available in order to enable developers of both non-commercial and commercial image analysis software to prepare for the introduction of RADARSAT-2 data products.

References

Alberta Environment. (2000). *Geotechnical Hazard Assessment - South Flank of Frank Slide*, Hillcrest, Alberta, Edmonton.

Alpers, W. and H. Hühnerfuss. (1989). “The damping of ocean waves by surface films: A new look at an old problem”, *Journal of Geophysical Research*, Vol. 94, No. C5, pp. 6251-6265.

Bannari, A., D. Haboudane, H. McNairn, and F. Bonn. (2000). “Modified Soil Adjusted Crop Residue Index (MSACRI): A new index for mapping crop residue”, In: *Proceedings of the International Geoscience and Remote Sensing Symposium 2000 (IGARSS 2000)*, Honolulu, Hawaii, 24-28 July 2000, pp. 2936-2938.

Bouman, B.A.M. and H.W.J. van Kasteren. (1990). “Ground-based X-Band (3-cm wave) radar backscattering of agricultural crops. II. Wheat, barley, and oats; the impact of canopy structure”, *Remote Sensing of Environment,* Vol. 34, pp. 107-118.

Brisco, B., R.J. Brown and M.J. Manore. (1989). "Early season crop discrimination with combined SAR and TM data", *Canadian Journal of Remote Sensing*, Vol. 15, pp. 44-54.

Brisco, B. and R.J. Brown. (1995). “Multidate SAR/TM synergism for crop classification in western Canada”, *Photogrammetric Engineering and Remote Sensing*, Vol. 61, pp. 1009-1014.

Cameron, W.L., N.N. Youssef and L.K. Leung. (1996). “Simulated Polarimetric Signatures of Primitive Geometrical Shapes”, *IEEE Transactions on Geoscience and Remote Sensing,* Vol. 34, No. 3, pp. 793-803.

Chiu, S. (2000). “An Analysis of RADARSAT2 SAR-GMTI Performance for Standard Beam Mode”, DREO report TR 2000-088.

Chiu, S. (2002). “Parameter Estimation for the Phase Statistics in Interferometric SAR”, In: *Proceedings IASTED International Conference on Signal and Image Processing*, Kauai, Hawaii, USA, 12-14 August 2002.

Chiu, S. and C. E. Livingstone. (2001). “Spaceborne GMTI Processor Development for Canada's RADARSAT 2 Satellite”, In: *Proceedings of the NATO SCI conference*, Lisbon, 21-23 May 2001.

Chiu, S. and C. E. Livingstone. (2002). *A Comparison of Displaced Phase Center Antenna and Along-Track Interferometry Techniques for RADARSAT 2 Ground Moving Target Indication*. Defence Research Establishment Ottawa (DREO), Technical Report.

Cloude, R. and E. Pottier. (1996). “A review of target decomposition theorems in radar polarimetry”, *IEEE Transactions on Geoscience and Remote Sensing,* Vol. 34, No. 2, pp. 498-518.

Cloude, S.R. and E. Pottier. (1997). “An entropy based classification scheme for land applications of polarimetric SAR”, *IEEE Transactions on Geoscience and Remote Sensing*, Vol. 35, No. 1, pp. 68-78.

Cruden, D.M. and O. Hungr. (1986). "The debris of Frank Slide and theories of rockslide-avalanche mobility", *Canadian Journal of Earth Science*, Vol. 23, pp. 425-432.

Cyr, I. and T. Toutin. (2001). “RADARSAT-1 Stereo Advisor on CCRS Web”, *Canadian Journal of Remote Sensing*, Vol. 27, No. 1, pp.62-66.

DeAbreu R., D. Flett, B. Scheuchl, and B. Ramsay. (2003). “Operational Sea Ice Monitoring with RADARSAT-2 – A Glimpse into the Future,” In: *Proceedings of the International Geoscience and Remote Sensing Symposium (IGARSS 2003)*, Toulouse, France, 21-25 July 2003.

Drinkwater, M.R., R. Kwok, E. Rignot, H. Israelsson, R.G. Onstott, and D.P. Winebrenner. (1992). “Potential Applications of Polarimetry to the Classification of Sea Ice,” In: F. Carsey (Ed.), Microwave Remote Sensing of Sea Ice, AGU Geophysical Monograph 68, 1992.

Du, Y., P.W. Vachon and J.J. van der Sanden. (2002). “Satellite Image Fusion with Multi-scale Wavelet Analysis for Marine Applications: Preserving Spatial Information and Minimizing Artifacts (PSIMA)”, *Canadian Journal of Remote Sensing*, Vol. 29, No. 1, pp. 14-23.

Eriksson, L., M. Drinkwater, B. Holt, E. Valjavek, and O. Nortier. (1998). “SIR-C Polarimetric Radar Results from the Weddel Sea, Antarctica,” In: *Proceedings of the International Geoscience and Remote Sensing Symposium (IGARSS 1998)*, Seattle, USA, 6-10 July 1998.

Espedal, H.A. and T. Wahl. (1999). “Satellite SAR oil spill detection using wind hasty information”, *International Journal of Remote Sensing*, Vol. 20, No 1, pp. 49-65.

Evans, D.L., T.G. Farr, J.P. Ford, T.W. Thompson, and C.L. Werner. (1986). "Multi-polarization Radar Images for Geologic Mapping and Vegetation Discrimination", *IEEE Transactions on Geoscience and Remote Sensing*, Vol. 26, pp. 774-789.

Evans, D.L., T.G. Farr, J.J. Van Zyl and H.A. Zebker (1988). “Radar Polarimetry: Analysis Tools and Applications”, *IEEE Transactions on Geoscience and Remote Sensing*, Vol. 26, No. 6, pp. 774-789.

Freeman T., and S.L. Durden. (1998). “A Three-Component Scattering Model for Polarimetric SAR Data,” *IEEE Transactions on Geoscience and Remote Sensing*, Vol. 36, No. 3, pp. 963-973, May 1998.

Gade, M., W. Alpers, H. Hühnerfuss, H. Masuko and T. Kobayashi. (1998a). “Imaging of biogenic and anthropogenic ocean surface films by multifrequency/multipolarization SIR-C/X-SAR”, *Journal of Geophysical Research*, Vol. 103, No. C9, pp. 18851 – 18866.

Gade, M., W. Alpers, H. Hühnerfuss, V.R. Wismann, and P.A. Lange. (1998 b). “On the reduction of the radar backscatter by oceanic surface films : Scatterometer measurements and their theoretical interpretation”, *Remote Sensing of Environment*, Vol. 66, pp. 52-70.

Gierull, C. H., (2001). “Unbiased coherence estimator for SAR interferometry with application to moving target detection”, *Electronics Letters*, 2001.

Gierull, C. H. (2002). “Statistics of Multilook SAR Interferograms for CFAR Detection of Ground Moving Targets”, In: *Proceedings of EUSAR2002*, 7 March 2002.

Gierull, C. H. and I. Sikaneta, (2002). “Estimating the Effective Number of Looks in Interferometric SAR Data”, *IEEE Transactions on Geoscience and Remote Sensing*, Vol. 40, No. 8, pp.1733-1742.

Hajnsek, I., K.P. Papathanassiou, A. Moreira, and S.R. Cloude. (2002). "Surface parameter estimation using interferometric and polarimetric SAR", In: *Proceedings of IGARSS'02, Remote Sensing: Integrating Our View of the Planet,* Toronto*,* 24-28 June 2002, pp. 420-422.

Hawkins R. K., R. Touzi, A. Wind, K. Murnaghan and C.E. Livingstone. (1999). “Polarimetric calibration results and error budget for SAR-580 system”, In: *Proceedings of CEOS Workshop*, Toulouse, France, 26-29 October 1999.

Hawkins, R.K., C.E. Brown, K.P. Murnaghan, A. Alexander and R. Marois. (2002). “The SAR-580 Facility – System Update”, In: *Proceedings of the IEEE 2002 International Geoscience and Remote Sensing Symposium (IGARSS 2002)*, 24-28 June 2002, Toronto, Ontario, Canada, pp. 1705-1707.

Hochheim, K., and D. Barber. (2002). “The seasonal backscatter of agricultural crops as observed by RADARSAT-1. Part I. Wheat”, *International Journal of Remote Sensing* (in press).

Horgan, G.W. (1998). “Wavelets for SAR image smoothing”, *Photogrammetric Engineering & Remote Sensing*, Vol. 64, No. 12, pp. 1171-1177.

Jackson, C., H. Rais and B. Huxtable. (1997). “Polarimetry and Its Use in Automatic Target Detection with Examples from Search and Rescue”, In: *Proceedings of SPIE Conference on Automatic Target Recognition VII,* Orlando, Florida, USA, 22-24 April 1997, SPIE Vol. 3069, pp. 204-214.

Jackson, C.R., H. Rais and A.W. Mansfield. (1998). "Polarimetric target detection techniques and results from the Goddard Space Flight Center Search and Rescue Synthetic Aperture Radar (SAR2) program", In: *Proceedings of SPIE Conference on Automatic Target Recognition VIII*, Orlando, Florida, USA, 13-17 April 1998, F.A. Sadjadi (Ed.), SPIE Vol. 3371, pp. 185-193.

Jackson, C.R. and H. Rais. (1999). “Detection of aircraft crash sites from space using fully polarimetric SIR-C SAR imagery for Search and Rescue applications*”,* In: *Proceedings of SPIE Conference on Automatic Target Recognition IX*, Orlando, Florida, USA, 7-9 April 1999, SPIE Vol. 3718, pp. 213-217.

Lambert, R.A., J.T. Bortell, D.C. Carmer, B.E. Morey, D.F. Paskausky, and M. Fisher. (1992). “Recommanding remote sensing requirements to the United States Coast Guard”, In: *First Thematic Conference on Remote Sensing for Marine and Coastal Environments*, New Orleans, USA, 15-17 June 1992, pp. 191-204.

Lee, J.-S., M.R. Grunes, T.L. Ainsworth, L.-J. Du, D.L. Schuler, and S.R. Cloude. (1999). “Unsupervised Classification Using Polarimetric Decomposition and the Complex Wishart Classifier,” *IEEE Transactions on Geoscience and Remote Sensing*, Vol. 37, No. 5, pp.2249-2258, September 1999.

Livingstone, C.E., A.L. Gray, R.K. Hawkins, P.W. Vachon, T.I. Lukowski and M. Lalonde. (1995). “The CCRS Airborne SAR Systems: Radar for Remote Sensing Research”, *Canadian Journal of Remote Sensing*, Vol. 21, No. 4, pp. 468 – 490.

Livingstone, C.E., I. Sikaneta, C. H. Gierull, A. Beaudoin, J. Campbell, J. Beaudoin, S. Gong and T.A. Knight. (2002). “An airborne SAR experiment to support RADARSAT 2 GMTI”, *Canadian Journal of Remote Sensing*, Vol. 28, No. 6, pp.794-813.

Lowman, P. (1994). "Radar geology of the Canadian Shield - A 10 year review", *Canadian Journal of Remote Sensing*, Vol. 20**,** No. 3, pp. 198-209.

Lukowski, T.I., F. Khellah, F.J. Charbonneau and B. Yue. (2002a). “Synthetic Aperture Radar for Search and Rescue: Evaluation of Advanced Capabilities in Preparation for RADARSAT-2”, In: *Proceedings of SPIE Conference on Automatic Target Recognition XII*, Orlando, Florida, USA, 2-4 April 2002, SPIE Vol. 4726, pp. 343-352.

Lukowski, T.I. and F.J. Charbonneau. (2002b). “Synthetic Aperture Radar and Search and Rescue: Detection of Crashed Aircraft Using Imagery and Interferometric Methods”, *Canadian Journal of Remote Sensing,* Vol. 28, No. 6, pp. 770-781.

Lukowski, T.I. and B. Yue. (2003a). “Synthetic Aperture Radar for Search and Rescue: Studies at Natural Resources Canada-Update”, In: *Proceedings of the IEEE 2003 International Geoscience and Remote Sensing Symposium* (*IGARSS 2003*), Toulouse, France, 21-25 July 2003, pp.1311-1313.

Lukowski, T.I. and B. Yue. (2003b). “Man-Made Target Detection in SAR Imagery”, In: *Proceedings of Canadian Symposium on Remote Sensing*, Montreal, PQ, Canada, 14-16 October 2003, 6p.

Lukowski, T.I., B. Yue, F.J. Charbonneau, F. Khellah, and R.K. Hawkins. (2004). “Detection of Crashed Aircraft in Polarimetric Imagery”, *Canadian Journal of Remote Sensing, RADARSAT-2 Special Issue,* Vol. 30, No. 3, pp. 384-395.

Mattia, F., T. Le Toan, J.C. Souyris, G. De Carolis, N. Floury, F. Posa, and G. Pasquariello. (1997). "The effect of surface roughness on multifrequency polarimetric SAR data", IEEE Transactions on Geoscience and Remote Sensing, Vol. 35, No. 4, pp. 954-965.

McNairn, H., D. Wood, Q.H.J. Gwyn and R.J. Brown. (1998). “Mapping tillage and crop residue management practices with RADARSAT”, *Canadian Journal of Remote Sensing*, Vol. 24, pp. 28-35.

McNairn, H., J.J. van der Sanden, R.J. Brown, and J. Ellis. (2000). "The potential of RADARSAT-2 for crop mapping and assessing crop condition", In: *Proceedings of the Second International Conference on Geospatial Information in Agriculture and Forestry,* Lake Buena Vista, Florida, 10-12 January 2000, Vol. II, pp. 81-88.

McNairn, H., K. Hochheim and N. Rabe. (2002a). ″Applying polarimetric radar imagery for mapping the productivity of wheat crops″, *Canadian Journal of Remote Sensing, RADARSAT-2 Special Issue,* Vol. 30, No. 3, pp. 517-524.

McNairn, H., V. Decker and K. Murnaghan. (2002b). ″The sensitivity of C-Band polarimetric SAR to crop condition ″, In: *Proceedings of the International Geoscience and Remote Sensing Symposium 2002 (IGARSS 2002)*, Toronto, 24-28 June 2002.

MDA, MacDonald, Dettwiler and Associates. (2003). *RADARSAT-2 mission requirements specification*, CDRL SE-01, February 25, 2003, Fifth Issue, First Revision, 60 p.

Meteorological Service of Canada (MSC), (2002). *MANICE – Manual of Standard Procedures for Observing and Reporting Ice Conditions*. Ninth Edition, April 2002.

Murphy, W. and R. J. Inkpen. (1996). "Identifying landslide activity using airborne remote sensing data", In: *GSA Abstracts with Programs*, Denver, Vol. A-408, pp. 28-31.

Nghiem, S.V. and C. Bertoia. (2001). “Study of Multi-Polarization C-Band Backscatter Signatures for Arctic Sea Ice Mapping with Future Satellite SAR,” *Canadian Journal of Remote Sensing*, Vol. 27, No. 5, October 2001.

Novak, L.M., M. C. Burl, and W. W. Irving. (1993). “Optimal Polarimetric Processing for Enhanced Target Detection”, *IEEE Transactions on Aerospace and Electronic Systems*, Vol. 29, No. 1, pp. 234-243.

Rais, H., A. W. Mansfield, B. D. Huxtable and K. Chotoo. (2000). “The Virginia Beach Search and Rescue Experiment”, In: *Proceedings of SPIE Conference on Automatic Target Recognition X*, Orlando, Florida, USA, 26-28 April 2000, SPIE Vol. 4050, pp. 169-178.

Rignot, E., R. Chellappa, and P. Dubois. (1992). “Unsupervised Segmentation of Polarimetric SAR Data Using the Covariance Matrix,” *IEEE Transactions on Geoscience and Remote Sensing*, Vol. 30, No. 4, pp. 697-705.

Rosenthal, W.D. and B.J. Blanchard. (1984). “Active microwave responses: An aid in improved crop classification”, *Photogrammetric Engineering And Remote Sensing*, Vol. 50, pp. 461-468.

Rott, H., B. Scheuchl, A. Siegel, and B. Grasemann. (1999). "Monitoring very slow slope movements by means of SAR interferometry: A case study from a mass waste above a reservoir in the Ötztal Alps, Austria", *Geophysical Research Letters*, Vol. 2, No. 11, pp. 1629-1632.

Saint-Jean, R., V. Singhroy, and S.M. Khalifa. (1995). “Geological interpretation of integrated SAR images in the Azraq Area of Jordan”, *Canadian Journal of Remote Sensing*, Vol. 21, pp. 511-517.

Saint-Jean R., V. Singhroy, and M. Rheault. (1999). "Understanding multi-polarized airborne C-SAR images for geological mapping in Precambrian Shield terrains", In: *Proceedings Applied Geologic Remote Sensing*, Vancouver, 1-3 March 1999.

Scheuchl, B., R. Caves, I. Cumming, and G. Staples. (2001a). "Automated Sea Ice Classification Using Spaceborne Polarimetric SAR Data," In: *Proceedings of the International Geoscience and Remote Sensing Symposium (IGARSS 2001),* Sydney, Australia, 9-13 July 2001.

Scheuchl, B., R. Caves, I. Cumming, and G. Staples. (2001b). "H/A/α-based classification of sea ice using SAR polarimetry", In: *Proceedings 23rd Canadian Symposium on Remote Sensing*, Quebec, Canada, 21-24 August 2001.

Scheuchl, B., I.G. Cumming, and I. Hajnsek. (2003a). "Classification of Ice Types from Convair-580 data of Northumberland Strait, PEI," In: *Proceedings ASAR 2003,* Montreal, Quebec, Canada.

Scheuchl, B., D. Flett, G. Staples, G. Davidson, and I. Cumming. (2003b). "Preliminary Classification Results of Simulated RADARSAT-2 Polarimetric Sea Ice Data," In: *Proceedings POLinSAR 2003 Workshop*, Frascati, Italy, 14-16 January.

Scheuchl B., D. Flett, R. Caves, and I. Cumming. (2004). "Potential of RADARSAT-2 for Operational Sea Ice Monitoring," *Canadian Journal of Remote Sensing, RADARSAT-2 Special Issue*, Vol. 30, No. 3, pp. 448-461.

Schuler, D.L., J.S. Lee, D. Kasilingam, and G. Nesti. (2002). "Surface roughness and slope measurements using polarimetric SAR data", *IEEE Transactions on Geoscience and Remote Sensing*, Vol. 40, No. 3, pp. 687-698.

Sikaneta, I. (2002). Personal communication, May 2002.

Sikaneta, I. and C. H. Gierull. (2002). "Parameter Estimation for the Phase Statistics in Interferometric SAR", In: *Proceedings of the International Geoscience and Remote Sensing Symposium (IGARSS 2002),* Toronto, 24-28 June 2002.

Singh, K.P., A.L. Gray, R.K. Hawkins, and R.A. O'Neil. (1986). "The influence of surface oil on C- and Ku- Band ocean backscatter", *IEEE Transactions on Geoscience and Remote Sensing*, Vol. GE-24, No. 5, pp. 738-744.

Singhroy, V. (1992). "Radar Geology, Techniques and Results", *EPISODES*, Vol. 15, No. 1, pp. 15-20.

Singhroy, V. (1996). "Environmental and Geological site characterization in vegetated areas: Image enhancement guidelines", In: V. Singhroy, D. Nebert, and A. Johnson (Eds.), Remote Sensing and GIS: Applications and Standards, ASTM Special Technical Publication no. 1279, American Society for Testing and Materials, pp. 5-17.

Singhroy, V. and R. Saint-Jean. (1997). "Effects of relief on the selection of RADARSAT beam modes for geological mapping", In: *Proceedings ERIM, Applied Geologic Remote Sensing Conference*, Denver, USA, 17-19 November 1997, 14 pp.

Singhroy, V., K. Mattar, and L. Gray. (1998). "Landslide characterization in Canada using interferometric SAR and combined SAR and TM images", *Advances in Space Research*, Vol. 2, No. 3, pp. 465-476.

Singhroy, V. and R. Saint-Jean. (1999). "Effects of Relief on the Selection of RADARSAT-1 incidence angle for Geological Applications", *Canadian Journal of Remote Sensing*, Vol. 25, No. 3, pp. 211-217.

Singhroy, V. and K. Mattar. (2000). "SAR image techniques for mapping areas of landslides", In: *Proceedings XIXth ISPRS Congress,* Amsterdam, 16-23 July 2000, pp. 1395-1402.

Singhroy, V. and K. Molch. (2004). "Characterizing and monitoring Rockslides from SAR techniques", *Advances in Space Research,* Vol. 33, Issue 3, pp. 290-295.

Skriver, H. and L.T. Pedersen. (1995). "Polarimetric Signatures of Sea Ice in the Greenland Sea", In: *Proceedings of the International Geoscience and Remote Sensing Symposium, IGARSS '95*, Florence, Italy, 10-14 July 1995, pp. 1792-1794.

Smith, A.M., D.J. Major, R.L. McNeil, W.D. Willms, B. Brisco, and R.J. Brown. (1995). “Complementarity of radar and visible-infrared sensors in assessing rangeland condition”, *Remote Sensing of Environment,* Vol. 52, pp. 173-180.

Solberg, A.H.S., G. Storvik, R. Solberg, and E. Volden. (1999). “Automatic Detection of Oil Spills in ERS SAR Images”, *IEEE Transactions on Geoscience and Remote Sensing*, Vol. 37, No. 4, pp. 1916-1924.

Swartz, A.A., H.A. Yueh, J.A. Kong, L.M. Novak, and R.T. Shin. (1988). "Optimal polarizations for achieving maximum contrast in radar images", *Journal of Geophysical Research*, Vol. 93, No. B12, pp. 15,252-15,260.

Thompson, A.A. and C. E. Livingstone. (2000). “Moving target performance for RADARSAT 2”, In: *Proceedings of the International Geoscience and Remote Sensing Symposium (IGARSS 2000),* Honolulu, Hawaii, 24-28 July 2000.

Touzi R., S. Goze, T. Le Toan, A. Lopes, and E. Mougin. (1992). “Polarimetric discriminators for SAR images”, *IEEE Transactions on Geoscience Remote Sensing*, Vol. 30, No. 5, pp. 973-980.

Touzi, R. and F. Charbonneau. (2002). *Polarimetric Workstation User Guide*, Canada Centre for Remote Sensing, 13 p.

Ulaby, F.T., R.K. Moore and A.K. Fung. (1986). *Microwave remote sensing, active and passive, vol. III: From theory to applications*, Artech House Inc., Dedham, Ma, 2162 p.

van der Sanden, J.J., P.W. Vachon and J.F.R. Gower. (2000). “Combining optical and radar satellite image data for surveillance of coastal waters”. In: *Proceedings of the Sixth International Conference on Remote Sensing for Marine and Coastal Environments*, Charleston, 1-3 May 2000, Vol. 1, pp. 109-116.

van der Sanden, J.J. and S.G. Ross (Eds.). (2001). *Applications Potential of RADARSAT-2 - A Preview*. Ottawa, Natural Resources Canada, Canada Centre for Remote Sensing, 117 p.

van der Sanden, J.J. (2004). "Anticipated applications potential of RADARSAT-2 data", *Canadian Journal of Remote Sensing*, Vol. 30, No. 3, pp. 369-379.

Vietmeier, J., W. Wagner, and R. Dikau. (1999). “Monitoring moderate slope movements (landslides) in the southern French Alps using Differential SAR Interferometry”, In: *Proceedings 2nd International Workshop on ERS SAR Interferometry*, *FRINGE'99*, Liège, Belgium, 10-12 November 1999.

Wismann, V. (1993). “Radar signatures of mineral oil spills measured by an airborne multi-frequency radar and the ERS-1 SAR”, In: *Proceedings of the International Geoscience and Remote Sensing Symposium (IGARSS 1993),* Tokyo, Japan, 18-21 August 1993, pp. 940-942.

Zebker, H.A., J.J van Zyl, and C. Elachi. (1990). "Polarimetric SAR applications", In: F. T. Ulaby and C. Elachi (Eds.), Radar Polarimetry for Geoscience Applications, Artech House Inc., 364 p.

Appendix I – Applications Summary Paper

Source: *Canadian Journal of Remote Sensing*, 2004, Vol. 30, No. 3, pp. 369-379.

Anticipated Applications Potential of RADARSAT-2 Data

J.J. van der Sanden

Natural Resources Canada, Canada Centre for Remote Sensing, Applications Division, 588 Booth Street, Ottawa, ON, K1A 0Y7. Tel: + 1-613-947-1324, Fax: + 1-613-947-1385, E-mail: sanden@ccrs.nrcan.gc.ca

Abstract. In this paper we assess how RADARSAT-2's technical enhancements in terms of polarization, spatial resolution, look direction and orbit control will impact the potential utility of its data products for 32 applications in the fields of agriculture, cartography, disaster management, forestry, geology, hydrology, oceans, and sea and land ice. Our assessment relies on bibliographic sources and, in particular, case studies drawn from ongoing applications development work at the Canada Centre for Remote Sensing and the Canadian Ice Service. The applications potential of RADARSAT-2 data, compared to that of RADARSAT-1 data, is anticipated to improve in a major, moderate, and minor fashion for 3, 18, and 10 of the identified applications, respectively. For one of the applications considered the increase in potential of RADARSAT-2 vis-à-vis RADARSAT-1 cannot be assessed because this application relies completely on RADARSAT-2's new full polarimetric capability.

Introduction

RADARSAT-2 will provide all imaging modes of the current RADARSAT-1 satellite, as well as some new modes that incorporate significant technical innovations and improvements (cf. Ali *et al.*, 2004a; Ali *et al.*, 2004b; Fox *et al*., 2004; Morena *et al*., 2004). Hence, the satellite will offer data continuity to RADARSAT-1 users and new data that support the development of new applications and the refinement of existing ones. From an applications perspective, the most prominent technical enhancements embodied by RADARSAT-2 are those relating to polarization, spatial resolution, look direction, and orbit control. In this

paper, we assess how these enhancements will impact the potential of RADARSAT-2 data products for applications in the fields of agriculture, cartography, disaster management, forestry, geology, hydrology, oceans, and sea and land ice. Evidently, the utility of the RADARSAT-2 data products will govern the satellite's economic viability and as such its role in the operationalisation of space-borne radar remote sensing.

The presented assessment is primarily based on an evaluation of data information content and largely disregards other conditions that may affect the promise of particular applications, e.g. economic or legal circumstances. After all, such conditions may vary widely from one geographical application area to another. Our evaluation relies on bibliographic sources and, in particular, case studies drawn from ongoing applications development work at the Canada Centre for Remote Sensing and the Canadian Ice Service (van der Sanden and Ross, 2001; CCRS, 2004). Logically, the evaluation will focus on data products that are not currently available from RADARSAT-1. Even so, the applications potential as demonstrated vis-à-vis RADARSAT-1 data products will often provide the starting-point for our discussions concerning RADARSAT-2.

Anticipated Applications Potential

Table 1 summarises our assessment of the specific effect of the most important technical enhancements of RADARSAT-2 on the data information content and hence on the associated applications potential. Our evaluation of the combined effect of these technical enhancements on the anticipated overall applications potential of RADARSAT-2 data is summarised in Table 2. This table also lists our ratings for the overall applications potential of RADARSAT-1 data products. As such, Table 2 illustrates the degree in which progress in space-borne SAR technology is expected to enhance the overall applications potential of RADARSAT-2 data products. With regard to Table 2 it is important to mention that we assume application of single date SAR images. The use of images acquired on different dates is known to enhance the application potential in fields dealing with vegetation in particular. As an example, the application potential of RADARSAT-1 data for crop type mapping would rate as 'moderate' rather than 'limited'

Table 1. Anticipated effect of new RADARSAT-2 features on applications potential in terms of data information content. Key: '-' minor, '-/+' moderate, '+' major.

Application	RADARSAT-2 Feature: Selective Single Polarization (SSP)	Selective Dual Polarization (SDP)	Quad Polarization (QP)	Ultra-Fine Spatial Resolution	Selective Look Direction	Improved Orbit Control
Agriculture						
Crop type	-	-/+	+	-	-	-
Crop condition	-	-/+	+	-/+	-/+	-
Crop yield	-	-	-/+	-/+	-	-
Cartography						
DEM interferometry	-	-	-	+	-	+
DEM stereoscopy	-	-	-	+	-	-/+
DEM polarimetry	N.A.	N.A.	+	N.A.	-	-/+
Cartographic feature extraction	-	-	-/+	+	-	-/+
Disaster Management						
Floods	-	-	-	-	+	-
Geological hazards	-	-/+	-/+	-/+	+	- (+) [1]
Hurricanes	-/+	-	-/+	-	+	-
Oil spills	-/+	-	-	-/+	+	-
Search and rescue	-	-	+	-/+	+	-/+ (+) [1]
Forestry						
Forest type	-	-	-/+	-/+	-	-
Clearcuts	-/+	-	-	-/+	-	-
Fire-scars	-/+	-	-	-/+	-	-
Biomass	-	-	-	-	-	-
Geology						
Terrain mapping	-	-/+	-/+	-/+	-	- (+) [1]
Structure	-	-/+	-/+	-/+	-	-
Lithology	-	-	-	-	-	-
Hydrology						
Soil moisture	-	-	-/+	-	-/+	-
Snow	-	-	-/+	-	-/+	-
Wetlands	-	-/+	-/+	-/+	-	-
Oceans						
Winds	-/+	-	-	-	-	-
Ships	-/+	-/+	-/+	+	-/+	-/+
Waves	-	-	-/+	-	-	-
Currents	-/+	-	-	-	-	-
Coastal zones	-/+	-/+	-/+	-/+	-	-
Sea and Land Ice						
Sea ice edge and ice concentration	-/+	-	-/+	-	-/+	-
Sea ice type	-	-	-/+	-	-	-
Sea ice topography and structure	-/+	-	-/+	-	-/+	-
Icebergs	-/+	-	-/+	+	-/+	-/+
Polar glaciology	-/+	-	-/+	-	+	- (+) [1]

1) Using InSAR techniques

Table 2. Applications potential [1] of RADARSAT-1 and RADARSAT-2. Key: '-' minimal, '-/+' limited, '+' moderate, '++' strong.

Application	Satellite: RADARSAT-1	RADARSAT-2
Agriculture		
Crop type	-/+	++
Crop condition	-/+	++
Crop yield	-	-/+
Cartography		
DEM interferometry	+	+
DEM stereoscopy	++	++
DEM polarimetry	N.A.	-/+
Cartographic feature extraction	+	++
Disaster Management		
Floods	++	++
Geological hazards	-/+	+
Hurricanes	+	+
Oil spills	+	+
Search and rescue	-/+	+
Forestry		
Forest type	-/+	-/+
Clearcuts	-/+	+
Fire-scars	-/+	+
Biomass	-	-
Geology		
Terrain mapping	-/+	+
Structure	+	++
Lithology	-/+	-/+
Hydrology		
Soil moisture	-/+	+
Snow	-/+	+
Wetlands	-/+	+
Oceans		
Winds	+	++
Ships	+	++
Waves	-/+	-/+
Currents	-/+	+
Coastal zones	-/+	+
Sea and Land Ice		
Sea ice edge and ice concentration	+	++
Sea ice type	+	+
Sea ice topography and structure	-/+	++
Icebergs	-/+	+
Polar glaciology	-/+	+

1) Use of single date images assumed

if the use of multi-temporal images had been considered. In addition – and perhaps unnecessarily – it is noted that the ratings in Table 2 are general in nature. In specific cases or under certain conditions the true application potential may therefore differ from the one shown. For instance, it is well-known that mountainous conditions have an overall adverse effect on the applications potential of any type of SAR data.

In the sections following we will motivate our ratings shown in Tables 1 and 2 for each application field identified.

Agriculture

Crop type and crop condition mapping are among the three applications that are expected to benefit the most from the technical enhancements embodied by RADARSAT-2. As shown in Table 2, the potential of RADARSAT-1 data for these applications is rated 'limited' while the applications potential for RADARSAT-2 data is anticipated to be 'strong'. Table 1 shows that the introduction of the Selective Dual Polarization (SDP) mode and, to a greater extent, the Quad Polarization (QP) mode contribute to the increase in potential for both applications. In addition, the crop condition mapping application is anticipated to benefit from RADARSAT-2's enhancements in terms of spatial resolution and look direction.

The improved applications potential of images acquired in the SDP and QP modes results from an increase in information content with respect to the structural characteristics of the crops observed. It is well known that the polarization of backscattered microwaves is a function of the polarization of the transmitted microwaves and the structural characteristics of the features observed. Moreover, the polarization of the transmitted microwaves dictates which components of the vegetation and soil contribute to the total amount of energy scattered back to the SAR sensor. Vertically-polarized microwaves (V) couple with the predominant vertical structure of most vegetation and as a result, penetration of the signal through the canopy is reduced. VV-polarized radar returns thus provide good contrast among crop types that have different vertical canopy structures. Differences in this vertical structure that result from changes in growth stage or health may also be detected in VV-polarized images. Horizontally-polarized microwaves (H) tend to penetrate the canopy to a greater extent than vertically-polarized waves. At steep incidence angles, HH images therefore tend to provide information about the underlying soil condition. Cross-polarized radar returns (HV

or VH) result from multiple reflections within the vegetation volume. C-HV and C-VH images are sensitive to crop structure within the total canopy volume and thus provide information that is complementary to HH and VV imagery. RADARSAT-2's capability to acquire full polarimetric data in the QP mode can be expected to extend its sensitivity to crop structural characteristics and hence potential for crop type and condition mapping beyond that of the SDP mode. McNairn and Brisco (2004) present a detailed review of the utility of C-band polarimetric data for agriculture. Buckley (2004) discusses the potential of RADARSAT-2 type data for the characterization of prairie landscapes.

Whereas crop type mapping calls for information at the level of individual fields, crop condition mapping requires information at the level of specific zones within individual fields. RADARSAT-2 images acquired in the Ultra-Fine mode will contain more detailed spatial information than any other commercially available space-borne SAR data product and are therefore anticipated to advance the potential for crop condition mapping (cf. McNairn *et al.*, 2004). The capability to image to either the right or the left of the sub-satellite track potentially shortens - on average - RADARSAT-2's acquisition response time and increases its revisit frequency in all but the most northerly regions on Earth. In the context of crop condition mapping, this improves application potential because it enhances the likelihood of acquiring multiple images immediately following and during critical events such as infestations, hailstorms etc.

Table 1 shows that images acquired in the QP and Ultra-Fine resolution modes are expected to contain moderately improved information in support of crop yield mapping. Accordingly, the application potential of RADARSAT-2 is rated one level above that of RADARSAT-1, i.e. 'limited' instead of 'minimal' (see Table 2). As in the case of crop condition mapping, the improved potential of the QP and Ultra-Fine resolution data products for crop yield mapping can be explained from the increased sensitivity to crop structure and the capacity to obtain within-field zonal information, respectively. The anticipated potential of RADARSAT-2 for crop yield mapping does not exceed the 'limited' rating because the employed C-band radar signal is known to saturate for larger biomass crops.

Cartography

Digital Elevation Models (DEMs) are currently one of the most important data sources used in geo-spatial analysis. Like RADARSAT-1, RADARSAT-2 will have the capacity to support the generation of DEMs by means of repeat-pass interferometry and stereoscopy. In addition, RADARSAT-2 data acquired in the QP mode can be applied to the generation of DEMs from polarimetry. While the techniques for the production of DEMs from interferometric or stereoscopic SAR image pairs are operational, the technique for the generation of DEMs from polarimetric SAR data is experimental.

DEM polarimetry involves the direct measurement of terrain slopes and the inference of terrain elevations from known elevation points. The generation of a two-dimensional DEM requires two (quasi-)orthogonal SAR overpasses since the capability to measure slopes is restricted to the azimuth direction. In addition, slope measurement requires the availability of a scattering model for the target observed (cf. Toutin, 2004). The requirements for DEM polarimetry in terms of elevation points, overpasses and scattering models explain why the associated application potential has been rated as ‘limited’ in Table 2.

Both the repeat-pass DEM interferometry and DEM stereoscopy applications will benefit from RADARSAT-2’s enhancements in terms of spatial resolution and orbit control. DEMs generated from data acquired in RADARSAT-2’s Ultra-Fine resolution mode can be expected to comprise more spatial details and have higher spatial accuracies than DEMs generated from any other commercially available space-borne SAR data source. Improved knowledge about and control over the orbit will enhance the absolute positional accuracy of image products as well as the accuracy with which baselines between interferometric image pairs can be computed. The anticipated effect of improved orbit control for DEM stereoscopy and DEM interferometry is rated as ‘moderate’ and ‘major’, respectively. The effect on the former application is rated lower because, in many cases, the positional accuracy of image products can also be improved through the identification of ground control points. In contrast, an alternative for more accurate calculation of baselines between repeat-pass interferometric image pairs is lacking. Table 2 shows that, while beneficial, the technical enhancements embodied by RADARSAT-2 are not anticipated to improve its overall application potential for DEM interferometry and DEM stereoscopy to a level above that of RADARSAT-1. The potential associated with repeat-pass DEM interferometry is assessed to

halt at ‘moderate’ for both satellites because of two well-known problems with this technique – that is - the loss of coherence and changes in atmospheric propagation between subsequent image acquisitions. As for RADARSAT-1, the overall application potential of RADARSAT-2 for DEM stereoscopy is rated at the highest level, i.e. ‘strong’.

As shown in Table 2, the overall potential for cartographic feature extraction is rated ‘moderate’ for RADARSAT-1 and ‘strong’ for RADARSAT-2. The most important feature contributing to this increase in application potential is the Ultra-Fine spatial resolution mode. RADARSAT-2’s Ultra-Fine resolution data products will comprise more detailed spatial information. These products can thus be expected to enable the mapping of cartographic features with reduced errors of omission and increased positional accuracies (cf. Toutin, 2004). The enhancement in terms of orbit control improves the application potential because it will facilitate more accurate absolute positioning of features extracted. RADARSAT-2’s capability to acquire QP data products is anticipated to enhance its potential for cartographic feature extraction because the polarimetric information comprised in these data (e.g. information re scattering mechanisms) is likely to ease the detection and hence the subsequent extraction of features of interest. It should be noted that, due to technical limitations, the QP data products will have a lower spatial resolution than the Ultra-Fine data products.

Disaster Management

The urgency associated with disaster management dictates that applications in this field require instantaneous and frequent image acquisition. RADARSAT-2’s selective look direction capability will (on average) shorten the response time and increase the revisit frequency in all but the most northerly regions on Earth. Consequently the effect of selective look direction capability on the information content of RADARSAT-2 data products for all disaster management applications is rated as ‘major’. With the exception of polar glaciology, no other application is anticipated to benefit from the selective look direction feature in such a paramount fashion (see Table 1). It should be noted that even though look direction switching will be an operational RADARSAT-2 feature, the right-looking configuration is regarded as the default mode of operation. The left-looking mode is expected to be deployed

primarily to meet data requirements for disaster management and Antarctic mapping (see section on Sea and Land ice).

RADARSAT-2's enhancements in terms of polarization are anticipated to have a mostly 'moderate' effect on the information content of its data for all of the disaster management applications identified with the exception of flood mapping. When operating in the Selective Single Polarization (SSP) mode, RADARSAT-2 will be able to acquire a single image in either the HH-, VV-, VH- or HV-polarization (note; RADARSAT-1 operates in HH only). The capability to image in VV will benefit the hurricanes application because available wind retrieval models are best developed for this particular polarization. Moreover, the oil spills application will gain from the VV imaging capability since VV-polarized images provide better oil-water contrast than HH and HV (VH) images. The option to simultaneously acquire both a VV and VH image in the SDP mode is not considered beneficial for either the hurricanes or oil spills application since the extra cross-polarized band does not contain additional information. In fact, the extra image band would hamper these applications by adding to the data volume to be handled. Accordingly, the effect of the SSP feature for the hurricanes and oil spills applications has been rated higher than the effect of the SDP feature (Table 1). RADARSAT-2's QP feature has been given the 'moderate' rather than 'minor' rating in connection with hurricanes because there is evidence in the literature that co- and cross-polarized ratios at C-band provide a mechanism to estimate rain rates (Braun *et al.*, 2000). Rain rates would represent important additional quantitative information on the state and evolution of hurricanes. It is therefore unfortunate that, due to technical limitations, QP data cannot be acquired in ScanSAR imaging mode, that is, the preferred mode for hurricane studies. The use of the narrow swath QP mode (25 km nominally) will considerably reduce the probability of obtaining a hurricane image.

As shown in Table 1, RADARSAT-2's SDP and QP data products are anticipated to offer moderately improved information content for the mapping of geological hazards. This can be explained from the difference in the sensitivity of (linear) like- and cross-polarized data to surface roughness, which is an important variable in the mapping of landslides and volcanoes. Indeed, QP data have been shown to hold promise for the quantification of surface roughness in agricultural terrain (e.g. Mattia *et al*., 1997; Schuler *et al*., 2002). Introduction of the QP mode is also expected to benefit the application of space-borne SAR to the search

and rescue of crashed airplanes (cf. Lukowski *et al.*, 2004). Unlike any other image types, QP images can be evaluated for the occurrence of dihedrals formed by parts of the airplane structure. This is a particularly effective detection approach given that these highly reflective dihedral structures have been found to often survive the crash and are unusual features in natural environments.

The enhanced spatial information that will be available in RADARSAT-2's Ultra-Fine mode images is anticipated to be of value for search and rescue as well as the mapping of geological hazards and oil spills. Improved orbit control will simplify the extraction of accurate geographic coordinates for (candidate) crash sites and hence be of benefit to the search and rescue application. Moreover, this feature will facilitate the computation of accurate baselines between satellite overpasses. Consequently, it is anticipated to represent a 'major' improvement for applications that are known to use repeat-pass SAR interferometry techniques, e.g. geological hazards mapping and search and rescue.

Like other disaster management applications, the flood mapping application is expected to benefit in a 'major' fashion from RADARSAT-2's selective look direction capability. In contrast, the effects of enhancements in terms of polarization, spatial resolution and orbit control are anticipated to be 'minor' (see Table 1). In fact, the technical capabilities of the current RADARSAT-1 satellite are very well suited to the mapping of floods. Hence, RADARSAT-2 data products are not anticipated to be able to advance the floods application. Accordingly, the overall potential of both RADARSAT-1 and RADARSAT-2 for flood mapping has been rated in Table 2 as 'strong'.

Forestry

Table 2 rates the respective overall potential of RADARSAT-1 and RADARSAT-2 for the mapping of clearcuts and fire-scars as 'limited' and 'moderate'. RADARSAT-2's moderately improved potential for these applications results primarily from its capability to acquire HV-(VH-) polarized images in SSP mode. Compared to HH- and VV-polarized images, HV-(VH-) polarized images offer improved information content in the sense that they show better contrast between the clearcuts or fire-scars and the surrounding forest cover (Ahern and Drieman, 1988; Kneppeck and Ahern, 1989). This superior contrast results from the scarcity of HV backscatter generating multiple reflections in the lightly vegetated clearcuts or

fire-scars and the abundance of such reflections in the heavily vegetated forest. RADARSAT-2's capability to acquire images in the SDP or QP mode is not considered beneficial for either application since the extra image bands do not contain additional information but rather add to the volume of data to be handled. Accordingly, the ratings in Table 1 associated with clearcuts and fire-scars are higher for the SSP mode of operation than for either the SDP or QP mode of operation. Thanks to increased spatial information content, RADARSAT-2's images can be expected to facilitate clearcut and fire-scar mapping with reduced errors of omission and increased positional accuracies. However, the potential of Ultra-Fine resolution data for application to large-scale clearcut and fire-scar mapping is compromised by the associated limited coverage (20 km by 20 km nominally).

As shown in Table 2, RADARSAT-2 data are not expected to contain the information required to improve the application potential for forest type and forest biomass mapping to levels above that of RADARSAT-1 data. Forest type mapping is likely to benefit moderately from the introduction of the QP and Ultra-Fine spatial resolution modes but the resulting overall application potential is anticipated to be at the RADARSAT-1 level, i.e. 'limited'. The moderately increased information content of full polarimetric RADARSAT-2 data can be explained from the enhanced sensitivity of this data type to differences in forest canopy structure (cf. Touzi *et al*., 2004b). Similarly, the improved spatial detail available in Ultra-Fine mode data will represent an enhanced source of information for forest type mapping by means of analysis of image texture. Like RADARSAT-1, RADARSAT-2 is anticipated to offer only 'minimal' potential for application to the mapping of forest biomass. The main impediment of both satellites for operational forest biomass mapping is the high frequency of operation, i.e. C-band. It is well known that the sensitivity of C-band radar signals to differences in aboveground biomass is restricted to a level below that of most forests, i.e. below ca. 50 t ha^{-1} in dry biomass (Dobson *et al*., 1992; Le Toan *et al*., 1992).

Geology

RADARSAT-2 is anticipated to offer a moderately improved potential for application to terrain mapping and structure mapping. The overall potential for these respective applications is rated as 'limited' and 'moderate' for RADARSAT-1 and as 'moderate' and 'strong' for RADARSAT-2 (see Table 2). This increase in potential for both applications results

primarily from the introduction of the SDP, QP and Ultra-Fine spatial resolution modes. RADARSAT-2's capability to acquire dual-polarized or full polarimetric data increases its sensitivity to differences in vegetation structure and relief. Thanks to geobotanical relationships, differences in vegetation structure often reflect the properties and extent of underlying surficial deposits and rock units. Hence, more information concerning structural characteristics of vegetation translates in improved potential for terrain mapping (Singhroy, 1996). Greater sensitivity to relief can be observed in cross-polarized data in particular and explains the anticipated increase in application potential of RADARSAT-2 for the mapping of geological structures, including fracture zones and fault scarps (Huadong *et al*., 1997; Schaber *et al*., 1997). Like other applications that rely on repeat-pass SAR interferometry techniques, the mapping of terrain displacements can be expected to benefit in a major way from RADARSAT-2's enhancements in terms of orbit control.

The potential of both RADARSAT-1 and RADARSAT-2 for application to lithological (or rock type) mapping is rated as 'limited'. C-band SAR images have been reported to contain information in support of the mapping of lava flows and other rock types with distinct differences in surface roughness (Gaddis, 1992; MacKay and Mouginis-Mark, 1997). However, in most cases the lithological mapping application will be served much better with data acquired by optical sensor systems in general and hyperspectral sensor systems in particular.

Hydrology

Table 2 shows that the potential of RADARSAT-2 for application to the mapping of soil moisture, snow and wetlands is anticipated to be one level above that of RADARSAT-1, i.e. 'moderate' rather than 'limited'. The increased potential for the soil moisture and snow mapping applications results mainly from the introduction of the QP mode and the selective look direction capability. In turn, the wetland mapping application is expected to benefit from RADARSAT-2's SDP, QP and Ultra-Fine resolution mode (see Table 1). Sokol *et al.* (2004) present a detailed review of the utility of RADARSAT-2 type data for hydrology.

It is well known that the radar return signal of a soil surface is a function of both the soil's moisture content and effective surface roughness. Hence, reliable mapping of soil moisture with the help of SAR images requires information about the soil surface roughness

and vice versa. SAR-assisted assessment of both soil moisture and soil surface roughness is feasible with systems that can provide a minimum of two independent observations, i.e. measure backscatter in two or more polarizations. A combination of HH- and VV-polarized signals constitutes the preferred polarization combination for soil moisture (and soil roughness) mapping. This results from the fact that HH-polarized radar signals and, to a lesser extent, VV-polarized radar signals have the best capacity to penetrate overlying vegetation cover. The foregoing explains the anticipated effect of the QP mode on the potential of RADARSAT-2 for application to soil moisture mapping. Given the narrow swath width of the QP mode (25 km nominally), it is unfortunate that RADARSAT-2 will not have the capability to acquire a combination of HH- and VV-polarized images in the SDP mode. The swath width of images that can be acquired in the SDP mode will range from about 50 km in the Fine spatial resolution mode to about 500 km in the ScanSAR Wide mode. RADARSAT-2's selective look direction feature potentially increases the revisit frequency in all but the most northerly regions on Earth. A capacity to map soil moisture more frequently should facilitate the work of water resource managers, for example, by providing more frequent and more up-to-date input for hydrological and crop-growth models. It must be noted that RADARSAT-2 data will support the mapping of moisture in the upper soil layers only. This is due to the limited penetration depth at C-band.

The positive effect of RADARSAT-2's QP mode on its potential for application to the mapping of snow can be explained from the greater information content of full polarimetric radar data concerning the snow pack. Sokol *et al.* (2003) report that parameters derived from polarimetric radar data can provide information on snow state (wet/dry) and complexities (e.g. ice layers) in the snow pack structure. Knowledge of these conditions can be used to improve the mapping of an important snow parameter, i.e. snow water equivalent (SWE). Typically, SWE is mapped on the basis of brightness temperature recorded by microwave radiometers. Temporal information on snow state can also be used as an indicator of the onset of snowmelt. Onset of snowmelt and SWE are important variables for activities such as flood forecasting and reservoir management. Once again, the selective look direction feature has the potential to improve the quality of the information on snow cover by providing more frequent imaging and thus mapping opportunities.

The wetland mapping application is anticipated to benefit from RADARSAT-2's SDP and QP modes because of the enhanced sensitivity of dual-polarized and full polarimetric radar data to the structural characteristics of the target observed. The structural characteristics of wetlands are governed by the structure of the vegetation and the presence/absence of water. Please refer to the section on agriculture for a discussion concerning the relationship between microwave polarization and vegetation structure. The presence of water leads to the dominance of the double-bounce scattering mechanism. Full polarimetric radar data facilitate the classification of scattering mechanisms and as such provide increased information content in support of wetland mapping. RADARSAT-2's Ultra-Fine resolution data can be expected to facilitate the mapping of smaller wetland units. In addition, the greater spatial information content in these data will enhance the potential of wetland mapping on the basis of image texture.

Oceans

With the exception of the waves application, all oceans applications identified are anticipated to moderately benefit from the introduction of RADARSAT-2. The potential of both RADARSAT-1 and RADARSAT-2 for the waves application can be seen to halt at the 'limited' rating. This can be explained from the satellites' polar orbit, which restricts the information content of the images acquired to specific ranges of the total available ocean wave spectrum (e.g. Vachon *et al.*, 1997; Dowd *et al.*, 2001). Even so, the capability of RADARSAT-2 to simultaneously acquire HH- and VV-polarized data in the QP mode can be considered a technical enhancement that benefits the wave application. As reported by Engen *et al.* (2000), the combination of HH- and VV-polarized images permits more accurate and more complete retrieval of ocean wave spectra.

The added capability to acquire VV-polarized images explains the increase in application potential for wind speed retrieval from 'moderate' for RADARSAT-1 to 'strong' for RADARSAT-2. Compared to HH-polarized data, VV-polarized data offer a better signal-to-noise ratio for higher incidence angles in particular. This will be especially beneficial for the extraction of lower wind speeds. In addition, existing models for wind speed retrieval from VV-polarized data are more mature than those developed for HH-polarized data (cf. Vachon *et al*., 2004). The benefit of the VV imaging capability for wind speed retrieval is

acknowledged in the rating for RADARSAT-2's SSP mode only. Indeed, the SDP and QP mode can be used to acquire VV-polarized images but the data volume of the associated images needlessly complicates image handling and thus hinders the application.

Like wind speed retrieval, the mapping of ocean currents is anticipated to benefit from the introduction of the SSP mode. Ocean currents may appear in SAR images through several mechanisms (Johannessen *et al*., 1996). Natural surfactants are known to express spiral eddies and to concentrate in zones parallel to the mean flow direction. VV-polarized images will provide a better contrast between natural surfactants and water and can therefore be expected to provide better potential for this indirect approach to current mapping. On the other hand, meandering fronts may appear in SAR images due to short wave-current interactions that locally modify the surface roughness. According to Ufermann and Romeiser (1999), the effect of this type of interaction is more apparent in HH-polarized images than in VV-polarized images. It follows, that the polarization diversity offered in the RADARSAT-2 SSP mode will benefit the ocean current mapping application. The applications potential associated with full polarimetric data is largely unknown but it is likely that this data type will be beneficial to improving the understanding of the imaging of ocean currents.

The potential for ship detection and tracking increases from 'moderate' for RADARSAT-1 to 'strong' for RADARSAT-2. As shown in Table 1, all new RADARSAT-2 features are expected to contribute to this increase in applications potential. The most important technical enhancement for the tracking of previously detected ships is the Ultra-Fine resolution mode (nominal resolution 3 m by 3 m). Imagery from this mode will allow a more detailed analysis of ship structures and should facilitate the estimation of ship type, size and orientation. However, the high spatial resolution comes at the expense of spatial coverage. The limited swath width (20 km nominally) of the Ultra-Fine resolution data precludes its operational use for the detection of ships over extensive areas.

Full polarimetric images acquired in the QP mode have similar limitations in terms of coverage (nominal swath width 25 km) and are therefore also better suited for operational application to the tracking of known ships than to ship detection over large areas. On the other hand, full polarimetric data have been shown to facilitate the enhancement of ship-sea contrast. A better ship-sea contrast will improve results of ship detection by reducing errors of omission (cf. Touzi *et al*., 2004a). The information in full polarimetric data pertaining to

microwave scattering mechanisms has the potential to improve ship detection results because it can be used to facilitate discrimination between ships and ship look-alikes (e.g. protruding rocks or icebergs). In addition, this type of scattering information is expected to be of value for ship classification.

With the introduction of the SSP and SDP modes, RADARSAT-2 will be in a better position to support the two basic approaches to ship detection using SAR, that is, detection of the ship wake signature and detection of the ship target itself. Thanks to a greater sensitivity to sea state, VV-polarized images offer better potential for ship wake detection than either HH- or HV-polarized images. At the same time, this sensitivity to sea state decreases the ship-sea contrast in VV-polarized images as compared to the contrast in HH- and HV-polarized images. Hence, HH- and HV-polarized images are the better choice for the detection of ship targets. HH-polarized images will show the best ship-sea contrast at large incidence angles (> ca. 35°), while HV-polarized images will do so at small angles of incidence. It follows that a combination of VV and VH-polarized images can be expected to offer good potential for ship detection because these data support both ship detection approaches. This combination of images can be acquired in the RADARSAT-2 SDP mode.

The benefits of the selective look direction and improved orbit control features for ship detection are easily explained. The selective look direction potentially facilitates more continuous ship detection by increasing the number of imaging opportunities, while the improved orbit control will simplify the extraction of accurate geographic coordinates for ships detected.

The moderate increase in the overall applications potential of RADARSAT-2 vis-à-vis RADARSAT-1 for coastal zone mapping results from the enhancements in terms of polarization diversity and spatial resolution. The capacity to acquire HV-polarized data in the SSP mode is anticipated to improve the potential for the mapping of the high water shoreline. Unlike in HH and VV images, the land-water contrast in HV images will be largely unaffected by the angle of incidence and high wind conditions. The SDP and QP modes of operation will enable RADARSAT-2 to detect structural differences in the features observed, e.g. differences in vegetation cover/type and soil surface roughness. As such, these modes facilitate the mapping of land cover in coastal zones. Please refer to the preceding sections on agriculture, geology and hydrology (wetlands) for discussions regarding the relationships

between microwave polarization and the structure of natural targets. The potential of the SSP, SDP and QP modes for the mapping of near-shore bathymetry is largely unknown. However, results reported by Ufermann and Romeiser (1999) indicate that HH- and HV-polarized images are more suited for application to bathymetric mapping than VV-polarized images. The Ultra-Fine spatial resolution images can be expected to enable more detailed shoreline and land cover mapping. Moreover, these images will make a better source of information for coastal mapping by means of textural analysis.

Sea and Land Ice

Table 2 shows that the introduction of RADARSAT-2 is anticipated to increase the overall potential for all applications identified with the exception of the mapping of sea ice types. Indeed, sea ice topography and structure mapping is among the three applications that are expected to benefit the most from the technical enhancements embodied by RADARSAT-2. The (anticipated) potential for this application increases from 'limited' for RADARSAT-1 to 'strong' for RADARSAT-2. This increase in applications potential results primarily from RADARSAT-2's capability to acquire HV-polarized images in the SSP mode. Compared to HH- and VV-polarized images, HV-polarized images are more suited to the mapping of ice surface topography and structural features resulting from ridging or other types of deformation. Consequently, HV-polarized images offer better potential for the routing of ships around hazardous sea ice areas. RADARSAT-2 QP mode data products are likely to display even more sensitivity to ice topography and structure. However, the value of this data type for operational sea ice mapping is limited by its narrow swath width (nominally 25 km). The difference in the information content between images acquired in the SSP and SDP modes is not expected to be significant. The lower rating for the SDP mode can be explained from the redundancy in data volume. The potential increase in revisit frequency resulting from the capability to switch from left- and right-looking would be of benefit to sea ice mapping/monitoring at mid-latitudes where the current revisit with RADARSAT-1 is every 2 to 3 days.

Like in the case of sea ice topography and structure mapping, the increase in application potential for sea ice edge and ice concentration mapping results mostly from the HV imaging capability in the SSP mode. Unlike in HH and VV images, the ice-water

contrast in HV images will be largely unaffected by the angle of incidence and high wind conditions. Consequently, HV images can be expected to offer improved potential for sea ice edge and ice concentration mapping (Scheuchl *et al.*, 2004). Full polarimetric data products as acquired in the QP mode of operation can likely be manipulated to enhance the ice-water contrast to a level above that of HV data. However, as mentioned before, the value of this data type for operational application to sea ice is limited by the swath width. The promise of the selective look direction feature for applications potential was discussed previously in this paper.

Data from single frequency and single polarization SAR systems like RADARSAT-1 are known to offer moderate potential for the mapping of multi-year and first-year ice types. On the other hand, this type of data has shown little promise as a source of information for discrimination of thin/new ice and open water. According to Drinkwater *et al*. (1991) and Thomsen *et al*. (1998), C-band full polarimetric data, that is, the type of data acquired in RADARSAT-2's QP mode, offer considerably more potential for sea ice type mapping. For example, a polarimetric parameter known as the co-polarization phase difference is reported to allow for separating water from a range of thin ice types. As mentioned before, the value of the QP data products for operational mapping of ice types is limited by the narrow swath width.

Icebergs, like ships, manifest themselves in radar images as bright point targets against a dark background of ocean clutter. Consequently, much of the ratings in Table 1, and justifications thereof, for icebergs and ships are identical. Only the effect of SDP feature rates differently, i.e. 'minor' for icebergs and 'moderate' for ship detection. In the case of iceberg detection, a dual-polarization image pair (e.g. VV and VH) is not expected to contain any more relevant information than a single VH-polarized image. Ship detection, on the other hand, will benefit from the capability to acquire images in the SDP mode since ship targets often have higher contrast in VH-polarization while ship wakes are most evident in VV-polarization. Generally speaking, iceberg detection by means of SAR creates a bigger challenge than ship detection. This is reflected in the applications potential ratings for both RADARSAT-1 and RADARSAT-2 in Table 2. Differences in material, shape, and size as well as the effects of environmental conditions on the radar signature of icebergs contribute to this discrepancy in applications potential.

By far the most beneficial feature of RADARSAT-2 for the polar glaciology application is its selective look direction. The ability to easily change from right- to left-looking will enable RADARSAT-2 to image parts of Antarctica not accessible by other high-resolution remote sensing satellites. As such, RADARSAT-2 will facilitate the study of Antarctic ice flows and floating ice shelves in a way and at a scale not previously possible. The capability to acquire cross-polarized data in the SSP mode and full polarimetric data in the QP mode is likely to benefit the application since these data types are more sensitive to differences in both surficial and internal ice structure. However, more research is required to assess the potential for application to polar glaciology of full polarimetric C-band data in particular. Repeat-pass SAR interferometry techniques have been shown to yield information on ice motion (e.g. Gray *et al.*, 2001; Short and Gray, 2004). Thanks to improved orbit control RADARSAT-2 can be expected to offer better interferometric capabilities than RADARSAT-1.

Summary

RADARSAT-2's Selective Single Polarization (SSP) mode is shown to moderately advance the potential for applications for which information needs can generally be met by single channel C-band data, but for which the HH-polarization as offered by RADARSAT-1 is not the most favourable. As a rule, the information needs associated with hurricanes, oil spills, and winds are better met through application of VV-polarized images. Similarly, the requirements pertaining to clearcuts, fire-scars, ships, and selected sea and land ice applications are more easily satisfied when HV or VH images can be applied. On the other hand, the current application can benefit from information contained in both HH- and VV-polarized images.

The capability to operate in the Selective Dual Polarization (SDP) mode is projected to moderately improve the potential of RADARSAT-2 to provide information in support of applications dealing with targets that include transparent (at C-band) vegetation volumes with varying structural properties or land surfaces with varying degrees of roughness. The hurricanes, oil spills, clearcuts, fire-scars, winds, current and sea and land ice applications are expected to gain little information from SDP image acquisitions. In fact, the larger data volume of SDP products is anticipated to burden these applications in terms of data handling.

Data acquired in the Quad Polarization (QP) mode will facilitate the computation of a wide variety of variables that relate to the strength, polarization or phase of the received backscatter signal. Introduction of this imaging mode is expected to moderately advance the potential of RADARSAT-2 for most of the applications identified. The QP mode data are anticipated to be particularly valuable or essential for the crop type, crop condition, DEM polarimetry, and search & rescue applications. On the other hand, the oil spills, clearcuts, fire-scars, winds and currents applications are not expected to benefit from the QP mode imaging capability. Due to technical limitations, the swath width of the images acquired in the QP mode is restricted to 25 km (nominally). This will definitely constrain the operational use of QP mode data in support of applications that require information over large areas, e.g. forestry, oceans and sea ice applications.

RADARSAT-2's capacity to acquire images with Ultra-Fine spatial resolutions is restricted to the SSP imaging mode. The expectation is that this capability will be most beneficial to cartographic applications and applications dealing with point targets, that is, ship and iceberg detection. In addition, a considerable number of applications are foreseen to moderately benefit from Ultra-Fine resolution space-borne SAR data. Like QP data products, Ultra-Fine resolution data products will have a limited swath width (20 km nominally). Again, this can be expected to obstruct the operational use of this data type in certain applications.

The selective look direction feature of RADARSAT-2 is anticipated to have a major effect on its potential for applications in the fields of disaster management and polar glaciology. Disaster management applications will benefit form the reduced average response time and the generally increased revisit frequency. On the other hand, the polar glaciology application will gain from the fact that the left-looking configuration will enable routine imaging of the most southerly regions on Earth including Antarctica. Applications concerned with crop condition, soil moisture, snow, ships, icebergs and sea ice are expected to benefit from the selective look direction capability in a more moderate fashion.

Improved knowledge about and control over the RADARSAT-2 orbit will lead to enhanced potential of its images for applications that make use of interferometric processing techniques in particular. This includes applications dealing with DEM interferometry, geological hazards, search and rescue, terrain mapping and polar glaciology. Applications

such as DEM stereoscopy, DEM polarimetric, cartographic feature extraction, search and rescue, and ship and iceberg detection will moderately benefit from the associated improved image georeferencing accuracy.

Comparison of ratings for the overall applications potential of RADARSAT-1 and RADARSAT-2 (anticipated) shows that the technical enhancements of RADARSAT-2 will be most beneficial to applications concerned with crop type, crop condition, and sea ice topography / structure. The improvement in overall potential for these three applications, from 'limited' for RADARSAT-1 to 'strong' for RADARSAT-2, results primarily from the enhancements in terms of polarization. For 18 out of the 32 applications identified, the introduction of RADARSAT-2 is anticipated to result in a moderate increase in applications potential, i.e. an increase in potential vis-à-vis RADARSAT-1 by one level. The technical enhancements that lead to these improvements in potential may differ depending on the application. The number of applications for which no increase in applications potential is foreseen amounts to ten. This 'no increase' group of applications includes the DEM stereoscopy and flood mapping, that is, applications for which the potential of RADARSAT-1 is already ranked at the highest level. The application potential for DEM interferometry and hurricanes stalls at the 'moderate' rating because of restraints imposed by atmospheric conditions and swath width, respectively. Orbital characteristics of RADARSAT-1 and RADARSAT-2 restrict the potential for the waves application to a 'limited' rating. Generally speaking, the information requirements of other applications in the 'no increase' group are better met by low- or multi-frequency SAR systems (e.g. forest type, forest biomass, sea ice type) or by optical remote sensing systems (e.g. oil spills, lithology). The potential of RADARSAT-2 for the one remaining application, that is, DEM polarimetry is rated as 'limited'. DEMs produced from full polarimetric RADARSAT-2 data will not be complete since the elevation information will only be available in two specific directions, i.e. the azimuth directions of ascending and descending overpasses.

Acknowledgements

The author wishes to acknowledge the contributions of the following colleagues to the report that provided the basis for this paper (van der Sanden and Ross, 2001): Paul Budkewitsch, Dean Flett, Laurence Gray, Robert Hawkins, Shannon Kaya, Robert Landry, Tom Lukowski,

Heather McNairn, Terry Pultz, Vern Singhroy, Jennifer Sokol, Thierry Toutin, Ridha Touzi, and Paris Vachon. In addition, he would like to thank Sylvia Thomas as the internal reviewer and the two anonymous external reviewers for their advice and comments on the manuscript.

References

Ahern, F.J. and J.A. Drieman. (1988). "Assessment of clearcut mapping accuracy with C-band SAR", In: *Proceedings of the IGARSS 1988 Symposium; Remote Sensing: Moving Towards the 21st Century*, Edinburgh, 12-16 September 1988, Vol. III, pp. 1335-1338.

Ali, Z., I. Barnard, P. Fox, P. Duggan, R. Gray, P. Allan, A. Brand, and R. Ste-Mari. (2004a). "The RADARSAT-2 Synthetic Aperture Radar design description", *Canadian Journal of Remote Sensing*, Vol. 30, No .3, pp. 246-257.

Ali, Z., G. Kroupnik, G. Matharu, J. Graham, I. Barnard, P. Fox, and G. Raimondo. (2004b). "RADARSAT-2 space segment design and enhanced capabilities from RADARSAT-1", *Canadian Journal of Remote Sensing*, Vol. 30, No .3, pp. 235-245.

Braun, N., M. Gade, and G. Schymura. (2000). "Multi-frequency/multi-polarization measurements of radar backscatter under different rain and wind conditions", In: *Proceedings of the IGARSS 2000 Symposium; Taking the Pulse of the Planet: The Role of Remote Sensing in Managing the Environment*, Honolulu, 24-28 July 2000, Vol. 1, pp. 123-125.

Buckley, J. (2004). "Enhanced classification of prairie landscapes using simulated RADARSAT-2 imagery", *Canadian Journal of Remote Sensing*, Vol. 30, No. 3, pp. 510-516.

CCRS. (2004). RADARSAT-2 Demonstration Website, http://www.ccrs.nrcan.gc.ca/ccrs/data/satsens/radarsat/r2demo/r2demo_e.html.

Dobson, M.C., F.T. Ulaby, T. Le Toan, A. Beaudoin, E.S. Kasischke, and N.L. Christensen. (1992). "Dependence of radar backscatter on coniferous forest biomass", *IEEE Transactions on Geoscience and Remote Sensing*, Vol. 30, No. 2, pp. 412-415.

Dowd, M., P.W. Vachon, F.W. Dobson, and R.B. Olsen. (2001). "Ocean wave extraction from RADARSAT synthetic aperture radar inter-look image cross-spectra", *IEEE Transactions on Geoscience and Remote Sensing*, Vol. 39, No. 1, pp. 21-37.

Drinkwater, M.R., R. Kwok, D.P. Winebrenner, and E. Rignot. (1991). "Multifrequency polarimetric synthetic aperture radar observations of sea ice", *Journal of Geophysical Research*, Vol. 96, No. C11, pp. 20,679-20,698.

Engen, G., P.W. Vachon, H. Johnson, and F.W. Dobson. (2000). "Retrieval of ocean wave spectra and RAR MTFs from dual-polarization SAR data", *IEEE Transactions on Geoscience and Remote Sensing*, Vol. 38, No. 1, pp. 391-403.

Fox, P., A. Luscombe, and A. Thompson. (2004). "RADARSAT-2 SAR modes development and utilization", *Canadian Journal of Remote Sensing*, Vol. 30, No. 3, pp. 258-264.

Gaddis, L. (1992). "Lava-flow characterization at Pisgah volcanic field, California, with multiparameter imaging radar", *Bulletin of the Geological Society of America*, Vol. 104, pp. 695-703.

Gray, A.L., N. Short, K.E. Mattar, and K.C. Jezek. (2001). "Velocities and flux of the Filchner Ice Shelf and its tributaries determined from speckle tracking Interferometry", *Canadian Journal of Remote Sensing*, Vol. 27, No. 3, pp. 193-206.

Huadong, G., L. Jingjuan, W. Changlin, W. Chao, T.G. Farr, and D.L. Evans. (1997). "Use of multifrequency, multipolarization Shuttle Imaging Radar for volcano mapping in the Kunlun Mountains of Western China", *Remote Sensing of Environment*, Vol. 59, No. 4, pp. 364-374.

Johannessen, J.A., R.A. Shuchman, D.R. Lyzenga, C. Wackerman, O.M. Johannessen, and P.W. Vachon. (1996). "Coastal ocean fronts and eddies imaged with ERS-1 synthetic aperture radar", *Journal of Geophysical Research*, Vol. 101, No. C3, pp. 6651-6667.

Kneppeck, I.D. and F.J. Ahern. (1989). "Stratification of a regenerating burned forest in Alberta using Thematic Mapper and C-SAR images", In: *Proceedings of the IGARSS 1989 Symposium; Quantitative Remote Sensing: An Economic Tool for the Nineties*, Vancouver, 10-14 July 1989, Vol. III, pp. 1391-1396.

Le Toan, T., A. Beaudoin, J. Riom, and D. Guyon. (1992). "Relating forest biomass to SAR data", *IEEE Transactions on Geoscience and Remote Sensing*, Vol. 30, No. 2, pp. 403-411.

Lukowski, T.I., B. Yue, F.J. Charbonneau, F. Khellah, and R.K. Hawkins. (2004). "Detection of crashed aircraft in polarimetric imagery: studies at Natural Resources Canada", *Canadian Journal of Remote Sensing*, Vol. 30, No. 3, pp. 484-495.

MacKay, M.E. and P.J. Mouginis-Mark. (1997). "The effect of varying acquisition parameters on the interpretation of SIR-C radar data: the Virunga volcanic chain", *Remote Sensing of Environment*, Vol. 59, No. 2, pp. 321-336.

Mattia, F., T. Le Toan, J.C. Souyris, G. De Carolis, N. Floury, F. Posa, and G. Pasquariello. (1997). "The effect of surface roughness on multifrequency polarimetric SAR data", *IEEE Transactions on Geoscience and Remote Sensing*, Vol. 35, No. 4, pp. 954-965.

McNairn, H. and B. Brisco. (2004). "The application of C-band polarimetric SAR for agriculture: a review", *Canadian Journal of Remote Sensing*, Vol. 30, No. 3, pp. 525-542.

McNairn, H., K. Hochheim, and N. Rabe. (2004). "Applying polarimetric radar imagery for mapping the productivity of wheat crops", *Canadian Journal of Remote Sensing*, Vol. 30, No. 3, pp. 517-524.

Morena, L., K. James, and J. Beck. (2004). "An introduction to the RADARSAT-2 mission", *Canadian Journal of Remote Sensing*, Vol. 30, No. 3, pp. 221-234.

Schaber, G.G., J.F. McCauley, and C.S. Breed. (1997). "The use of multifrequency and polarimetric SIR-C/X SAR data in geologic studies of Bir Safsaf, Egypt", *Remote Sensing of Environment*, Vol. 59, No. 2, pp. 337-363.

Scheuchl, B., D. Flett, R. Caves, and I. Cumming. (2004). "Potential of RADARSAT-2 multiple polarization and polarimetric data for operational sea ice monitoring", *Canadian Journal of Remote Sensing*, Vol. 30, No. 3, pp. 448-461.

Schuler, D.L., J.S. Lee, D. Kasilingam, and G. Nesti. (2002). "Surface roughness and slope measurements using polarimetric SAR data", *IEEE Transactions on Geoscience and Remote Sensing*, Vol. 40, No. 3, pp. 687-698.

Short, N. and A.L. Gray. (2004). "Potential of RADARSAT-2 interferometry: glacier monitoring using speckle tracking", *Canadian Journal of Remote Sensing*, Vol. 30, No. 3, pp. 504-509.

....Singhroy, V. (1996). "Environmental and geological site characterization in vegetated areas: image enhancement guidelines", In: V.Singhroy, D.Nebert, & A.Johnson (Eds.), Remote Sensing and GIS: Applications and Standards, American Society for Testing and Materials, pp. 5-17.

Sokol, J., T.J. Pultz, and A.E. Walker. (2003). "Passive and active airborne microwave remote sensing of snow cover", *International Journal of Remote Sensing*, Vol. 24, No. 24, pp. 5327-5344..

Sokol, J., H. McNairn, and T.J. Pultz. (2004). "Case studies demonstrating hydrological applications of C-band multi-polarized and polarimetric SAR", *Canadian Journal of Remote Sensing*, Vol. 30, No. 3, pp. 470-483.

Thomsen, B.B., S.V. Nghiem, and R. Kwok. (1998). "Polarimetric C-band SAR observations of sea ice in the Greenland Sea", In: *Proceedings of the IGARSS 1998 Symposium; Sensing and Managing the Environment*, Seattle, 6-10 July 1998, Vol. V, pp. 2502-2504.

Toutin, T. (2004). "RADARSAT-2 stereoscopy and polarimetry for 3D mapping", *Canadian Journal of Remote Sensing*, Vol. 30, No. 3, pp. 496-503.

Touzi, R., F.J. Charbonneau, R.K. Hawkins, and P.W. Vachon. (2004a). "Ship detection and characterization using polarimetric SAR", *Canadian Journal of Remote Sensing*, Vol. 30, No. 3, pp. 552-559.

Touzi, R., R. Landry, and F.J. Charbonneau. (2004b). "Forest type discrimination using calibrated C-band polarimetric SAR data", *Canadian Journal of Remote Sensing*, Vol. 30, No. 3, pp. 543-551.

Ufermann, S. and R. Romeiser. (1999). "Numerical study on signatures of atmospheric convective cells in radar images of the ocean", *Journal of Geophysical Research*, Vol. 104, No. C11, pp. 25,707-25,719.

Vachon, P.W., J.W.M. Campbell, and F.W. Dobson. (1997). "Comparison of ERS and RADARSAT SARs for wind and wave measurement", In: *Proceedings of the 3rd ERS*

Symposium on Space at the Service of our Environment, Florence, 17-21 March 1997, Vol. 3, pp. 1367-1372.

Vachon, P.W., J. Wolfe, and R.K. Hawkins. (2004). "Comparison of C-band wind retrieval model functions with airborne multipolarization SAR data", *Canadian Journal of Remote Sensing*, Vol. 30, No. 3, pp. 462-469.

van der Sanden, J.J. and S.G. Ross. (2001). *Applications Potential of RADARSAT-2 - A Preview*. Ottawa, Natural Resources Canada, Canada Centre for Remote Sensing, 117 p. (http://dweb.ccrs.nrcan.gc.ca/ccrs/db/biblio/paper_e.cfm?BiblioID=13103)

BLANK PAGE

Appendix II – Convair-580 SAR Data

Table 1 Convair-580 SAR data sets available from the GeoGratis website[1)] hosted by Natural Resources Canada.

Application area(s)	Location	Website
Agriculture	Indian Head, Saskatchewan	http://geogratis.cgdi.gc.ca/download/cv580/28june2000l3p6/
Hydrology / wetlands	Alfred Bog, Ontario	http://geogratis.cgdi.gc.ca/download/cv580/AlfredBog/
Multiple / land cover	Annapolis Valley, Nova Scotia	http://geogratis.cgdi.gc.ca/download/cv580/Annapolis/
Oceans / coastal zones	Muskadobit, Nova Scotia	http://geogratis.cgdi.gc.ca/download/cv580/Coastline/
Multiple / land cover	Orillia, Ontario	http://geogratis.cgdi.gc.ca/download/cv580/Orillia/
Multiple / land cover	Orillia, Ontario	http://geogratis.cgdi.gc.ca/download/cv580/Pipeline/
Hydrology	Winnipeg, Manitoba	http://geogratis.cgdi.gc.ca/download/cv580/RedRiver/
Oceans / coastal zones	Seal Harbour, Nova Scotia	http://geogratis.cgdi.gc.ca/download/cv580/SealHarbour/
Agriculture	Barhaven, Ontario	http://geogratis.cgdi.gc.ca/download/cv580/a_SAR1/
Urban / calibration	Shirley's Bay, Ottawa, Ontario	http://geogratis.cgdi.gc.ca/download/cv580/a_SAR2/

1) http://geogratis.cgdi.gc.ca/clf/en?action=entrySummary&entryId=325&entryType=productCollection&keymap=outlineCanada

BLANK PAGE

Appendix III – PWS Functionality

1 Tools panel

Figure 1 represents the PWS tool panel. Users can select one of the following functions:

- Load image
- Local Area Analysis
- Image Synthesis
- View data
- Demo

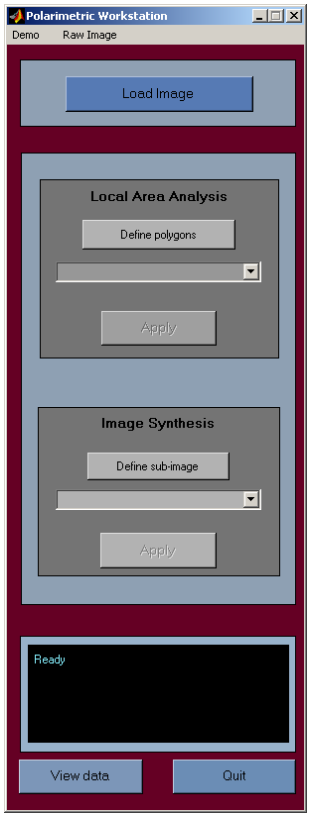

Figure 1 PWS tool panel. All major analysis functions are accessed from this panel. Processing status is displayed in bottom window.

2 Local Area Analysis Tools

Local analysis tools are the following functions that provide polarization information of a given sample selected with the Polygon function:

Polarimetric signature: Generate the co-polarized and cross-polarized polarimetric signatures of the selected polygon (Figure 2). The pedestal of the polarimetric signature is provided as well as the antenna illumination (incidence) angle.

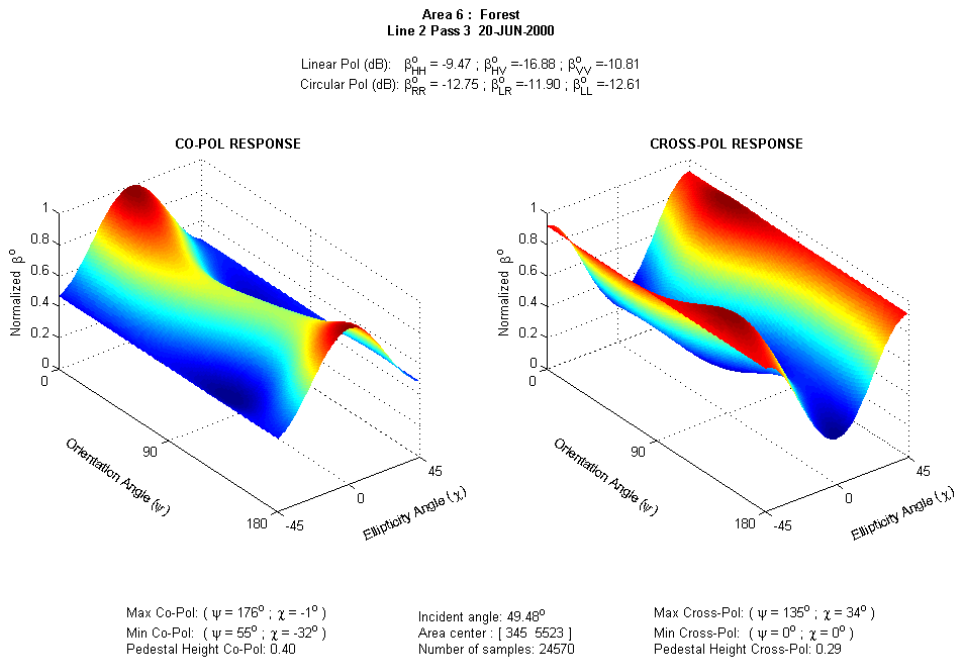

Figure 2 Polarimetric signatures of a forested area in a SAR scene. Co-polarization signature is shown on the left and cross-polarization signature on the right. Physical quantitative parameters are also displayed.

Statistics: Provide estimates of the polarimetric parameters that characterize the scattered and the received waves. The parameters computed for each selected polygon are saved in an Excel file. The following parameters are estimated within the selected sample:

1) $\beta°$ (=$\sigma°$ sin θ_{inc}, where θ_{inc} is the incidence angle) in dB for the linear polarizations HH, VV, and HV.
2) $\beta°$ for the right (R) and left (L) circular polarizations RR, LL, and RL.
3) Span which corresponds to the total scattered wave intensity.
4) Extrema of the scattered wave intensity R_o^{max} and R_o^{min}.
5) Extema of the degree of polarization p_{max} and p_{min}. The combination of these two parameters with R_o^{max} and R_o^{min} permits an excellent characterization of the type of scattering mechanism and its heterogeneity (Touzi *et al.,* 1992).
6) Extrema of the completely polarized wave intensity CP_{MAX} and CP_{MIN}.
7) Extrema of the completely unpolarized wave intensity CUP_{MAX} and CUP_{MIN}.
8) Extrema of the received power P_{MAX} and P_{MIN}.

9) Extrema of the cross-matched power P_{XMAX} and P_{XMIN}; the scattered wave is maximized and the received antenna polarization is cross-matched to the scattered wave.
10) Van Zyl coefficient of variation P_{MIN}/P_{MAX}.
11) Polarization signature pedestals.
12) Channel coherence amplitude γ and phase ϕ (in degree) for HH-VV, HH-HV, and VV-HV.
13) The number of pixels per polygon, as well as the incidence angle, are saved.

Histogram: Generate the amplitude histogram of the 4 polarizations.

Poincaré Sphere: Map the polarization state of the scattered wave on the Poincaré sphere (Figure 3). Multi-look data polarization state of a partially polarized wave is mapped within the Poincaré sphere.

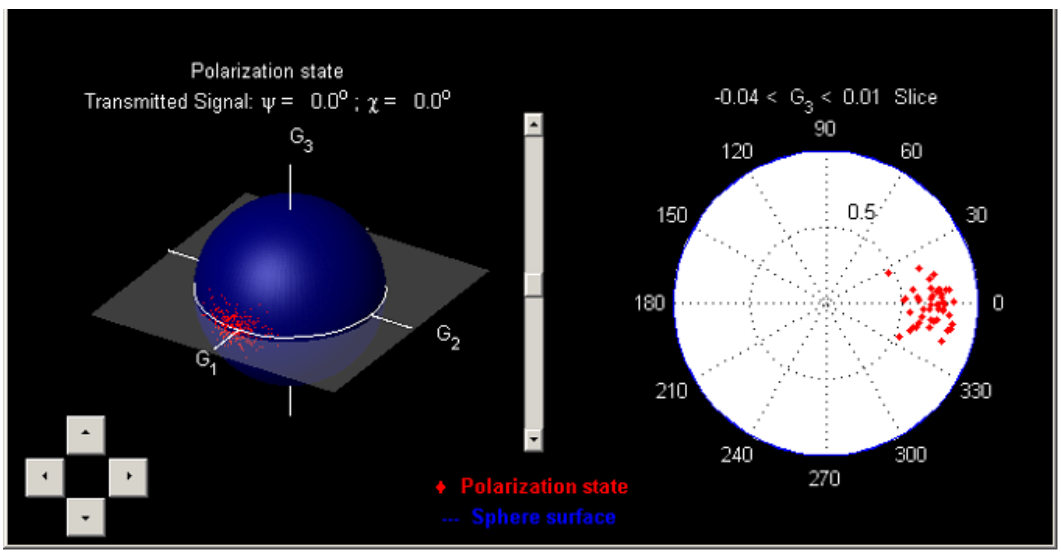

Figure 3 Poincaré sphere representation of the polarization state of the scattered wave. Analysis of the polarization state distribution in the sphere representation on the right reveals a large concentration of scattered waves in the Poincaré sphere equator that corresponds to linearly polarized waves with a dominating return at the horizontal polarization. The sphere transversal section on the right permits a better allocation of the polarization states of the partially polarized waves inside the Poincaré sphere; the large concentration of scattering at about 0.6 from the sphere origin indicates a significant unpolarized component in the target

Channel Coherence (magnitude and phase difference): The polar representation is used to present the magnitude and phase of the complex coherence (Figure 4).

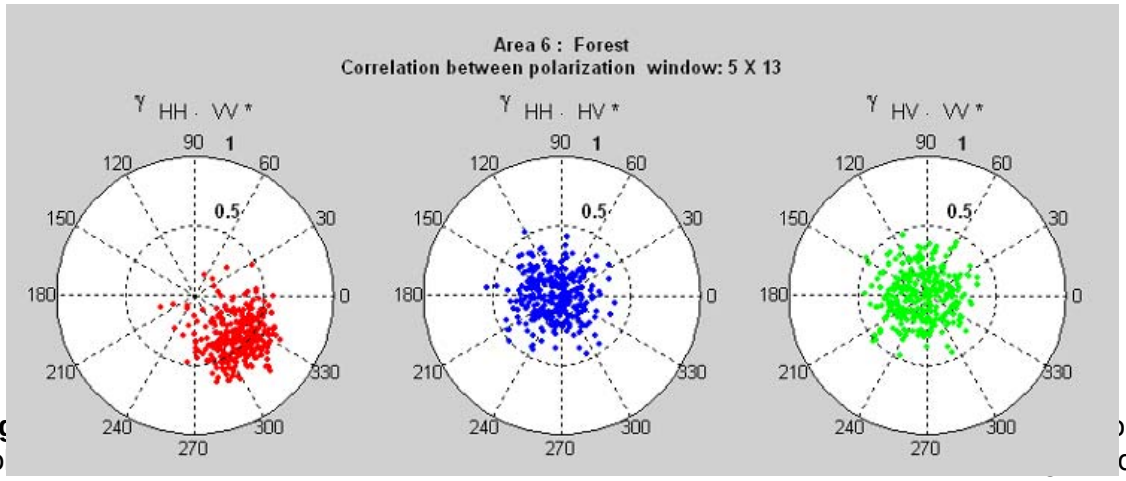

Fig on a
po dow
(5x13 in this case), where the magnitude of the coherence is represented by the radius length (0 to 1) and the coherence phase by the angle (0° to 360°).

Cloude's Decomposition: Derive Cloude's parameters (H), anisotropy (A), α and β, from Cloude's decomposition algorithm (Cloude and Pottier, 1996). Two options are offered:

1) Estimate of the means of Cloude's parameters H, A, α and β. To obtain unbiased estimates, the averaged coherency matrix is calculated over the polygon area under study, and used to derive the parameters.
2) Display the histogram of α as a function of entropy H within Cloude's parabola (Figure 5). α and H are derived using the coherency matrix derived from multi-look samples. The number of looks (i.e. number of independent samples per pixel) can be fixed in terms of pixel window size.

Batch-Tool: Execute the above functions in a batch processing over selected polygons.

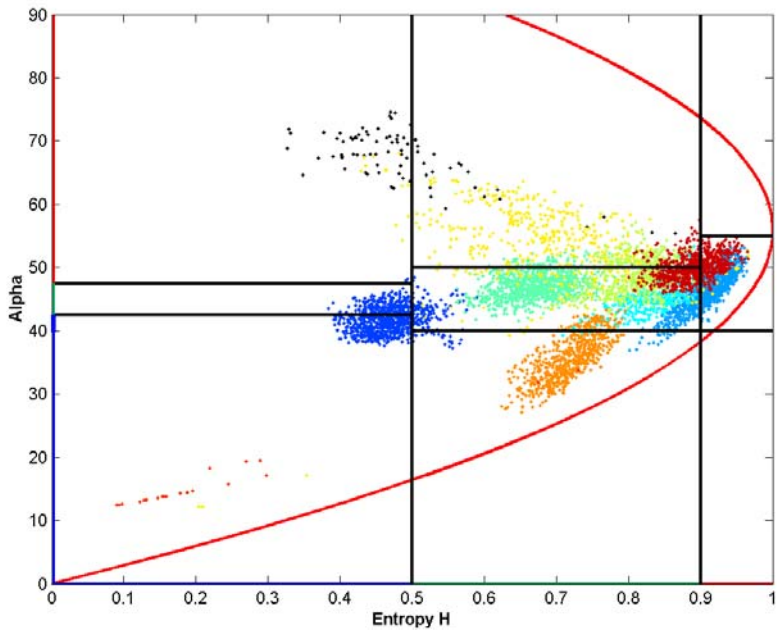

Figure 5 2-D representation of the Cloude's α angle function of the entropy H. Colour dots correspond to areas of different scattering mechanisms.

3 Image Synthesis Tools

a) Synthesis of the received radar reflectivity image, $\beta^\circ = \sigma^\circ \sin \theta_{inc}$, for any combination of transmitting-receiving antenna polarizations.
b) Channel Coherence for any combination of HH, VV, and HV channels.
c) Optimization of two-target contrast: generate the image at the antenna polarization combination which optimizes the contrast between two selected targets, using the Swartz method (Swartz *et al.,* 1988) developed for azimuthally symmetrical targets.
d) Generation of a file under the Kennaugh matrix format using the scattering matrix file.
e) Batch synthesis: Executes above points a, b and d, as well as Cloude's parameters, in a batch process for the defined sub-image.

4 Demo

By selecting "Demo" on the top-left corner of the control tools panel, a demonstration movie will launch. The demo represents a sequence of β° images synthesized for different configurations of the transmitting-receiving antenna polarizations. The transmitting and receiving polarization ellipses are displayed on each side of the synthesized image.